



Southern Ocean Long-term
Observation & MONitoring



Cruise Report 2023

For the Southern Ocean Expedition 2023 (ANA13B)
Using IBRV ARAON
January 5 ~ February 18, 2023
Ross Sea, Southern Ocean

Jisoo Park, Chief Scientist
Korea Polar Research Institute (KOPRI)

Report contributors:

Jisoo Park^{1*}, Tae-Wan Kim¹, Jaeill Yoo¹, Yeonggi Kim¹, Keyhong Park¹, Jung-OK Choi¹, Jinyoung Jung¹, Juyoung Son^{1,2}, Sun-Yong Ha¹, Jun-Oh Min¹, Taejin Kim², Ijin Lim², Jennifer Magnusson³, Youngju Lee¹, Hyeju Yoo¹, Jong Kuk Moon¹, Jee-Hoon Kim¹, Wuju Son¹, Hyoung Sul La¹, Sanghoon Park⁴

¹Division of Ocean Sciences, Korea Polar Research Institute (KOPRI), Republic of Korea

²Pukyong National University, Republic of Korea

³Monterey Bay Aquarium Research Institute; Moss Landing, CA

⁴Department of Oceanography, Pusan National University, Republic of Korea

*Chief Scientist, Jisoo Park

E-mail: jspark@kopri.re.kr

Tel.: +82-32760-5339

Korea Polar Research Institute

26 Songdomirae-ro, Yeonsu-gu

Incheon 21990, Republic of Korea

Editor's Note: All data and summaries provided herein is subject to revision or correction and should be treated as unpublished data with intellectual property reserved to the scientist contributing to the report. Please contact the individuals listed as having responsibility for each report section for additional information or Dr. Jisoo Park (jspark@kopri.re.kr), the chief scientist of 2023 ARAON Southern Ocean Cruise (2nd Leg, ANA13B).

How to cite this report:

Park, J. and et al. (2022) Cruise Report for the Southern Ocean Expedition 2023 using IBRV ARAON: The 2nd Leg, Report No. XXXX, Korea Polar Research Institute, pp100.

Contents

Summary	3
Acknowledgements	4
Cruise track	6
Chapter 1. Physical Oceanography	8
1.1. Hydrographic Survey	8
1.2. Ocean Moorings	13
Chapter 2. Chemical Oceanography	35
2.1. Inorganic Carbon System and Gas Measurement	35
2.2. Nutrient, Dissolved Organic Carbon, and Oxygen Isotope	44
2.3. Particulate Organic Carbon and Photochemistry	48
2.4. Trace Metal	57
2.5. Deploying Biogeochemical Profiling Floats in the Southern Ocean and Ross Sea	63
Chapter 3. Biological Oceanography	72
3.1. Phytoplankton Ecology	72
3.2. Microzooplankton Community and Grazing	82
3.3. Mesozooplankton Ecology	86
3.4. Krill Acoustics	90
3.5. Biochemical Composition of POM	96

IBRV ARAON Southern Ocean Cruise ANA13B

January 5 – February 18, 2023

Summary

The most important function of the Earth system in the Southern Ocean (SO) is the role of climate change control in which the cold waters of the SO cool the equator and absorb greenhouse gases. Our research goal is understanding current status of heat and carbon uptake capacity in the West Antarctic region and investigating the variability of material cycle and marine ecosystem response. To this, we are doing our effort to 1) assess of heat transport change and carbon uptake evolution in the Southern Ocean, 2) understand the variability of biogeochemical cycles in the Southern Ocean coastal region under shrinking cryosphere (global warming), 3) detect biological production change and tracing marine ecosystem response, and 4) establish an optimal site for the Southern Ocean long-term monitoring research station through the domestic and international research collaboration.

To achieve this goal, in this austral summer, the ARAON Antarctic Cruise (ANA13B) was conducted. Korean first Icebreaker ARAON departed Littleton Harbor on January 5th, 2023 and returned to Littleton on February 18th, 2023. With funding provided by Korea Polar Research Institute (KOPRI), the research effort was conducted for the Southern Ocean Long-term Observation & MONitoring (SOLOMON) Program to observe physical, chemical, and biological parameters in recent warming of western Southern Ocean and how quickly environmental changes affect the ecosystem in that regions. For ANA13B, a total of 20 scientists and other staffs have participated including 2 universities and US Southern Ocean Carbon and Climate Observation and Modeling project (SOCCOM) team.

The in-situ data were collected on the transit line between southern Australia and Ross Sea and shelf regions in the Ross Sea, Southern Ocean. Profiles of water temperature and salinity were obtained with CTD (Conductivity-Temperature-Depth). Additional sensors on the CTD profiler were collected in-situ data on phytoplankton concentrations (fluorometer), optical clarity (transmissometer), dissolved oxygen (DO) and photosynthetic active radiation (PAR). A rosette sampler was used with the CTD to obtain water samples from discrete depths for a

broad suite of biological and geochemical parameters, some for onboard analysis, others to be stored for later analysis in shore-based laboratories. Both bio-acoustic backscatter data and depth-varying current information were collected using a Lowered Acoustic Doppler Current Profiler (LADCP) attached to CTD at most of the science stations. Plankton samples were also obtained in vertical hauls by phyto- and bongo-nets lowered to 200 m.

Acknowledgements

We thank the IBRV ARAON captain and crew for well-executed hard work under difficult conditions. This research was supported by KOPRI grant (PE22110).

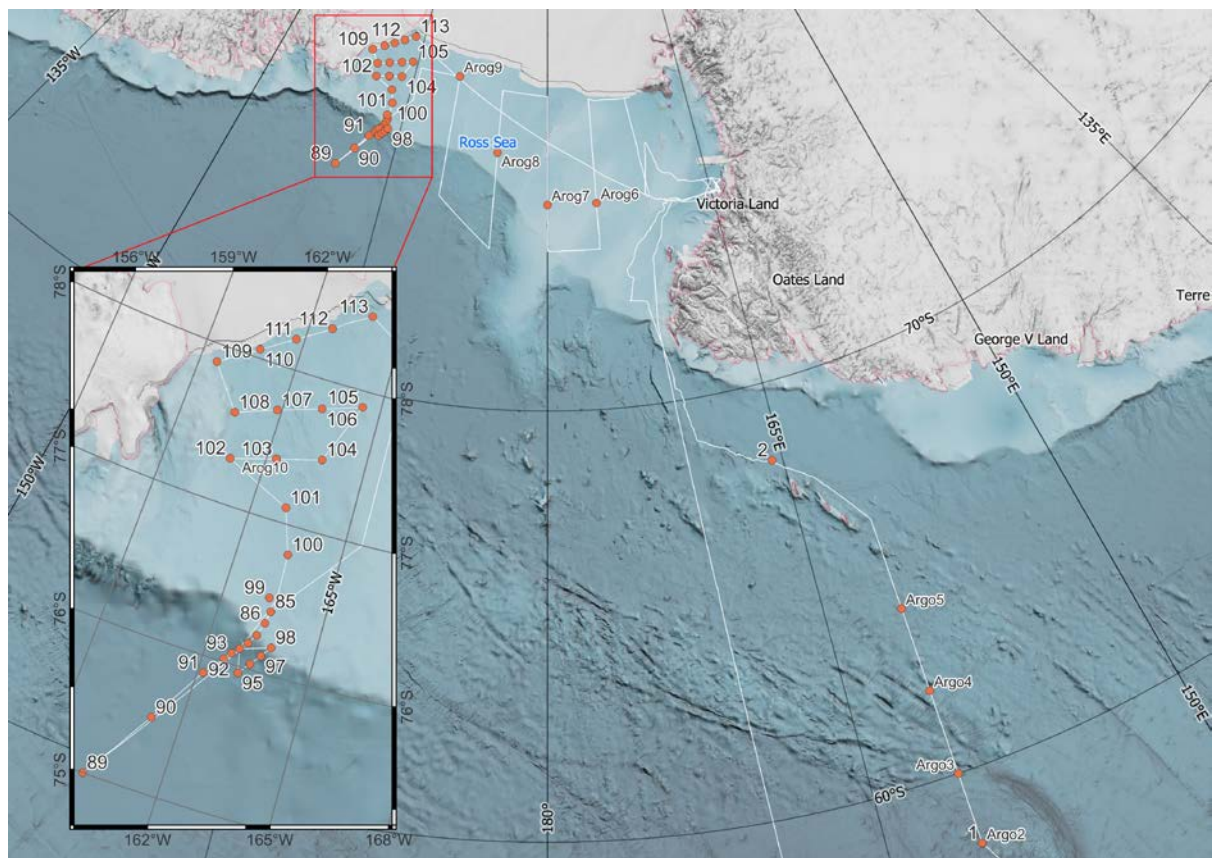
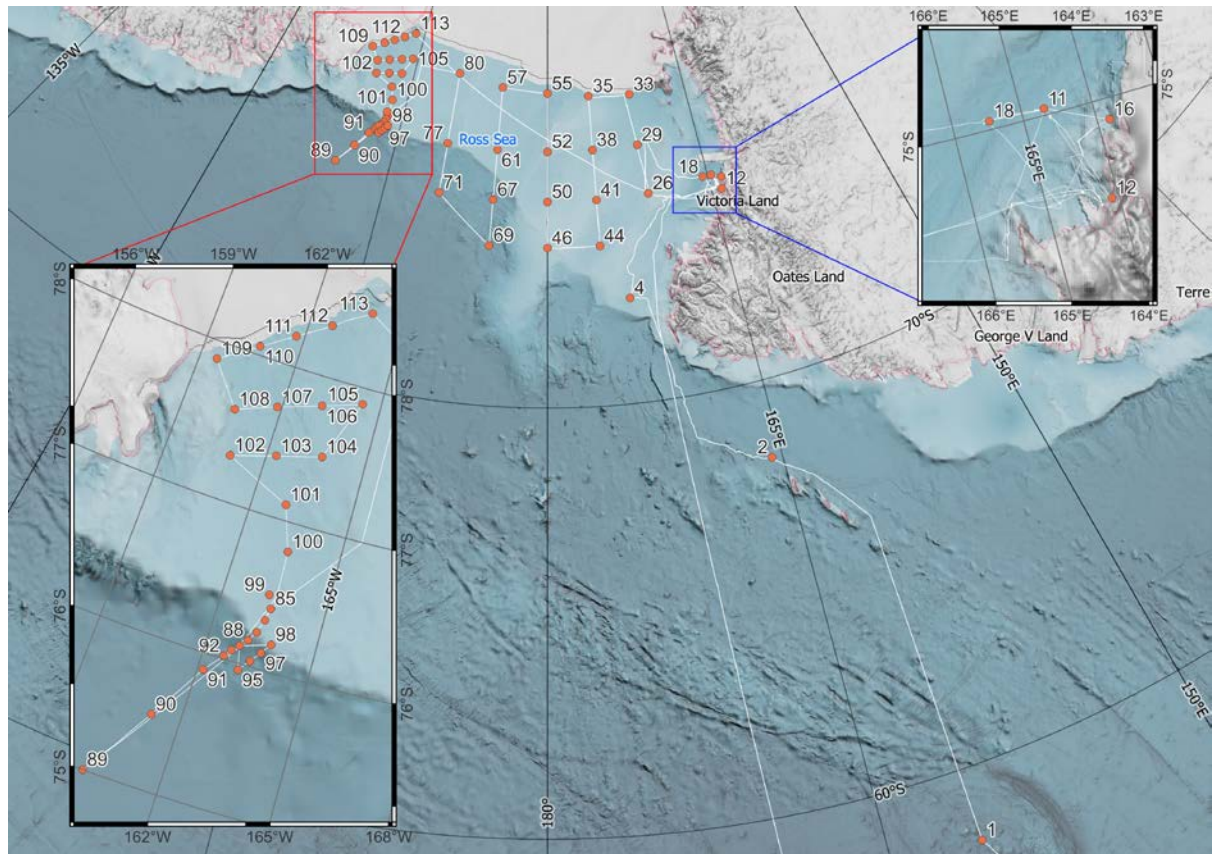
Projects

SOLOMON (Southern Ocean Long-term Observation and MONitoring), KOPRI Project No. PE22110, PI: Jisoo Park, KOPRI

Cruise Participants (research)

1. Jisoo Park, KOPRI, Republic of Korea (jspark@kopri.re.kr)
2. Tae-Wan Kim, KOPRI, Republic of Korea (twkim@kopri.re.kr)
3. Jaeill Yoo, KOPRI, Republic of Korea (jiyoo@kopri.re.kr)
4. Yeonggi Kim, KOPRI, Republic of Korea (ygkim@kopri.re.kr)
5. Keyhong Park, KOPRI, Republic of Korea (keyhongpark@kopri.re.kr)
6. Jung-OK Choi, KOPRI, Republic of Korea (jochoi@kopri.re.kr)
7. Jinyoung Jung, KOPRI, Republic of Korea (jinyoungjung@kopri.re.kr)
8. Juyoung Son, KOPRI, Republic of Korea (mh0980@kopri.re.kr)
9. Sun-Yong Ha, KOPRI, Republic of Korea (syha@kopri.re.kr)
10. Jun-Oh Min, KOPRI, Republic of Korea (jomin@kopri.re.kr)
11. Taejin Kim, Pukyong National University, Republic of Korea (tkim@pknu.ac.kr)
12. Ijin Lim, Pukyong National University, Republic of Korea (ijinlim@pknu.ac.kr)
13. Jennifer Magnusson, Monterey Bay Aquarium Research Institute, USA (jenn.magnusson@gmail.com)
14. Youngju Lee, KOPRI, Republic of Korea (yjlee@kopri.re.kr)
15. Hyeju Yoo, KOPRI, Republic of Korea (hjyoo@kopri.re.kr)
16. Jong Kuk Moon, KOPRI, Republic of Korea (jkmoon@kopri.re.kr)
17. Jee-Hoon Kim, KOPRI, Republic of Korea (jeehoonkim@kopri.re.kr)
18. Wuju Son, KOPRI, Republic of Korea (swj5753@kopri.re.kr)
19. Hyoung Sul La, KOPRI, Republic of Korea (hsla@kopri.re.kr)
20. Sanghoon Park, Pusan National University, Republic of Korea (mossinp@pusan.ac.kr)
21. Suk Hyun Haam, Neosea Tech, Republic of Korea (haam6481@gmail.com)

ANA13B Cruise Track (January 5 ~ February 18, 2023)



Survey components

- Water Column components
 - Water mass structure (water temperature, salinity, water velocity)
 - Pelagic ecosystems observations
(bacteria, phytoplankton, zooplankton, Ichthyoplankton, Fish)
 - Primary Production
 - Bio-geochemical measurements (nutrient, DOC, DIC, POC, DO)
 - Seawater dissolved gas (pCO₂, DMS)
 - Particulate organic matter (Carbohydrates, Proteins, Lipids, Transparent exopolymer Particles, Particulate organic carbon & nitrogen)
- Biological Acoustic
- Underway collection of meteorological and near-surface seawater
- Meteorological data from ship sensors
- CTD/rosette casts for hydrography and geochemistry
- Clean seawater sampling
 - Trace metal concentrations and chemical speciation
 - Rare earth elements concentrations and Nd isotopes
- LADCP (Lowered ADCP) for vertical profiles of water velocity at the CTD stations
- Ocean mooring systems recovered and re-deployed for measuring year-long water temperature, salinity, and water velocity

Chapter 1. Physical Oceanography

1.1. Hydrographic Survey

Tae-Wan Kim, Jaeill Yoo, Yeonggi Kim

Korea Polar Research Institute, Incheon, Republic of Korea

E-mail: twkim@kopri.re.kr; jiyoo@kopri.re.kr; ygkim@kopri.re.kr

1.1.1. Introduction

The Antarctic ice sheet is the largest ice mass on Earth, covering 98% of Antarctica, with an average thickness of about 2.16 km (Fretwell, P. et al., 2013). The ice shelf of the Antarctic coast, which the ice sheet flows toward the coast by gravity and floats on the sea, melts or calves due to the relatively warm seawater intrusion into the base of the ice shelf. The variability of ice shelf mass along the Antarctic coast showed significant regional differences (Paolo, F. S. et al., 2015), with the loss of ice shelf mainly in West Antarctica compared to East Antarctica. In particular, the fastest rate of decline in ice volume was recorded in the Amundsen and Bellingshausen Seas (Depoorter et al., 2013; Wåhlin et al., 2010). On the other hand, in East Antarctica and the Ross Sea, a distinct Antarctic Slope Front is formed on the continental slope under the influence of strong easterly winds, blocking the intrusion of warm and salty Circumpolar Deep Water onto the continental shelf (Thompson, A. F. et al., 2018). This study aims to identify the variability and mechanism of the Antarctic Slope Front and Currents based on observational data and evaluate the impact on the coastal environment caused by future climate change on these fronts.

1.1.2. Materials and methods

An intensive oceanographic survey was conducted from January 13 to February 8, 2023, using the IBRV Araon to understand the spatial and temporal variability of CDW on the eastern side of the Ross Sea and offshore (Figure 1.1.1). 31 CTD stations were visited to collect hydrographic data and water samples. At each hydrographic station, at least one CTD/Rosette

system cast with additional probes (e.g., dissolved oxygen, fluorometer, transmissometer, PAR, etc.) was conducted to measure the vertical profiles of temperature, salinity, and other related biochemical parameters. The serial numbers and calibration information of each sensor are given in Table 1.1.1. During the CTD upcasts, water samples were collected at several depths. For improved accuracy, the salinities of collected water samples were further analyzed by an Autosal salinometer (Guildline, 8400B). The measurement was performed when the temperature of water samples was stabilized to a laboratory temperature, usually within 48h after the collection. A lowered acoustic Doppler current profiler (LADCP, RDI, 300 kHz) was attached to the CTD frame to measure the complete profile of current velocities. The bin size was chosen as 5 m, and the number of bins was 20. During the cruise, the vessel-mounted ADCP (RDI, 38 kHz) was not operated due to the breaking of windows for protecting the ADCP's transducer.

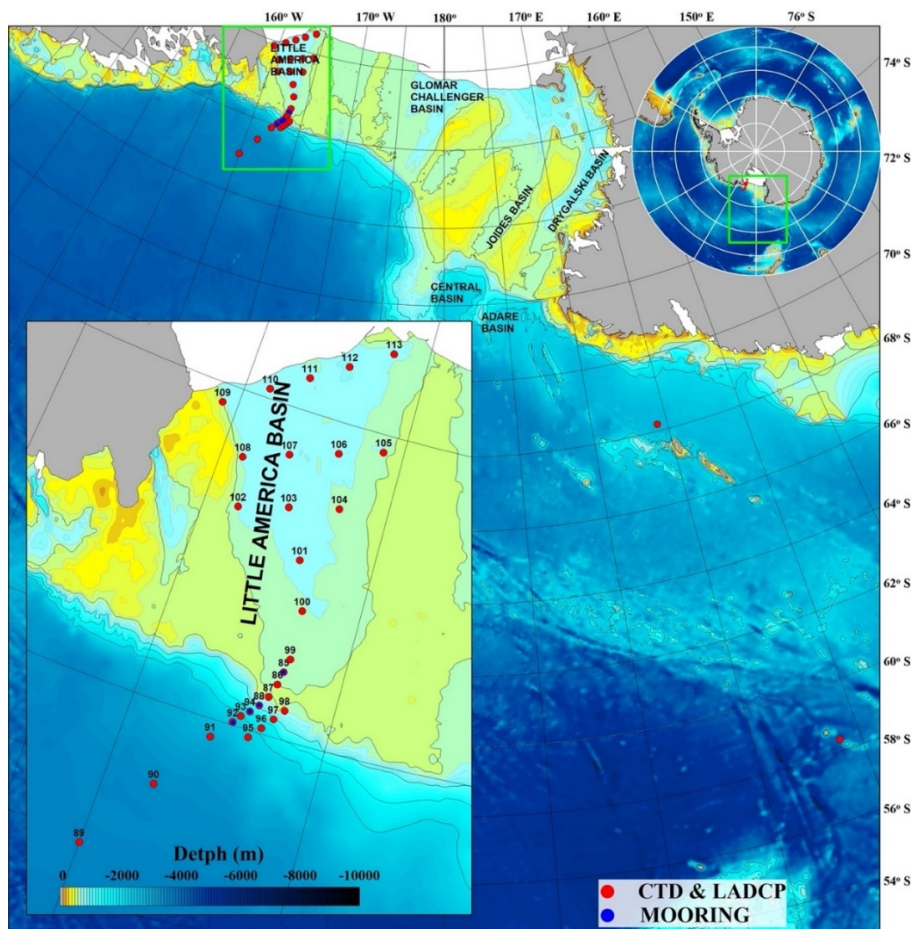


Figure 1.1.1. Map of study area. Red and blue dots denote the CTD and mooring stations visited during ANA13B expedition.

Table 1.1.1. Configuration of CTD (SBE 911plus) sensors used during ANA13B cruise

Sensor	S/N	Calibration date
Temperature 1	4995	Jun. 29, 2022
Temperature 2	5111	Jun. 30, 2022
Conductivity 1	4415	Jul. 08, 2022
Conductivity 2	4575	Jul. 08, 2022
Pressure	1241	Jul. 21, 2021
Oxygen	3434	Jun. 29, 2022
Fluorometer	FLRTD-1400	Jul. 06, 2022
(Changed sensor on Feb. 03 2023)	FLRTD-6763	Jul. 06, 2021
Transmissometer	CST-1227DR	Aug. 01, 2022
PAR	1023	Jun. 23 2015
Altimeter	51676	Nov. 15, 2010

1.1.3. Preliminary results

In February 2023, a total of 29 CTD stations were visited in Little America Basin to investigate the water mass composition and variety from the vertical profiles of temperature and salinity (Figure 1.1.1). The potential temperature-salinity diagram shows that the Little America Basin and the northern continental slope have three distinct water masses: (1) Circumpolar Deep Water (CDW); (2) Low Salinity Shelf Water (LSSW); (3) Ice Shelf Water (ISW); and (4) Antarctic Surface Water (AASW) (Fig. 1.1.2). LSSW generated the eastern Ross Sea in the process of expansion and contraction of polynya and distinguish with HSSW (High Salinity Shelf Water) by salinity. A mixture of LSSW and glacier meltwater forms the ISW. The water column in the stations (85, 86, 99-113) located in LAB's continental shelf composited by LSSW, ISW, WW (Winter Water), and ASSW, while the water column of offshore stations (90 and 91) occupied by CDW, WW, and ASSW. On the other hand, in stations, 87-89 and 92-98, located on the continental slope, the ASSW and CDW fill the upper and lower layers. A mixture of CDW, LSSW, ISW, and WW occupied showed a steep vertical variation in temperature and salinity profiles in the middle layer. In particular, relatively warm water of higher than -1.5 °C compared with shelf water was found in the lower station 85, located at the entrance of the trough beyond continental slopes. In 2023, the vertical temperature salinity's spatial

distribution was observed in higher resolution than the 2021 expedition from the front of the Ross ICE Shelf to the offshore along the LAB trough. The spatial distribution of the temperature and salinity in the continental slope and the LAB was similar to 2021. Isotherm and Isohaline are deepened as close to the continental slope from offshore. The vertical temperature and salinity profiles show a steep variation at shelf break due to the mixing with intruded CDW and outflows of shelf water. Additionally, the Isotherm and Isohaline were rapidly deepened at the entrance of the trough.

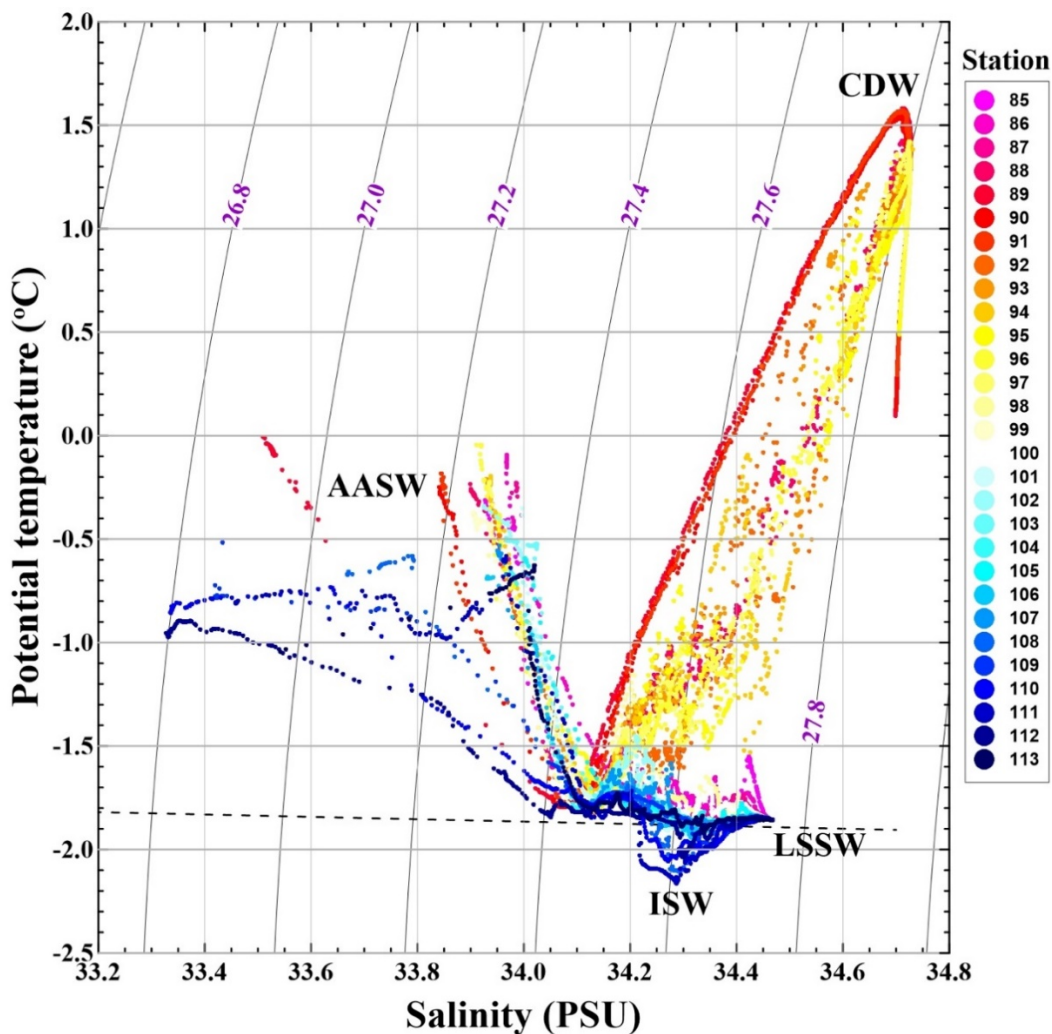


Figure 1.1.2. Potential temperature-salinity diagram at 29 stations in the Ross Sea. The color code indicates the stations, and the black dashed line indicates the freezing point temperature by salinity.

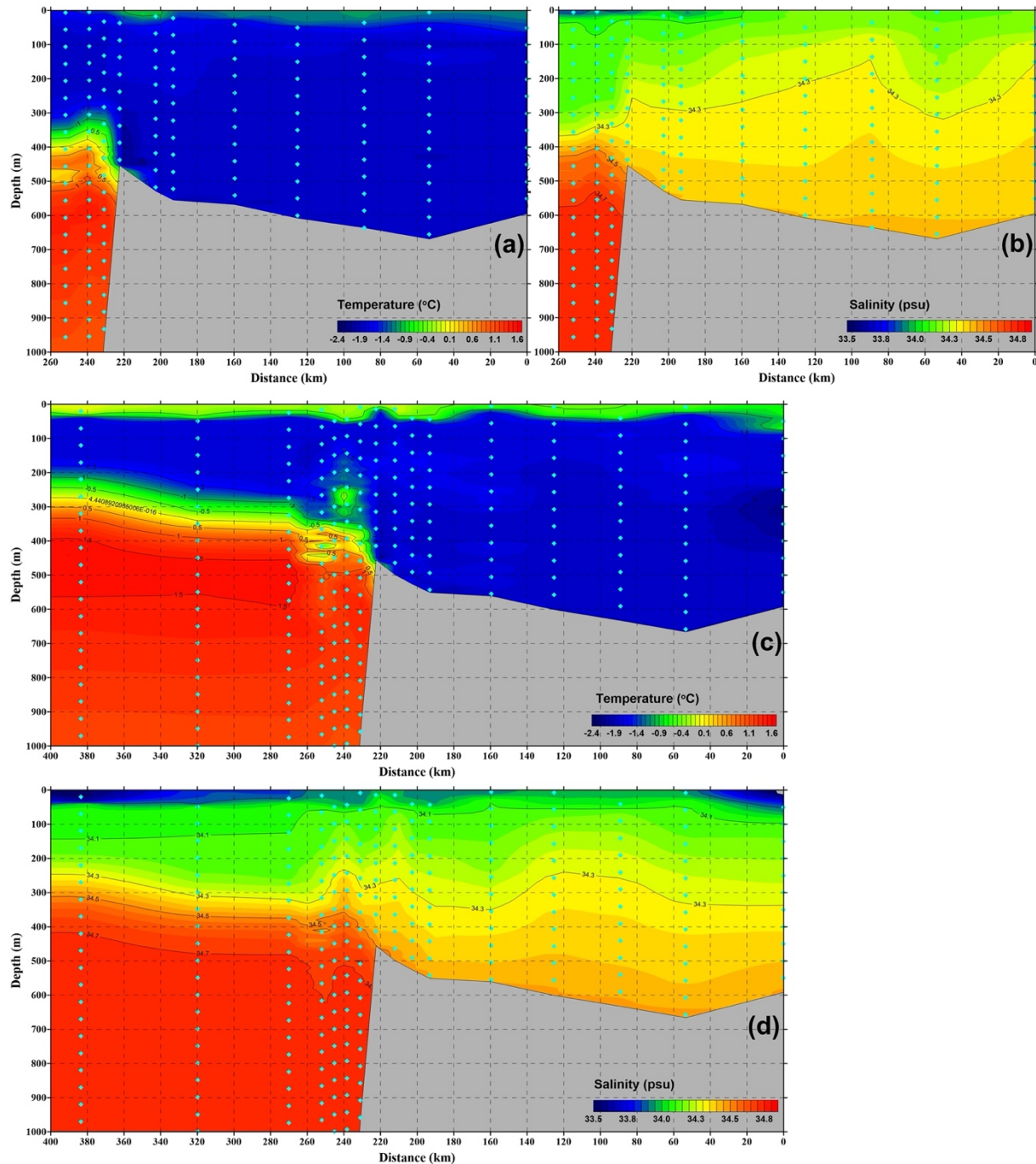


Figure 1.3. Vertical distribution of water mass properties along the Little America Basin through. (a) and (b) shows the spatial variation of temperature and salinity in the 2021 expedition. (c) and (d) shows the spatial variation of temperature and salinity in the 2023 expedition.

1.2. Ocean Moorings

Tae-Wan Kim, Jaeill Yoo, Yeonggi Kim

Korea Polar Research Institute, Incheon, Republic of Korea

E-mail: kcho@kopri.re.kr; jiyyoo@kopri.re.kr; ygkim@kopri.re.kr

It has been reported that the Antarctic Slope Front formed along the continental slope north of the Ross Sea blocks the intrusion of relatively warm Circumpolar Deep Water onto the continental shelf. However, previous in situ observations on the continental slope was limited to summer. Thus, such previous studies are insufficient to identify the temporal variability of the Antarctic Slope Front and Currents as the seasonal and inter-seasonal time scales. In this study, in order to observe the structure and variability of the Antarctic slope front and currents at the continental slope, A total of four long-term ocean moorings were installed at the north of the Little America Basin (KOP01, KOP02, KOP03) and entrance of the trough (KOP04) in December 2020. The KOP01 mooring, located in the northernmost part with a seabed depth of more than 2200m, consists of two RDI 150kHz ADCPs and eight MicroCat-CTDs and is designed to precisely observe the variability of temperature, salinity, and current in the 300-800 m depth. KOP02 mooring, located about 14km southwest of KOP01, consists of RDI 75 and 300kHz ADCP and eight MicroCat-CTDs and is designed to focus on the 300-700 m depth. A KOP03 mooring consisting of RDI 150 and 300kHz ADCP and eight MicroCat-CTDs was installed 7 km southwest of KOP02. The variability and spatial structure of the Antarctic Slope Front and Current are to be identified by maintaining three moorings that are spatially adjacent to the steep continental slope. Meanwhile, a mooring consisting of RDI 150 and 300 kHz ADCP and six MicroCat-CTDs was installed at the entrance of the trough beyond the continental slope to measure the variability of temperature, salinity, and current 250- 520 m depth. These moorings were recovered successfully in February 2023 and re-deployed at the same positions after data download and equipment inspection.

Recovery

On February 2nd, 2023, the first mooring position, KOP04, was visited to attempt mooring recovery. However, the signal could not be received from the Acoustic Release due to a communication problem between the Acoustic Release Deck Box (UTS9500) and the transducer. Thus, we used an extra Acoustic Release Deck Box and transducer and received wake-up and release signals from Acoustic Release. Afterward, we found a problem with the transducer during the communication test between Acoustic Release and Deck box on the board. At noon on February 2nd, Araon arrived at KOP03 and recovered the moorings safely. On February 4th, around 05:00 a.m., we arrived at KOP01, the deepest mooring station, and attempted to retrieve the mooring. After 20 minutes of arrival, all the mooring buoys floated on the sea surface. However, the rope connected to the top float was cut in the first attempt to recover the mooring due to rough sea conditions. And then, we can recover all the mooring equipment through several attempts to catch the buoys within 5 hours. At 02:00 on February 5th, an attempt was made to recover the KOP02 mooring, and all mooring equipment was successfully recovered in about 1.5 hours. We successfully recovered and measured the time series variation of temperature, salinity, and current over more than two years. Detailed information on the timetable for the recovery of mooring systems is given in Table 1.2.1.

Table 1.2.1. Time table for recovery of mooring systems in ANA13B

	KOP01	KOP02	KOP03	KOP04
Date	20230204	20230205	20230202	20230202
Latitude (S)	76°01.283'	76°06.759'	76°10.104'	76°24.794'
Longitude (W)	162°35.662'	162°55.371'	163°05.375'	163°27.389'
Arrival at station	05:43	02:44	12:36	00:38
First contact AR	05:48	02:50	12:38	01:00
Released	05:51	02:54	12:42	01:02
At surface	05:54	02:55	12:46	01:05
Recovered	11:08	03:57	13:48	01:59

Deployment

We immediately received all the data from the sequentially retrieved moorings, checked the data, and inspected the sensors, and it was confirmed that all sensors recorded stably. However, it takes more than 4 hours to download the two years of recorded data from ADCP. Thus it needs to improve the data download speed. On the other hand, when replacing the 150kHz ADCP battery of KOP01, the battery pack was partially damaged due to the overvoltage by battery pack connection failure. We repaired the damaged battery pack and used it for the 75kHz ADCP of the KOP02 mooring. The setups for MicroCats and ADCP were summarized in Table 1.2.2 (MicroCat) and Table 1.2.3 (ADCP). Detailed information on the deployment is given in Table 1.2.4. After the deployment, the triangulation was made to confirm the settlement status of the moorings and record the exact GPS location for future recovery. The design diagrams and triangulation results for individual moorings are given in Appendix II and III.

Table 1.2.2. Summary of setups for moored MicroCat

MicroCat	
	37-SM
Sample Interval	10 min
Deployment Endurance Calculator	1.5
Model Name	SBE 37 SM RS-232
Firmware	Firmware 3.0 and Higher
Pressure Sensor	Strain gauge
Sample Interval (sec)	600
Sampling Type	Autonomous
Transmit Real time	Not Enabled
Deployment Temperature	-
Deployment Pressure	-
Oxygen Time Constant (tau 20)	-
Battery Type	AA Lithium
Battery Capacity	8.8 Amp-Hours
Battery Endurance	5670 Days
	Batteries are not expected to last longer 2 years

Table 1.2.3. Summary of setups for moored ADCP

ADCP				
		75 kHz	150 kHz	300 kHz
Deployment Timing Setup	Duration(days)	800	800	800
	Ensemble interval	15 min	15 min	30 min
	Ping int.	2.5	2 sec	2 sec
Profiling Setup	Pings Per	20	20	20
	Number of Depth	60	44	37
	Depth Cell size	8	8	4
Environmental Setup	Transducer Depth	559 462(KOP04)	559(KOP01,03) 462(KOP04)	560(KOP02,03) 464(KOP04)
	Salinity (ppt)	35	35	35
	Transducer Variation	0	0	0
	Temperature	-1	-1	-1
Deployment Consequences	First cell range	15.03	12.21	6.17
	Last cell range	487.03	356.21	150.17
	Max range	478.58	355.47	105.61
	Standard deviation	3.27	1.59	0.79
	Ensemble size	1354	1034	894
	Storage required	99.17	75.73	32.74
	Power usage	1510.05	1568.77	401.68
	Battery usage	3.4	3.5	0.9
	Processing Bandwidth (BW)	Narrow BW	Narrow BW	Narrow BW
	Power	Low		

Table 1.2.4. Information about deployed moorings and positions

	KOP01	KOP02	KOP03	KOP04
<u>Anchor Release</u>				
Latitude	76°01.287'S	76°06.954'S	76°09.964'S	76°24.611'S
Longitude	162°34.940'W	162°55.634'W	163°05.899'W	163°27.586'W
Depth	2240 m	1560 m	995 m	536 m
Time (UTC)	20230204 22:45	20230205 15:05	20230202 22:26	20230202 08:42
<u>Triangulation</u>				
Sound velocity	1445	1445	1445	1445
Lat1	76°01.402'S	76°07.018'S	76°09.846'S	76°24.534'S
Lon1	162°34.671'W	162°56.278'W	163°05.952'W	163°27.990'W
Range1	1856 m	884 m	806 m	606 m
Lat2	76°01.160'S	76°06.649'S	76°10.149'S	76°24.574'S
Lon2	162°36.288'W	162°55.091'W	163°05.147'W	163°26.852'W
Range2	1876 m	862 m	817 m	595 m
Lat3	76°00.947'S	76°07.094'S	76°10.164'S	76°24.782'S
Lon3	162°34.588'W	162°54.340'W	163°06.700'W	163°27.567'W
Range3	1885 m	854 m	745 m	583 m
<u>Mooring Position (from 3-D)</u>				
Latitude	76°01.203'S	76°06.918'S	76°10.076'S	76°24.643'S
Longitude	162°35.169'W	162°55.147'W	163°06.122'W	163°27.448'W
2-D error	17 m	12 m	9m	1 m
Depth, triangulation	2222 m	1545 m	1006 m	534 m
<u>Acoustic release</u>				
SN	54245 (865)	57664 (865)	59823 (865)	57662 (865)
Address/Release	C/E	D/E	E/A	B/C
Rx/Tx (kHz)	9.50/12.0	10.50/12.0	9.25/12.0	9.50/12.0
SN	54246 (865)	59824(865)	72866 (865)	54244 (865)
Address/Release	B/D	A/F	H/G	D/F
Rx/Tx (kHz)	10.0/12.0	9.75/12.0	9.75/12.0	9.00/12.0
<u>Sensor Start Time</u>				
ADCP	20230204 20:00	20230205 13:00	20230202 22:00	20230202 08:00
MicroCat	20230204 18:00	20230205 13:00	20230202 22:00	20230202 08:00
Station Number	92	94	88	85

References

- Depoorter, M. A., Bamber, J. L., Griggs, J. A., Lenaerts, J. T., Ligtenberg, S. R., van den Broeke, M. R., et al. (2013) Calving fluxes and basal melt rates of Antarctic ice shelves. *Nature*, 502(7469), 89-92.
- Fretwell, P. et al. Bedmap2: improved ice bed, surface and thickness datasets for Antarctica. *Cryosphere* 7, 375–393 (2013).
- Paolo, F. S., Fricker, H. A., & Padman, L. (2015) Volume loss from Antarctic ice shelves is accelerating. *Science*, 348(6232), 327-331.
- Thompson, A. F., Stewart, A. L., Spence, P., & Heywood, K. J. (2018). The Antarctic Slope Current in a changing climate. *Reviews of Geophysics*, 56(4), 741-770.
- Wåhlin, A. K., Yuan, X., Björk, G., & Nohr, C. (2010) Inflow of warm circumpolar deep water in the central Amundsen shelf. *Journal of Physical Oceanography*, 40(6), 1427-1434.

Appendix 1.1. ANA13B cruise log spreadsheet

Ship: R/V Araon		Cruise: ANA13 . B										2023.01.12 ~ 2023.02.08					
STN No.	Gear	Cast No.	Date	Cast start	Cast end	Latitude	Longitude	Water depth	Cast depth	Wind speed	Wind direction	Ship speed	Heading	Remarks	Device Driver		
			UTC	UTC	UTC	(m)	(m)	m/s	(°)	knot	(°)						
CTD: CTD Casting, 150NET: 150 Net, BONGO: Bongo Net, ARGO: Argo Float Deploy, TM: Trace Metal, SECCHI: Secchi disk, PHY: Phytoplankton Net, MOC: Mocness Net, MD: Mooring Deploy, FTN: Frame Trawl Net, XCTD: xCTD																	
EK80CAL: EK80 Calibration, FT: Fish Trap, MR: Mooring Recovery, BOX: Box Corer																	
Argo1	ARGO	1	2023-01-12	01:00	01:01	49°59.992' S	153°04.973' E					1.92	134.2	Argo Float Deploy	J. Magnusson		
	CTD	1	2023-01-13	18:31	19:41	58°20.001' S	160°59.265' E	4290	1500	11.08	291	1.79	306.3	CTD Casting	Y. Kim		
	150NET	1		19:41	19:41	58°20.001' S	160°59.264' E	4290	200			0.75	305.1	150 Net	J. Kim		
	BONGO	1		19:41	19:41	58°20.001' S	160°59.264' E	4290	200			0.75	305.1	Bongo Net	J. Kim		
	Argo2	ARGO	1	20:47	20:49	58°19.669' S	160°58.631' E					2.12	295.1	Argo Float Deploy	J. Magnusson		
Argo3	ARGO	1	2023-01-14	04:03	04:04	59°59.963' S	160°59.244' E					3.26	152.3	Argo Float Deploy	J. Magnusson		
Argo4	ARGO	1	2023-01-14	12:30	12:30	62°00.021' S	160°59.318' E					4.70	181.3	Argo Float Deploy	J. Magnusson		
Argo5	ARGO	1	2023-01-14	21:05	00:00(+1)	63°59.911' S	160°59.256' E					2.06	321.4	Argo Float Deploy	J. Magnusson		
2	CTD	1	2023-01-15	20:49	21:57	68°10.786' S	165°40.086' E	2600	1500	5.50	259	0.01	160.2	CTD Casting	Y. Kim		
	TM	1		22:20	23:32	68°11.091' S	165°38.235' E	2600	1500			0.15	93.3	Trace Metal	TJ. Kim		
	SECCHI	1		23:33	23:33	68°11.121' S	165°38.202' E	2600				0.10	15	Secchi disk	S. Park		
	PHY	1		23:43	23:50	68°11.120' S	165°38.204' E	2600	100			0.10	15.6	Phytoplankton Net	J. Kim		
	150NET	1		23:57	00:08(+1)	68°11.120' S	165°38.203' E	2600	200			0.18	15.1	150 Net	J. Kim		
	BONGO	1	2023-01-16	00:14	00:25	68°11.119' S	165°38.203' E	2600	200			10.15	103	Bongo Net	J. Kim		
Argo6	ARGO	1	2023-01-26	00:15	00:15	74°54.074' S	175°29.649' E					2.40	212.8	Argo Float Deploy	J. Magnusson		
Argo7	ARGO	1		10:17	10:17	74°54.051' S	179°59.720' E					2.22	233.8	Argo Float Deploy	J. Magnusson		
Argo8	ARGO	1		14:00	14:00	76°05.991' S	175°00.359' W					2.35	260.9	Argo Float Deploy	J. Magnusson		
Argo9	ARGO	1		07:30	07:34	77°47.994' S	169°59.954' W					0.36	102.4	Argo Float Deploy	J. Magnusson		
85	MR	1	2023-02-02	01:02	02:01	76°24.791' S	163°27.349' W							Mooring Recovery	PO		
	CTD	1		02:26	02:56	76°24.630' S	163°27.487' W	539	525	7.50	331	0.40	284	CTD Casting	TW. Kim		
	TM	1		03:10	03:46	76°24.630' S	163°27.487' W	539	505			0.40	284	Trace Metal	TJ. Kim		
	CTD	2		04:00	04:14	76°24.628' S	163°27.493' W	539	100			0.27	331.3	CTD Casting	TW. Kim		
	PHY	1		04:26	04:36	76°24.630' S	163°27.497' W	539	100			0.53	310	Phytoplankton Net	J. Kim		
	150NET	1		04:43	04:56	76°24.630' S	163°27.499' W	539	200			0.04	309.9	150 Net	J. Kim		
	BONGO	1		05:07	05:19	76°24.629' S	163°27.500' W	539	200			0.27	310	Bongo Net	J. Kim		
86	MD	1		08:10	08:42	76°24.643' S	163°26.263' W							Mooring Deploy	PO		
	BOX	1		09:22	09:54	76°24.783' S	163°27.665' W	540	540			1.43	0.3	Box Corer	S. Ha		
	CTD	1	2023-02-02	06:07	06:30	76°19.549' S	163°23.577' W	505	498	6.50	304	0.06	319.6	CTD Casting	TW. Kim		
	CTD	1	2023-02-02	11:27	12:02	76°14.070' S	163°15.976' W	466	450	4.80	283	1.66	0.6	CTD Casting	TW. Kim		
	MR	1	2023-02-02	12:48	13:48	76°10.089' S	163°05.337' W							Mooring Recovery	PO		
88	CTD	1		14:19	15:04	76°10.053' S	163°05.955' W	981	965	9.00	344	0.82	93.3	CTD Casting	TW. Kim		
	TM	1		15:20	16:19	76°10.044' S	163°05.958' W	981	935			0.38	310.8	Trace Metal	TJ. Kim		
	CTD	2		16:36	16:51	76°10.051' S	163°05.922' W	981	100	7.32	339	0.65	143.4	CTD Casting	Y. Kim		
	PHY	1		17:02	17:14	76°10.039' S	163°05.944' W	981	100			0.10	330.9	Phytoplankton Net	J. Kim		
	150NET	1		17:23	17:36	76°10.038' S	163°05.947' W	981	200			0.33	330.3	150 Net	J. Kim		
89	BONGO	1		17:48	18:03	76°10.039' S	163°05.950' W	981	200			0.23	330.5	Bongo Net	J. Kim		
	BONGO	2		18:12	18:20	76°10.039' S	163°05.947' W	981	70			0.18	330.1	Bongo Net	J. Kim		
	BONGO	3		18:31	18:35	76°10.039' S	163°05.947' W	981	25			0.80	329.8	Bongo Net	J. Kim		
	BONGO	4		18:43	19:14	76°10.048' S	163°05.920' W	981	500			0.46	154.5	Bongo Net	J. Kim		
	MD	1		21:44	22:25	76°10.076' S	163°06.122' W							Mooring Deploy	PO		
89	SECCHI	1	2023-02-03	06:15	06:16	74°60.000' S	160°00.032' W					0.75	26.1	Secchi disk	S. Park		

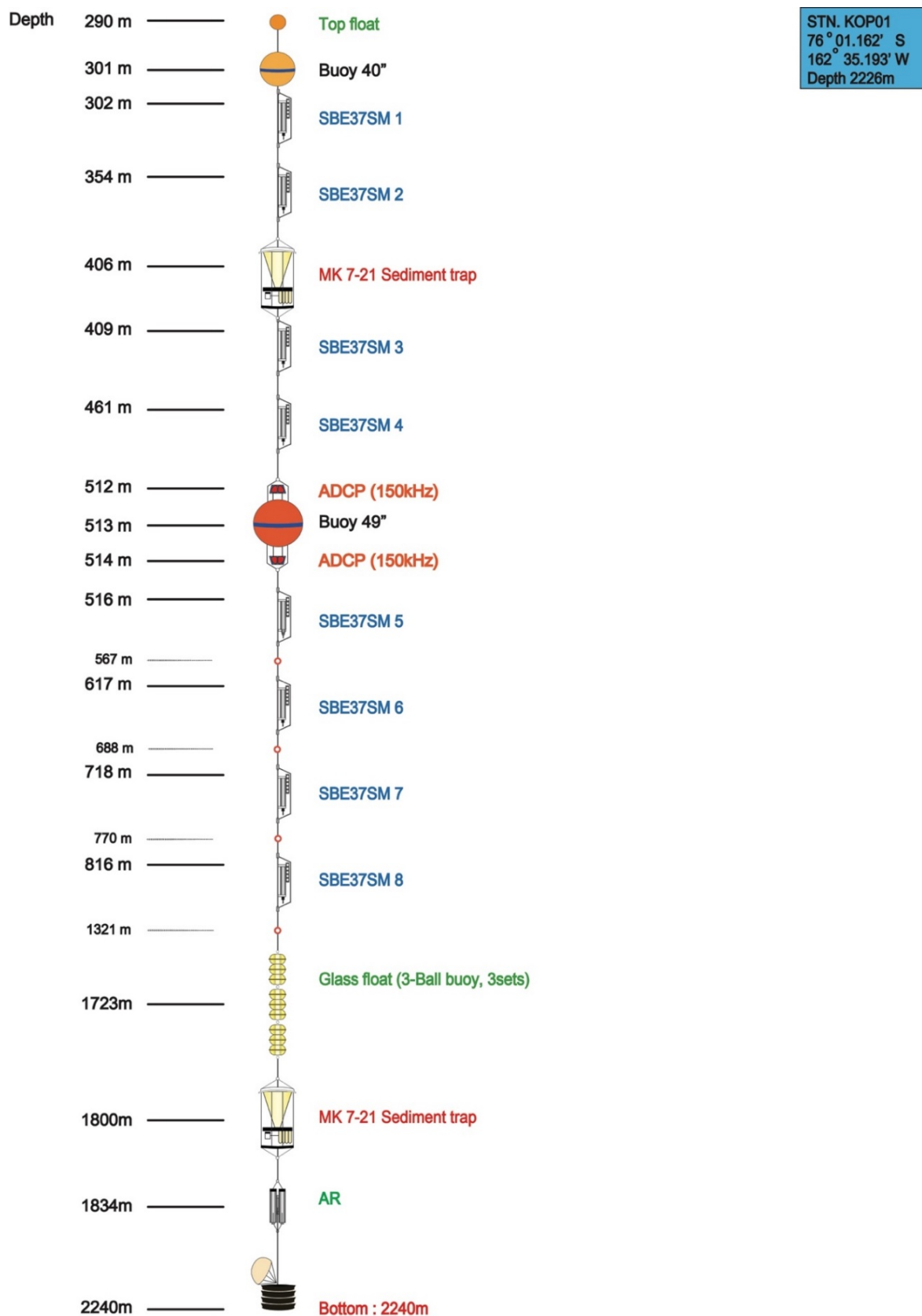
STN No.	Gear	Cast No.	Date	Cast start	Cast end	Latitude	Longitude	Water depth	Cast depth	Wind speed	Wind direction	Ship speed	Heading	Remarks	Device Driver
90	CTD	1		06:20	08:42	74°59.998' S	159°60.000' W	3588	3570	10.00	305	0.25	44.3	CTD Casting	TW. Kim
	PHY	1		08:50	08:59	74°59.997' S	160°00.011' W	3588	100			0.06	4.7	Phytoplankton Net	J. Kim
	150NET	1		09:04	09:19	74°59.997' S	160°00.013' W	3588	200			0.50	5.4	150 Net	J. Kim
	BONGO	1		09:24	09:38	74°59.997' S	160°00.012' W	3588	200			0.20	4.8	Bongo Net	J. Kim
	CTD	2		09:53	10:09	74°59.997' S	160°00.006' W	3588	100			0.54	20	CTD Casting	Y. Kim
	SECCHI	1	2023-02-03	13:14	13:14	75°30.007' S	161°12.706' W					1.53	39.7	Secchi disk	S. Park
91	CTD	1		13:19	15:31	75°30.002' S	161°12.715' W	3348	3328	8.42	22	0.54	39.2	CTD Casting	Y. Kim
	TM	1		15:47	18:47	75°30.001' S	161°12.719' W	3348	3270			0.20	41.1	Trace Metal	TJ. Kim
	CTD	2		19:03	19:20	75°30.001' S	161°12.706' W	3348	100	6.34	19	0.37	44.9	CTD Casting	J. Yoo
	PHY	1		19:33	19:41	75°30.001' S	161°12.711' W	3348	100			0.37	30.1	Phytoplankton Net	J. Kim
	150NET	1		19:48	20:02	75°30.001' S	161°12.713' W	3348	200			0.48	29.8	150 Net	J. Kim
	BONGO	1		20:09	20:22	75°30.001' S	161°12.714' W	3348	200			0.18	30.3	Bongo Net	J. Kim
92	SECCHI	1	2023-02-03	22:50	22:50	75°53.491' S	162°09.620' W					0.46	132	Secchi disk	S. Park
	CTD	1		22:55	00:50(+1)	75°53.490' S	162°09.663' W	2842	2823	6.50	269	0.50	90.7	CTD Casting	TW. Kim
	TM	1	2023-02-04	01:01	03:09	75°53.489' S	162°09.668' W	2842	2770			0.38	59.8	Trace Metal	TJ. Kim
	CTD	2		03:22	03:39	75°53.492' S	162°09.663' W	2842	100	4.19	38	0.59	84.4	CTD Casting	Y. Kim
	PHY	1		03:47	03:58	75°53.491' S	162°09.666' W	2842	100			0.48	78.1	Phytoplankton Net	J. Kim
	150NET	1		04:04	04:18	75°53.492' S	162°09.665' W	2842	200			0.29	85.6	150 Net	J. Kim
93	BONGO	1		04:27	04:41	75°53.492' S	162°09.661' W	2842	200			0.30	84.7	Bongo Net	J. Kim
	MR	1	2023-02-04	05:57	11:13	76°01.283' S	162°35.658' W							Mooring Recovery	PO
	CTD	1		12:57	14:38	76°01.161' S	162°35.195' W	2256	2240	8.60	136	0.23	123.4	CTD Casting	TW. Kim
	SECCHI	1		14:34	14:35	76°01.162' S	162°35.195' W					0.61	122.4	Secchi disk	S. Park
	TM	1		14:52	16:21	76°01.163' S	162°35.203' W	2256	2180			0.36	123.5	Trace Metal	TJ. Kim
	CTD	2		16:34	16:51	76°01.160' S	162°35.247' W	2256	100	5.40	187	0.19	313.9	CTD Casting	TW. Kim
94	PHY	1		17:05	17:15	76°01.158' S	162°35.238' W	2256	100			0.68	335.2	Phytoplankton Net	J. Kim
	150NET	1		17:21	17:36	76°01.171' S	162°35.212' W	2256	200			0.27	133.1	150 Net	J. Kim
	BONGO	1		17:43	17:58	76°01.203' S	162°35.212' W	2256	200			0.27	133.1	Bongo Net	J. Kim
	MD	1		21:07	22:45	76°01.203' S	162°35.169' W							Mooring Deploy	PO
	BOX	1		23:41	01:15(+1)	76°00.955' S	162°34.527' W	2256	2256			0.61	160.5	Box Corer	S. Ha
	CTD	1	2023-02-04	18:34	19:47	76°04.273' S	162°44.173' W	1948	1930	4.80	263	0.56	169	CTD Casting	TW. Kim
95	MR	1	2023-02-05	03:05	03:57	76°06.883' S	162°55.409' W							Mooring Recovery	PO
	CTD	1		04:16	05:24	76°06.922' S	162°55.275' W	1562	1542	7.10	342	0.50	189.6	CTD Casting	TW. Kim
	CTD	1	2023-02-05	06:30	07:54	75°57.479' S	163°04.063' W	2278	2262	6.06	140	0.09	200.1	CTD Casting	J. Yoo
	CTD	1	2023-02-05	08:38	09:44	76°02.209' S	163°19.035' W	1817	1800	4.96	168	0.26	219.4	CTD Casting	Y. Kim
	CTD	1	2023-02-05	10:25	11:08	76°06.575' S	163°32.705' W	1107	1092	4.89	223	1.11	240.2	CTD Casting	J. Yoo
	CTD	1	2023-02-05	11:46	12:07	76°10.850' S	163°45.290' W	453	440	3.90	34	12.05	252.9	CTD Casting	TW. Kim
96	MD	1	2023-02-05	14:21	15:05	76°06.918' S	162°55.147' W							Mooring Deploy	PO
	FTN	1	2023-02-05	17:25	17:44	76°24.664' S	163°23.232' W					12.75	196.9	Frame Trawl Net	W. Son
	CTD	1	2023-02-05	18:34	19:06	76°29.840' S	163°18.315' W	562	550	7.20	139	12.68	159.8	CTD Casting	TW. Kim
	SECCHI	1	2023-02-05	20:46	20:47	76°48.419' S	163°27.830' W					12.91	160.1	Secchi disk	S. Park
	CTD	1		20:54	21:33	76°48.419' S	163°27.830' W	572	560	3.90	178	12.91	160.1	CTD Casting	TW. Kim
	TM	1		21:40	22:30	76°48.419' S	163°27.830' W	572	540			12.91	160.1	Trace Metal	TJ. Kim
97	CTD	2		22:44	23:01	76°48.409' S	163°27.832' W	573	100	5.50	333	12.91	160.1	CTD Casting	TW. Kim
	PHY	1		23:10	23:21	76°48.409' S	163°27.832' W	573	100			12.91	160.1	Phytoplankton Net	J. Kim
	150NET	1		23:26	23:40	76°48.409' S	163°27.832' W	573	200			12.91	160.1	150 Net	J. Kim
	BONGO	1		23:44	00:00(+1)	76°48.409' S	163°27.832' W	573	200			12.91	160.1	Bongo Net	J. Kim
	CTD	1	2023-02-06	01:46	02:23	77°06.310' S	163°00.452' W	616	600	9.06	304	0.17	0	CTD Casting	Y. Kim
	CTD	1	2023-02-06	01:46	02:23	77°06.310' S	163°00.452' W								

STN No.	Gear	Cast No.	Date	Cast start	Cast end	Latitude	Longitude	Water depth	Cast depth	Wind speed	Wind direction	Ship speed	Heading	Remarks	Device Driver
15ONET	TM	1		02:38	03:05	77°06.312' S	163°00.470' W	616	590			0.24	300.2	Trace Metal	T.J. Kim
	CTD	2		03:20	03:33	77°06.311' S	163°00.472' W	616	100			0.25	299.8	CTD Casting	Y. Kim
	PHY	1		03:43	03:52	77°06.311' S	163°00.470' W	616	100			0.04	300.1	Phytoplankton Net	J. Kim
	BONGO	1		03:59	04:12	77°06.311' S	163°00.470' W	616	200			0.04	300.1	150 Net	J. Kim
	BONGO	1		04:18	04:31	77°06.312' S	163°00.470' W	616	200			0.13	300.1	Bongo Net	J. Kim
102	CTD	1	2023-02-06	07:12	07:47	77°18.221' S	160°56.886' W	571	562	3.86	343	0.42	350.2	CTD Casting	J. Yoo
103	SECCHI	1	2023-02-06	09:27	09:28	77°23.871' S	162°17.285' W	645	632	8.48	250	0.53	278.8	Secchi disk	S. Park
Argo10	CTD	1		09:34	10:12	77°23.865' S	162°17.335' W	645	610			0.25	289.4	CTD Casting	J. Yoo
	TM	1		10:29	11:06	77°23.863' S	162°17.333' W	645	100			0.19	309.8	Trace Metal	T.J. Kim
	CTD	2		11:18	11:32	77°23.864' S	162°17.330' W	645	100	8.34	237	0.37	300.7	CTD Casting	J. Yoo
	PHY	1		11:42	11:49	77°23.864' S	162°17.330' W	645	100			0.27	300	Phytoplankton Net	J. Kim
	15ONET	1		11:56	12:08	77°23.863' S	162°17.331' W	645	200			0.06	299.7	150 Net	J. Kim
	BONGO	1		12:16	12:31	77°23.863' S	162°17.330' W	645	200			0.41	299.9	Bongo Net	J. Kim
ARGO	ARGO	1		12:36	12:37	77°23.883' S	162°17.623' W					2.43	256	Argo Float Deploy	J. Magnusson
	FTN	1		13:36	14:11	77°26.285' S	162°55.630' W					0.32	70.1	Frame Trawl Net	W. Son
104	CTD	1	2023-02-06	15:29	16:06	77°28.786' S	163°38.784' W	579	569	10.48	233	0.91	253	CTD Casting	J. Yoo
105	CTD	1	2023-02-06	18:36	19:06	77°53.568' S	164°24.769' W	522	523	12.75	239	0.28	287.6	CTD Casting	Y. Kim
106	CTD	1	2023-02-06	21:00	21:34	77°48.459' S	163°11.402' W	618	601	8.06	282	0.45	30.6	CTD Casting	Y. Kim
107	CTD	1	2023-02-06	23:18	23:53	77°42.632' S	161°51.181' W	677	665	6.00	254	0.12	282.5	CTD Casting	Y. Kim
15ONET	TM	1	2023-02-07	00:07	00:50	77°42.633' S	161°51.184' W	677	645			0.50	269.3	Trace Metal	T.J. Kim
	CTD	2		00:59	01:18	77°42.632' S	161°51.181' W	677	100			0.40	268.9	CTD Casting	Y. Kim
	PHY	1		01:25	01:36	77°42.632' S	161°51.184' W	677	100			1.33	269.4	Phytoplankton Net	J. Kim
	BONGO	1		01:40	01:53	77°42.632' S	161°51.183' W	677	200			0.09	269	150 Net	J. Kim
	BONGO	1		01:58	02:10	77°42.632' S	161°51.182' W	677	200			0.66	269.2	Bongo Net	J. Kim
108	BONGO	2		02:14	02:28	77°42.632' S	161°51.183' W	677	200			0.43	270.3	Bongo Net	J. Kim
	CTD	1	2023-02-07	04:08	04:41	77°36.286' S	160°36.971' W	595	584	5.46	156	0.32	57.9	CTD Casting	J. Yoo
109	CTD	1	2023-02-07	06:42	07:11	77°52.933' S	159°32.494' W	459	439	7.37	38	0.56	55.2	CTD Casting	J. Yoo
15ONET	TM	1		07:29	08:03	77°52.933' S	159°32.495' W	459	420			0.60	46.4	Trace Metal	T.J. Kim
	CTD	2		08:22	08:35	77°52.937' S	159°32.498' W	459	100	9.38	49	0.17	57.2	CTD Casting	J. Yoo
	PHY	1		08:47	08:56	77°52.936' S	159°32.500' W	459	100			0.32	47.7	Phytoplankton Net	J. Kim
	BONGO	1		09:02	09:15	77°52.936' S	159°32.501' W	459	200			0.35	47.3	150 Net	J. Kim
	BONGO	1		09:22	09:34	77°52.936' S	159°32.501' W	459	200			0.30	46.6	Bongo Net	J. Kim
110	CTD	3		11:50	00:00(+1)	78°03.502' S	160°42.959' W					0.51	217.5	CTD Casting	J. Yoo
	CTD	1	2023-02-07	11:12	00:00(+1)	78°03.499' S	160°42.975' W	650	640	7.14	111	0.42	217.2	CTD Casting	J. Yoo
	SECCHI	1	2023-02-07	13:09	13:10	78°11.992' S	161°43.353' W					0.73	54.9	Secchi disk	S. Park
111	CTD	1		13:15	13:50	78°11.990' S	161°43.367' W	603	592	5.65	92	0.12	80.4	CTD Casting	J. Yoo
	TM	1		14:05	14:37	78°11.990' S	161°43.369' W	603	570			0.24	80.4	Trace Metal	T.J. Kim
	CTD	2		14:51	15:04	78°11.990' S	161°43.366' W	603	100	7.59	107	0.22	80	CTD Casting	J. Yoo
	PHY	1		15:12	15:23	78°11.990' S	161°43.368' W	603	100			0.22	79.7	Phytoplankton Net	J. Kim
	15ONET	1		15:29	15:42	78°11.990' S	161°43.369' W	603	200			0.26	80	150 Net	J. Kim
112	BONGO	1		15:48	16:03	78°11.990' S	161°43.369' W	603	200			0.24	80.1	Bongo Net	J. Kim
	CTD	1	2023-02-07	17:30	18:07	78°20.434' S	162°45.038' W	700	690	7.47	98	0.06	97.7	CTD Casting	Y. Kim
113	FTN	1		19:10	19:21	78°25.419' S	163°19.469' W					0.24	58.2	Frame Trawl Net	W. Son
	SECCHI	1	2023-02-07	20:15	20:16	78°29.737' S	163°55.379' W					0.23	27.2	Secchi disk	S. Park
	CTD	1		20:23	20:58	78°29.737' S	163°55.377' W	642	630	8.03	113	0.48	34.4	CTD Casting	Y. Kim
	TM	1		21:15	21:53	78°29.743' S	163°55.360' W	642	630			0.27	100	Trace Metal	T.J. Kim
114	CTD	2		22:14	22:31	78°29.748' S	163°55.399' W	642	100	9.10	110	0.10	120.1	CTD Casting	Y. Kim

STN No.	Gear	Cast No.	Date	Cast start	Cast end	Latitude	Longitude	Water depth (m)	Cast depth (m)	Wind speed m/s	Wind direction (°)	Ship speed knot	Heading (°)	Remarks	Device Driver
PHY	1			22:40	22:50	78°29.743' S	163°55.398' W	642	100	0.14	75	Phytoplankton Net		J. Kim	
150NET	1			22:50	23:08	78°29.743' S	163°55.398' W	642	200	0.14	75	150 Net		J. Kim	
BONGO	1			23:13	23:26	78°29.743' S	163°55.398' W	642	200	0.14	75	Bongo Net		J. Kim	
BONGO	2			23:32	23:37	78°29.743' S	163°55.397' W	642	60	0.24	74.6	Bongo Net		J. Kim	
BONGO	3	2023-02-08		00:10	00:10	78°29.743' S	163°55.398' W	642	500	0.08	75.1	Bongo Net		J. Kim	

Appendix 1.2. All design diagrams of moorings

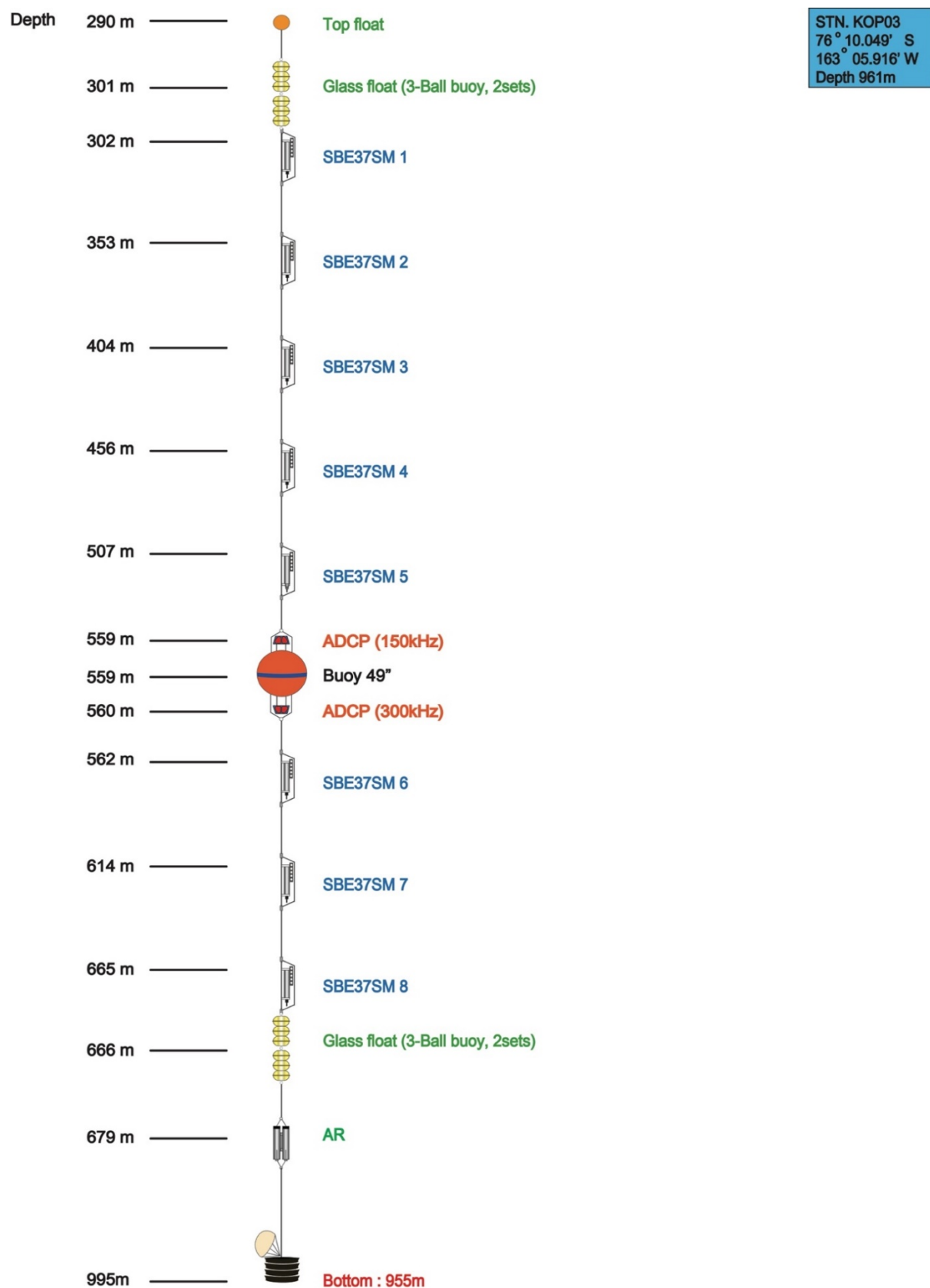
AP2 1 mooring design for KOP01 (recovery)



AP2 2 mooring design for KOP02 (recovery)



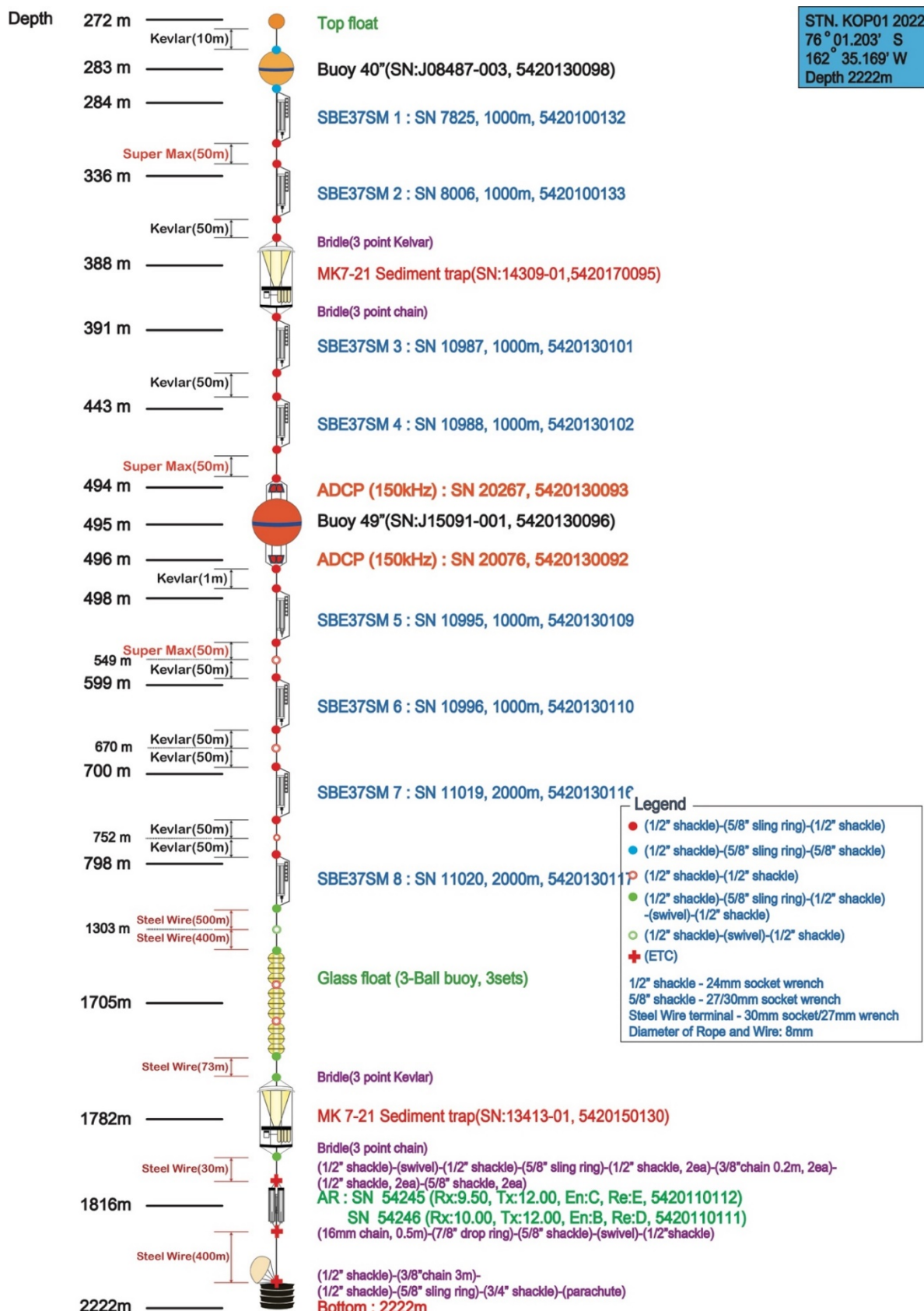
AP2 3 mooring design for KOP03 (recovery)



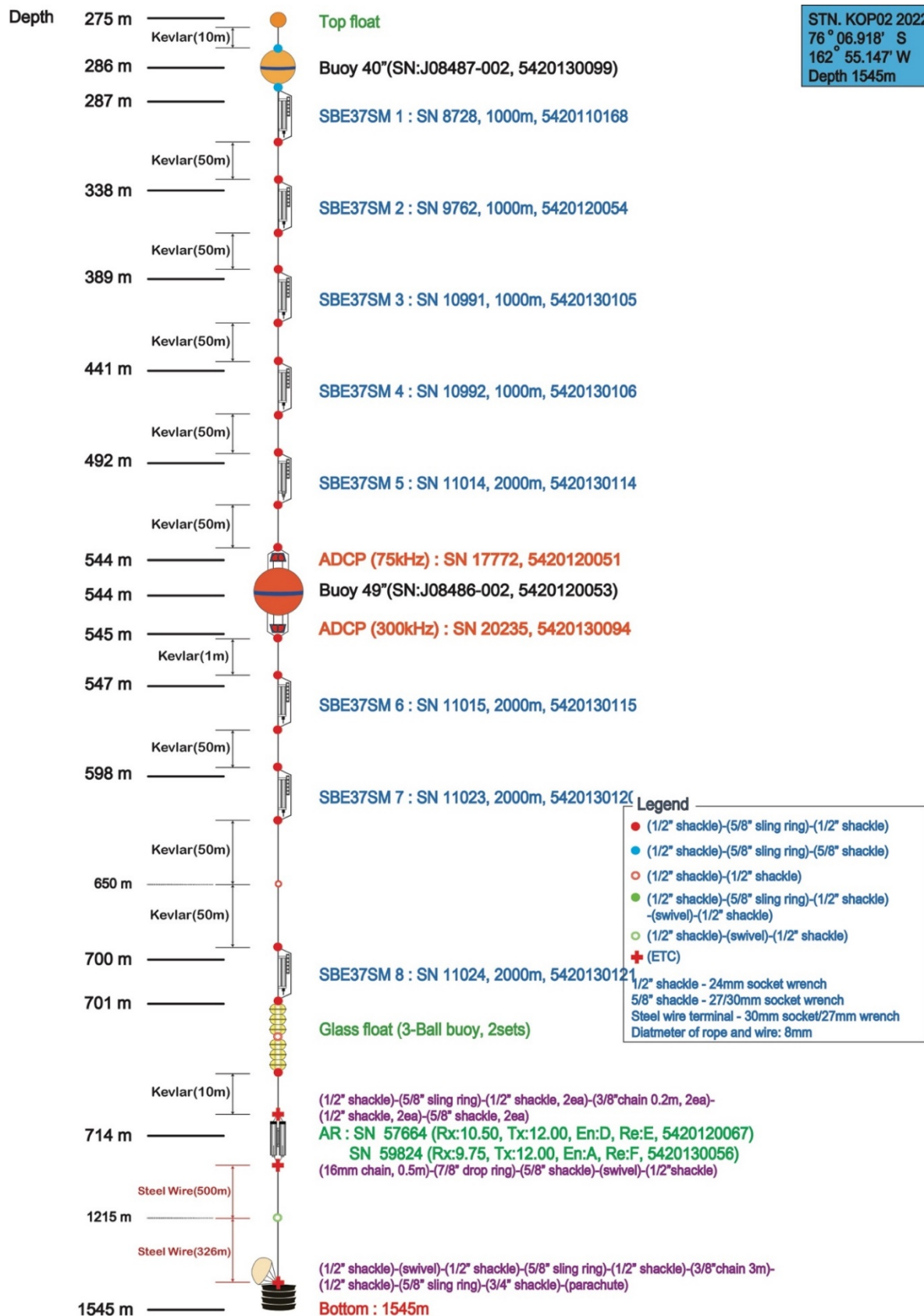
AP2 4 mooring design for KOP04 (recovery)



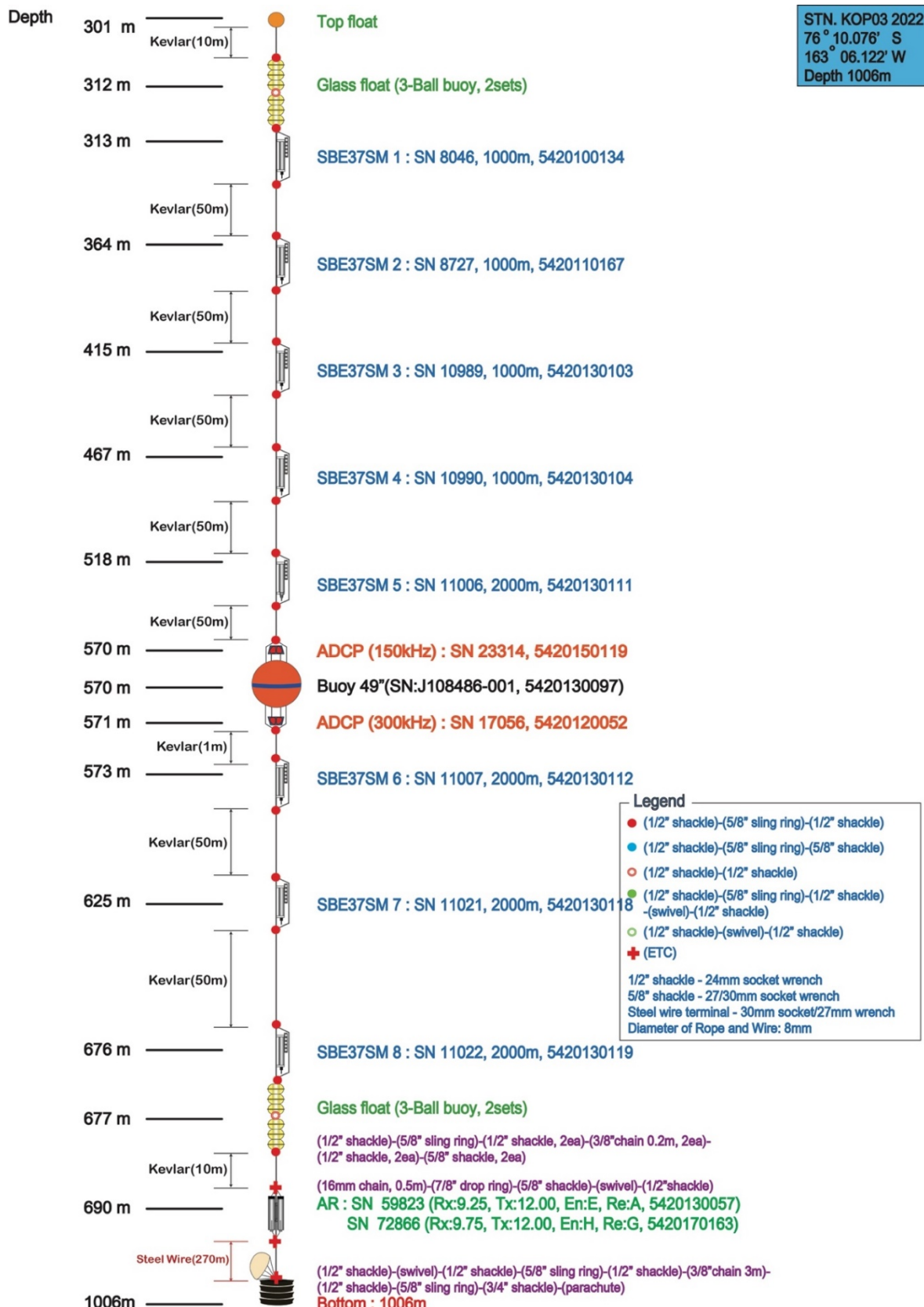
AP2 5 mooring design for KOP01 (deployment)



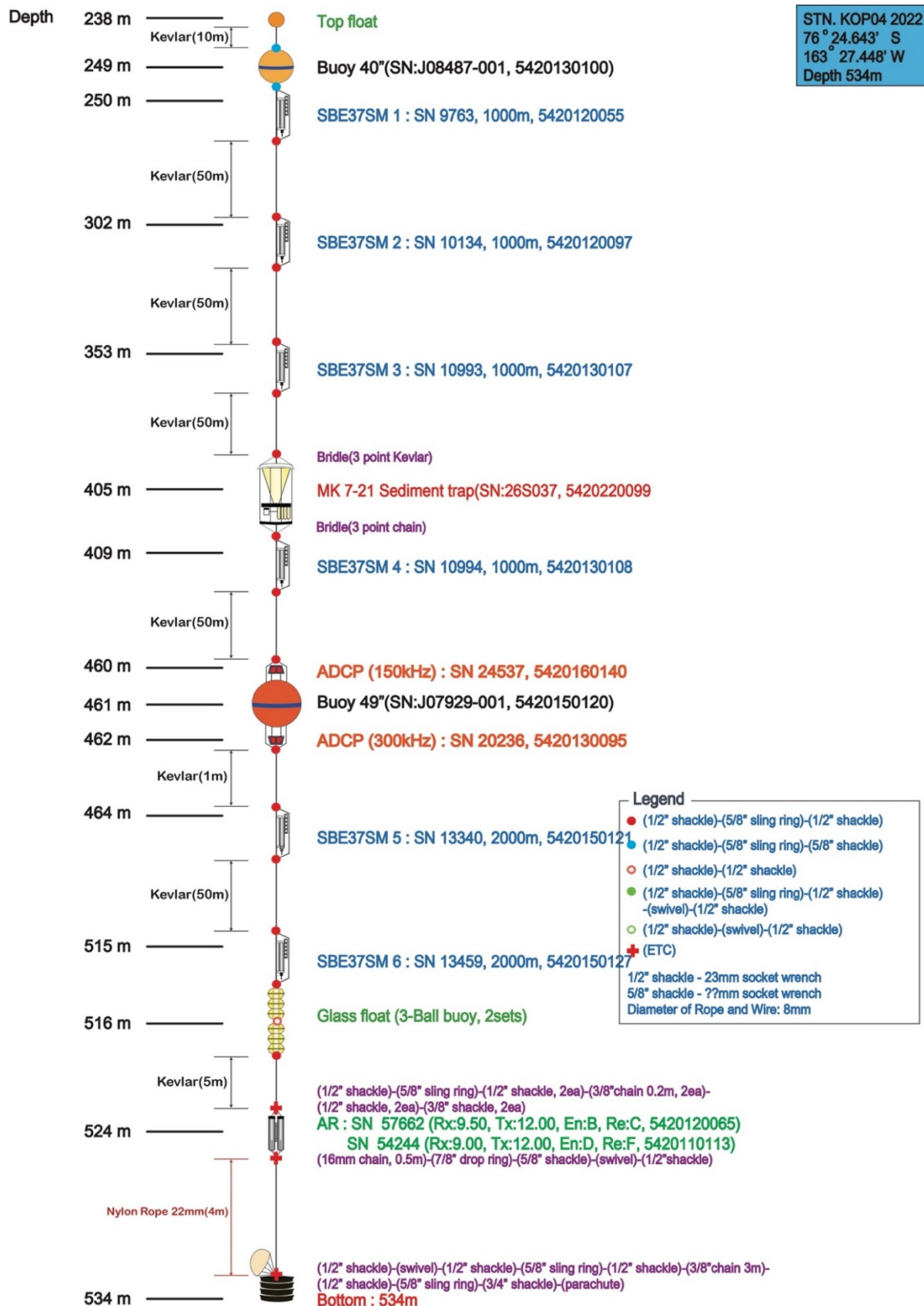
AP2 6 mooring design for KOP02 (deployment)



AP2 7 mooring design for KOP03 (deployment)

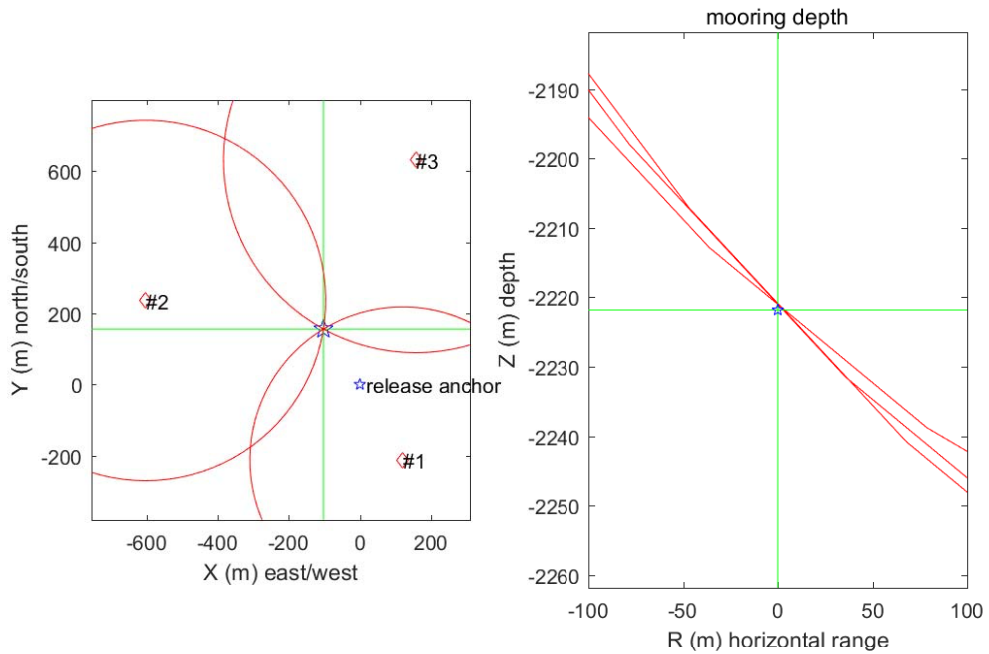


AP2 8 mooring design for KOP04 (deployment)



Appendix 1.3. Triangulation results

AP3 1 triangulation result for KOP01



anchor release position: 76°S 1.287' 162°W 34.940'; depth: 2240 m

3D mooring position: 76°S 1.203' 162°W 35.169'

drift: 186 m; direction: 327°

mooring depth: 2222 m; slant error: 0 m

2D mooring position: 76°S 1.197' 162°W 35.172'

drift: 198 m; direction: 328°

horizontal error: 17 m

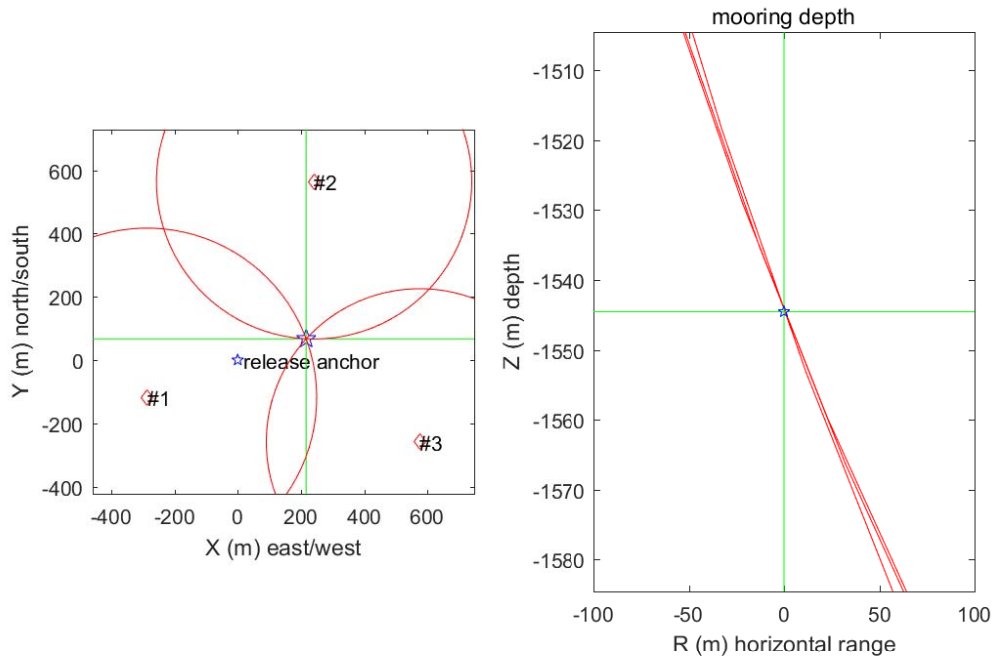
sound speed at site: 1445 m/s

#1 pos: 76°S 1.402' 162°W 34.671' range: 1856 m range soundspeed 1500

#2 pos: 76°S 1.160' 162°W 36.288' range: 1876 m range soundspeed 1500

#3 pos: 76°S 0.947' 162°W 34.588' range: 1885 m range soundspeed 1500

AP3 2 triangulation result for KOP02



anchor release position: 76°S 6.954' 162°W 55.634'; depth: 1560 m

3D mooring position: 76°S 6.918' 162°W 55.147'

drift: 227 m; direction: 73°

mooring depth: 1545 m; slant error: 0 m

2D mooring position: 76°S 6.918' 162°W 55.153'

drift: 224 m; direction: 73°

horizontal error: 12 m

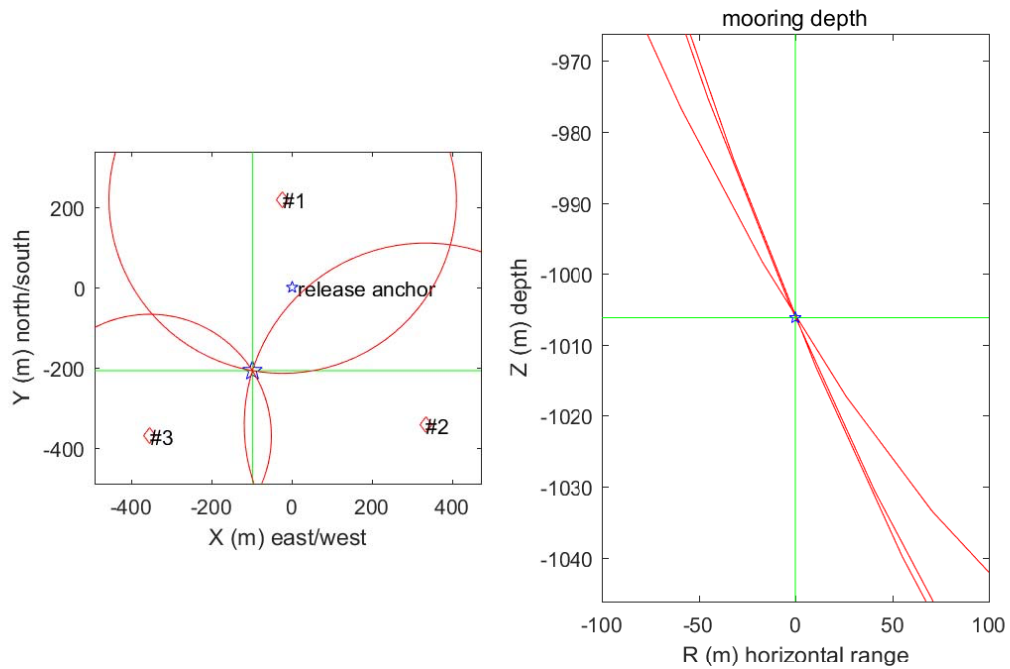
sound speed at site: 1445 m/s

#1 pos: 76°S 7.018' 162°W 56.278' range: 884 m range soundspeed 1500

#2 pos: 76°S 6.649' 162°W 55.091' range: 862 m range soundspeed 1500

#3 pos: 76°S 7.094' 162°W 54.340' range: 854 m range soundspeed 1500

AP3 3 triangulation result for KOP03



anchor release position: 76°S 9.964' 163°W 5.899'; depth: 995 m

3D mooring position: 76°S 10.076' 163°W 6.122'

drift: 230 m; direction: 205°

mooring depth: 1006 m; slant error: 0 m

2D mooring position: 76°S 10.078' 163°W 6.135'

drift: 235 m; direction: 206°

horizontal error: 9 m

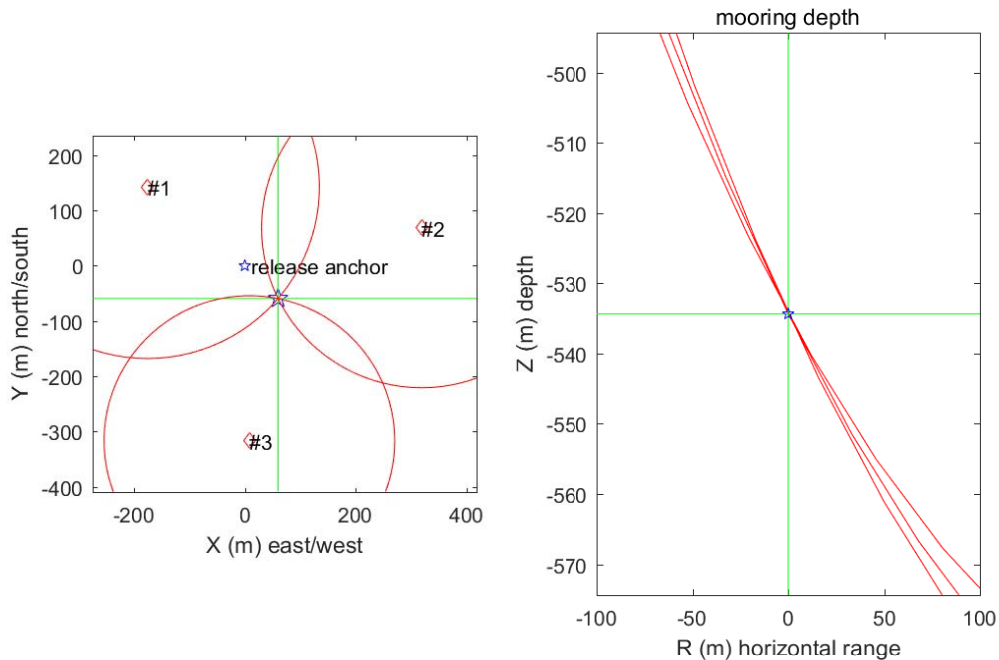
sound speed at site: 1445 m/s

#1 pos: 76°S 9.846' 163°W 5.952' range: 806 m range soundspeed 1500

#2 pos: 76°S 10.149' 163°W 5.147' range: 817 m range soundspeed 1500

#3 pos: 76°S 10.164' 163°W 6.700' range: 745 m range soundspeed 1500

AP3 4 triangulation result for KOP04



anchor release position: 76°S 24.611' 163°W 27.586'; depth: 536 m

3D mooring position: 76°S 24.643' 163°W 27.448'

drift: 84 m; direction: 135°

mooring depth: 534 m; slant error: 0 m

2D mooring position: 76°S 24.643' 163°W 27.449'

drift: 84 m; direction: 135°

horizontal error: 1 m

sound speed at site: 1445 m/s

#1 pos: 76°S 24.534' 163°W 27.990' range: 606 m range soundspeed 1500

#2 pos: 76°S 24.574' 163°W 26.852' range: 595 m range soundspeed 1500

#3 pos: 76°S 24.782' 163°W 27.567' range: 583 m range soundspeed 1500

Chapter 2. Chemical Oceanography

2.1. Inorganic Carbon System and Gas Measurement

Keyhong Park, Jung-OK Choi

Korea Polar Research Institute, Incheon, Republic of Korea

E-mail: keyhongpark@kopri.re.kr; jochoi@kopri.re.kr

2.1.1. Introduction

Ocean is a major sink of anthropogenic carbon dioxide and especially, the Southern Ocean has been known that which absorbs 40% of the carbon dioxide emitted by human activity. The Ross Sea is one of the most productive regions in the Southern Ocean however its carbon dioxide absorption capacity and carbonate system has not been clearly evaluated yet. Because the Southern Ocean is geographically isolated from the civilization and thus, its remoteness prevents making sufficient observations from proving reliable carbon dioxide sink strength estimates. Thus, direct observations are essential to improve current understanding on the carbon chemistry and biogeochemistry in the Ross Sea, and also significantly increase to enhance reliability of future environment of the ocean. Therefore, in this cruise, we have made an integrative oceanographic survey throughout the entire Ross Sea shelf region and observed pCO_2 , DIC, TA, pH, DO, and O₂/Ar.

2.1.2. Material and methods

2.1.2.1. General Oceanics GO-8050 Automated Flowing pCO_2 measuring system

CO_2 flux across the sea surface is usually determined by the concentration difference between the dissolved CO_2 in the surface mixed layer and the atmospheric CO_2 overlying the surface with a parameterized gas transfer velocity k . Dissolved CO_2 , so called pCO_2 , was determined using an aqueous and gaseous phase equilibration technique with a small Weiss-type equilibrator. The air above the surface was withdrawn from the intake cup mounted at the foremast at 29 m above sea-level. The CO_2 in the air and the equilibrator headspace was

analyzed with Li-cor 7000 (Figure 2.1.1) in which 4.5 μm wavelength of photon is selectively absorbed by CO₂. The analyzing system was calibrated every 6 hours using a series of calibration gases and one zero air. pCO₂ in the seawater was acquired every minute in a computer and atmospheric CO₂ every 6 hours. The raw data will then be corrected for the effect of temperature difference between the in-situ and the equilibrator after coming back to the institute, and gas transfer velocity k will also be determined using parameterization with wind speed which has been logged in DaDis onboard Araon.



Figure 2.1.1. GO-8050 pCO₂ underway measurement system.

2.1.2.2. Contros HydroC pCO₂ sensor

The instruments (Figure 2.1.2) were equipped with newly developed flow heads that made use of the platform movement to provide a constant and directed stream of water to the HydroC's membrane. Normally a submersible pump is used to create this water flow that is required to speed up the partial pressure equilibration between dissolved gases in the water and the gaseous headspace behind the membrane.



Figure 2.1.2. Contros HydroC $p\text{CO}_2$ sensor.

2.1.2.3. Underway DIC/TA sampling

Water sample is collected from the ships' seawater intake at 7 m for the analysis of DIC (Figure 2.1.3 and Table 2.1.1). These samples were poisoned with HgCl_2 . The samples will be analyzed with VINDTA system in Marine Environment Research Lab of Korea University after this cruise.



Figure 2.1.3. Bottled water samples for DIC/TA and d₁₃C analysis.

Table 2.1.1. DIC 250 mL or 500 mL sampling Log

No.	Datetime (UTC)	LATITUDE	LONGITUDE	Remarks
1	2023/1/11 07:56	46° 44.2' S	150° 22.2'E	
2	2023/1/11 07:56	46° 44.2' S	150° 22.2'E	duplicate
3	2023/1/12 15:45	51° 10.0' S	154° 06.0'E	
4	2023/1/12 15:45	51° 10.0' S	154° 06.0'E	duplicate
5	2023/1/13 21:01	58° 21.1' S	160° 59.4'E	
6	2023/1/14 05:38	60° 21.9' S	160° 59.3'E	
7	2023/1/14 05:38	60° 21.9' S	160° 59.3'E	duplicate
8	2023/1/15 05:56	66° 03.2' S	160° 59.2'E	
9	2023/1/15 05:56	66° 03.2' S	160° 59.2'E	duplicate
10	2023/1/15 12:40	67° 17.0' S	162° 55.2'E	
11	2023/1/15 13:10	67° 20.3' S	163° 03.1'E	
12	2023/1/16 23:35	71° 17.6' S	171° 26.5'E	
13	2023/1/22 22:47	76° 11.6' S	170° 06.3'E	
14	2023/1/26 02:17	74° 39.0' S	175° 29.9'E	
15	2023/1/26 02:17	74° 39.0' S	175° 29.9'E	duplicate
16	2023/1/27 00:40	74° 03.0' S	179° 59.9'W	
17	2023/1/27 00:40	74° 03.0' S	179° 59.9'W	duplicate
18	2023/2/5 18:23	76° 30.0' S	163° 31.1'W	
19	2023/2/7 09:53	77° 53.9' S	159° 40.0'W	

2.1.2.4. CTD samplings for DIC/TA and $\delta^{13}\text{C}$ analysis

The stable isotopes of carbon ($\delta^{13}\text{C}$) samples were collected at the hydrographic stations from the Niskin bottles attached in CTD/Rosette (Figure 2.1.4). The sample bottles were flushed 3 times before starting collection in 500 mL (or 250 mL) borosilicate glass bottle. Making small headspace, to prevent the seawater samples from being altered due to biological activities in the seawater, 200 μL (or 100 μL) of saturated HgCl_2 solution were injected upon injecting HgCl_2 solution. Then the sample bottles were tightened with rubber

band. The samples will be analyzed with an Apollo DIC analyzer coupled to a carbon dioxide Picarro cavity ring down spectrometer (CRDS) after this cruise.

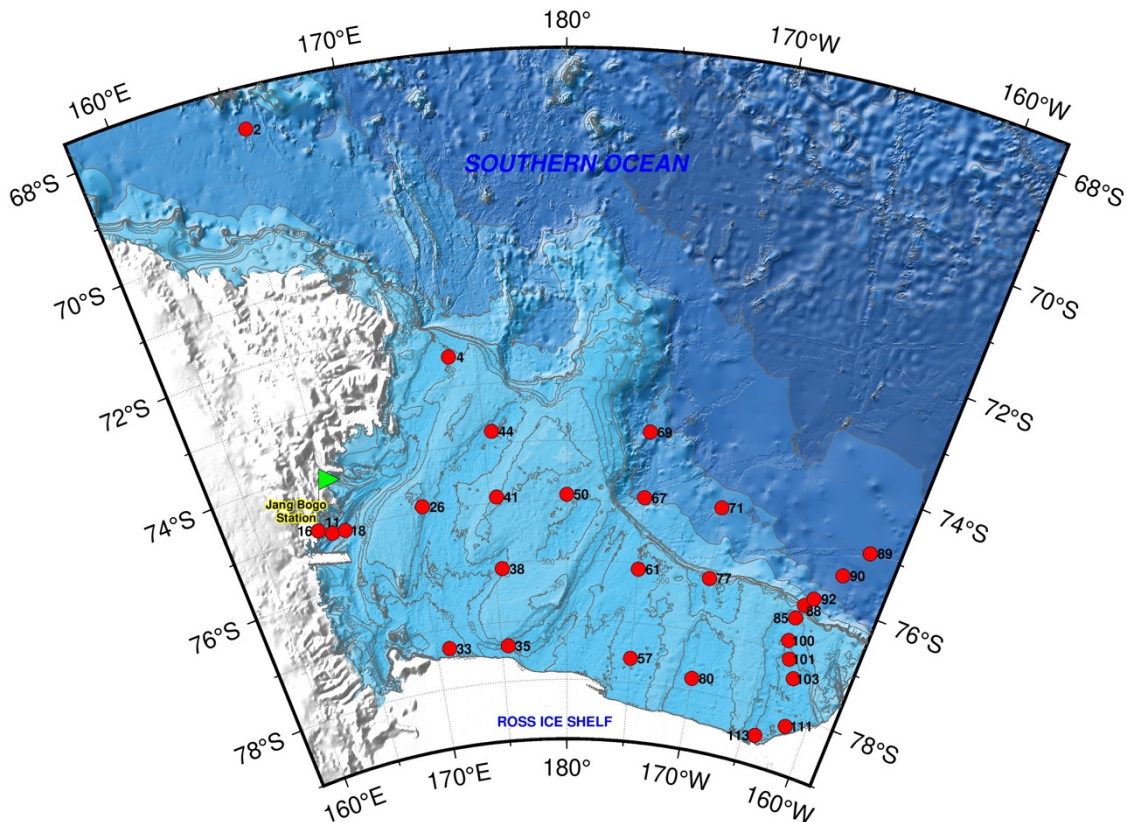


Figure 2.1.4. Sampling stations for DIC and d13C analysis. Station#1 (Lat 58.2°S, Lon 160.0°E) is not shown in the map

2.1.2.5. Continuous $\Delta O_2/Ar$ measurement as a proxy of net community production

Net community production (NCP), defined as the difference between autotrophic photosynthesis and (autotrophic and heterotrophic) respiration, produces O_2 proportional to the amount of net carbon. By measuring chemically and biologically inert Ar together with O_2 , it is possible to remove O_2 variation by physical processes (e.g., air temperature and pressure change and mixing of water masses) and deduce O_2 variation by biological processes (Craig and Hayward, 1987).

To determine the net community (oxygen) production underway, we adopted a continuous $\Delta O_2/Ar$ measurement system developed by Cassar et al. (2009). The so called ‘equilibrator inlet mass spectrometer (EIMS)’ is centered around a quadrupole mass spectrometer that measures dissolved gas molecules equilibrated with air in and supplied by an equilibrator (Figure 2.1.5). Water temperature, salinity, oxygen and fluorescence were also obtained to help the interpretation of temporal and spatial variation of $\Delta O_2/Ar$.

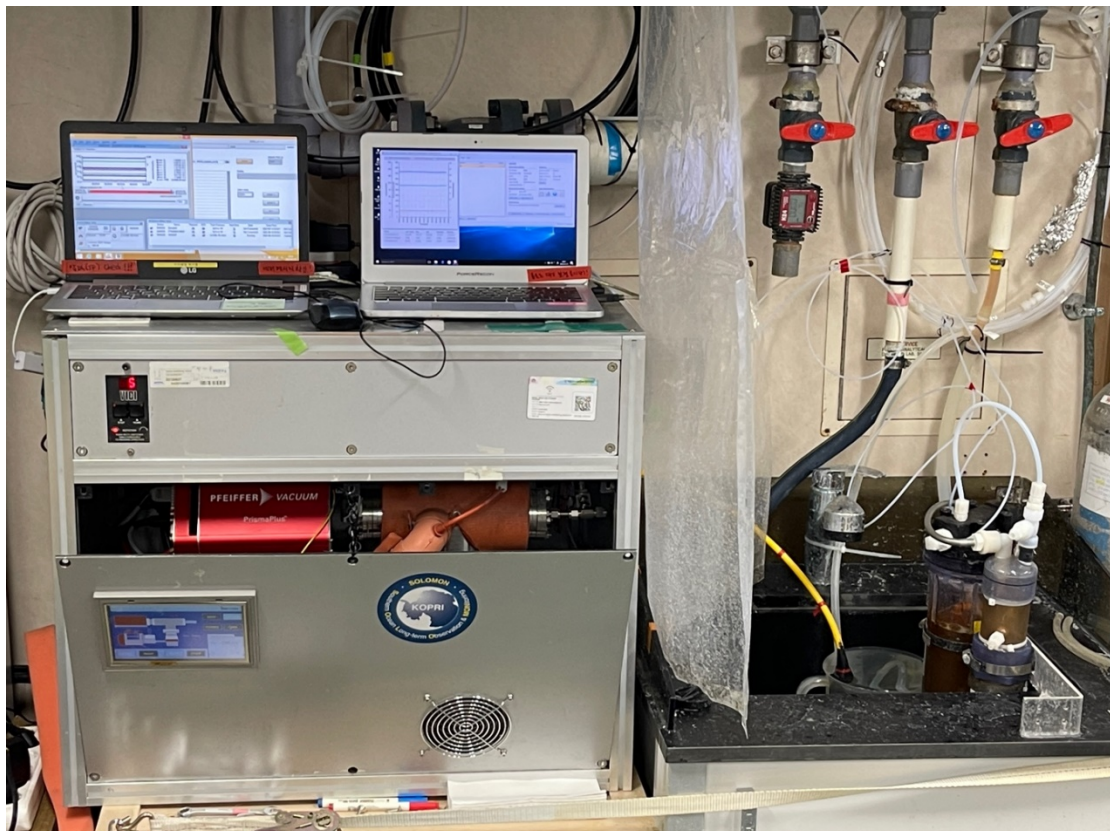


Figure 2.1.5. EIMS used for the underway measurements of $\Delta O_2/Ar$.

2.1.2.6. Underway surface water dissolved oxygen measurement

Dissolved oxygen was continuously measured from the ships’ seawater intake at a nominal depth of 7 meter using an optode from Aanderaa®. Oxygen concentration, saturation and water temperature were logged in the O₂ data log. The discrete 27 samples (including Triplicates) were collected from the scientific seawater system, using the same sampling point

as for the optode O₂ measurements. These were analysed by whole-bottle Winkler titration with amperometric endpoint detection. These Winkler data will be used to calibrate the optode sensor (Figure 2.1.6).

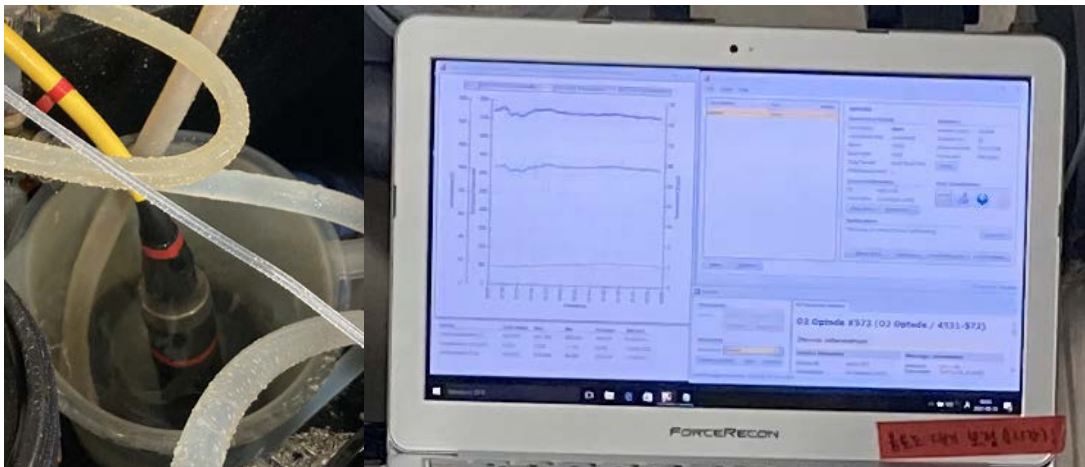


Figure 2.1.6. Aanderaa optode 4531 sensor.

2.1.2.7. Dissolved oxygen determined by automated amperometric titrator

Due to its central role in biological redox reactions and the availability of reliable sensors, dissolved oxygen is one of the most commonly measured chemical parameters in sea-going observations. In the cruise, along with the oxygen sensor (SBE-43) attached to the CTD-rosette system, we determined oxygen concentration by amperometric Winkler titration method (Langdon, 2010). The method involves applying a potential to electrodes placed in a solution and adding thiosulfate to react with I₂ to form 2I⁻. The gradual decrease of I₂ during the reaction results in the decrease of the current measured at the electrodes. The endpoint is determined as the point at which the current does not decrease further. The bottle oxygen measurements will be used to check whether SBE-43 oxygen sensor shows any drift or malfunctioning (Figure 2.1.7).



Figure 2.1.7. Automated amperometric titrator.

Water samples were collected from a selected number of CTD casts for calibration of the CTD oxygen sensor. A total of Six CTD casts were sampled for dissolved oxygen (DO) which were the first samples to be drawn from the Niskin bottles. Duplicate samples were collected from on average 10 depths. Seawater was collected directly into pre-calibrated glass bottles using a Tygon® tube. Before the sample was drawn, the bottles were flushed with seawater for several seconds (for about 3 times the volume of the bottle). The fixing reagents (i.e., manganese chloride and sodium hydroxide/sodium iodide solutions) were then added. Care was taken to avoid bubbles inside the sampling tube and sampling bottle. Samples were thoroughly mixed following the addition of the fixing reagents and were then kept for 30-40 min to allow the precipitate to settle to <50% the volume of the bottle. Once the precipitate had settled all samples were thoroughly mixed for a second time in order to maximize the efficiency of the reaction.

References

- Cassar, N., Barnett, B. A., Bender, M. L., Kaiser, J., Hamme, R. C., Tilbrook, B. 2009. Continuous high-frequency dissolved O₂/Ar. measurements by equilibrator inlet mass spectrometry. *Analytical Chemistry*, 81, 1855–1864.
- Craig, H., Hayward, T., 1987. Oxygen supersaturation in the ocean: Biological versus physical contributions. *Science* 235, 199–202.
- Dickson, A. G. (1995) Determination of dissolved oxygen in seawater by Winkler titration. WOCE Operations Manual. WHP Office Report WHPO 91–1, 1995.

- Fietzek, P., Steinhoff, T., Kortzinger, A. (2014) In situ quality assessment of a novel underwater pCO₂ sensor based on membrane equilibration and NDIR spectrometry. *Journal of Atmospheric and Oceanic Technology*, 31, 181-196.
- Hahm, D., T. S. Rhee, H.-C. Kim, J. Park, Y. N. Kim, H. C. Shin, and S. Lee (2014), Spatial and temporal variation of net community production and its regulating factors in the Amundsen Sea, Antarctica, *Journal of Geophysical Research*, 119(5), 2815–2826, doi:10.1002/2013JC009762.
- Langdon, C. (2010) Determination of dissolved oxygen in seawater by Winkler titration using the amperometric technique. GO-SHIP Repeat Hydrography Manual. IOCCP Report No. 14, ICPO Publication Series No. 134.
- Pierrot, D., Neill, C., Sullivan, K., Castle, R., Wanninkhof, R., Lüger, H., Johannessen, T., Olsen, A., Feely R.A., Cosca, C.E. (2008) Recommendations for Autonomous Underway pCO₂ Measuring Systems and Data Reduction Routines. *Deep-Sea Research Part II*.

2.2. Nutrient, Dissolved Organic Carbon, and Oxygen Isotope

Jinyoung Jung¹ and Juyoung Son^{1,2}

¹*Korea Polar Research Institute, Incheon, Republic of Korea*

²*Pukyong National University, Busan 48513, Republic of Korea*

E-mail: jinyoungjung@kopri.re.kr; mh0980@kopri.re.k

2.2.1. Introduction

It is well known that the growth of marine phytoplankton is directly dependent on their ability to utilize nutrients and photosynthesize in environments where neither nutrients nor light are necessarily optimal for these processes. Nitrogen (N) is the macro-nutrient thought to limit marine primary productivity in most coastal and oceanic areas. However, large portions of the world's ocean, including much of the Southern Ocean, are characterized as high nutrient, low chlorophyll regions (HNLC), where phytoplankton growth and nitrate (NO_3^-) uptake rates are modest despite the high concentrations of NO_3^- available for planktonic use. In these areas, other environmental factors, including the availability of essential trace metals (most notably iron) or inhibition by elevated concentrations of ammonium (NH_4^+) have been suggested to reduce the efficiency of NO_3^- uptake and phytoplankton growth (Cochlan and Bronk, 2001).

The Ross Sea, a highly productive region of the Southern Ocean, accounts for 25–30% of the annual Southern Ocean primary production (Orsi et al., 2002; Arrigo et al., 2008; Smith et al., 2014), thus playing an important role in the marine carbon cycle (Arrigo et al., 2008). Phytoplankton production contributes to significant accumulation of newly produced dissolved organic carbon (DOC) in the surface ocean and its subsequent export to the deep ocean (Hansell and Carlson, 2001; Carlson, 2002). DOC derived from primary production may originate from several biological processes including direct phytoplankton exudation, grazing interactions and viral lysis, while dissolved organic matter (DOM) removal processes include microbial mineralization and photodegradation (Carlson, 2002). In the Ross Sea, DOC concentration in late winter has been observed to be at a background level of ~42 μM (Carlson et al., 2000). An increase by as much as 30 μM of DOC in excess of that observed in late winter has been linked

to the high Ross Sea spring/summer production. However, the fraction of carbon fixed as DOC was found to be qualitatively more labile and enriched with nitrogen compared to the deeper refractory DOM (Carlson et al., 2000). Although studies have hypothesized on the role of plankton community structure on DOC production and accumulation, the absence of large DOC accumulation within the Ross Sea has been attributed to low bacterial activity (Ducklow et al., 2001). More recently, Bercovici et al. (2017) showed that DOC produced in the Ross Sea enriches the dense shelf water (DSW) by $\sim 7 \mu\text{M}$ and contributes to the export of $\sim 4 \text{ Tg C yr}^{-1}$ of DOC off the Ross Sea and into the abyssal Southern Ocean.

In this study, we examine water column nutrient and DOC concentrations, and oxygen isotope ($\delta^{18}\text{O}$) in conjunction with biophysical (e.g., salinity, temperature, and chlorophyll) properties obtained during a field campaign in the Little America Basin, the Ross Sea conducted onboard the Korean ice breaker and research vessel Araon in the austral summer of 2023.

2.2.2. Material and methods

2.2.2.1. Sample collection and Processing

2.2.2.1.1. Nutrient

Seawater sampling for nutrients, including phosphate (PO_4), nitrite + nitrate ($\text{NO}_2 + \text{NO}_3$), ammonium (NH_4), and silicic acid (Si(OH)_4), was carried out at 23 stations over the Little America Basin using a CTD/rosette sampler holding 24-10 L Niskin bottles (SeaBird Electronics, SBE 911 plus) during Korea research ice breaker R/V Araon cruise (ANA13B, February 2–February 7, 2023) (Fig. 2.2.1). Samples for nutrients were collected from the Niskin bottles into 50 ml conical tubes and immediately stored in a refrigerator at 4°C prior to chemical analyses. Concentrations of nutrients were measured using standard colorimetric methods adapted for use on a 4-channel continuous Auto-Analyzer (QuAAstro, Seal Analytical, Germany). The channel configurations and reagents were prepared according to the ‘QuAAstro Applications’. Standard curves were run with each batch of samples using freshly prepared standards that spanned the range of concentrations in the samples. The r^2 values of all the standard curves were greater than or equal to 0.99.

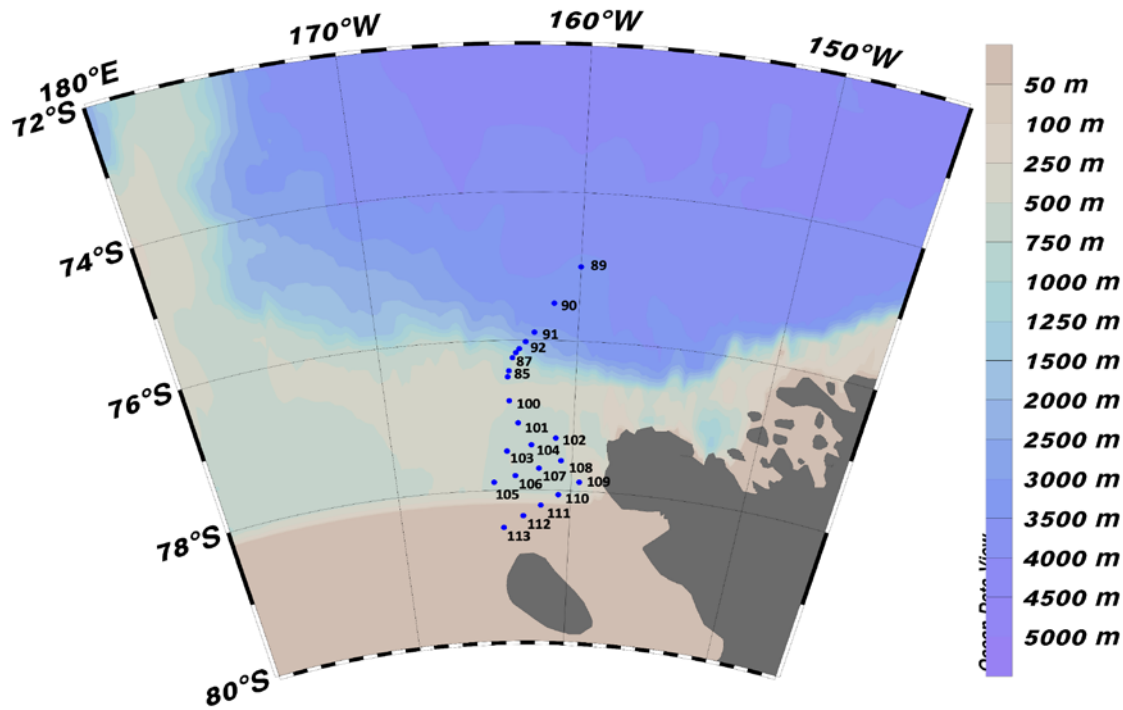


Figure 2.2.1. Map of study area. Blue dots show the CTD stations during the expedition. The numbers indicate the station numbers.

2.2.2.1.2. Dissolved organic carbon

For DOC measurements, a pre-cleaned (soaked in 10% HCl and rinsed with ultrapure water) Teflon tube was used to connect between the Niskin bottles spigot and a pre-cleaned 47 mm filtration holder made of PP (PP-47, ADVANTEC). About 200 ml of seawater was filtered through a pre-combusted (at 550°C for 6 hours) Whatman GF/F filter (47 mm in diameter) under gravity. The filtered seawater samples were collected directly into pre-cleaned glass bottles. The filtrate was distributed into two pre-combusted 20 ml glass ampoules using a sterilized serological pipette. Each ampoule was sealed with a torch, quick-frozen, and preserved at approximately -20°C until the analysis in our land laboratory. DOC analysis will be basically made with a HTCO system consisting of a commercial unit, the Shimadzu TOC-L system (Shimadzu Co.).

2.1.3. Oxygen isotope

For the determination of $\delta^{18}\text{O}$, seawater samples were collected using the same method as for DOC sampling (see Section 2.2.2.1.2). For each sample, the filtrate was placed in an acid-cleaned 20-mL glass vial, sealed with Parafilm, and stored at 4 °C until the analysis in our land laboratory analysis.

References

- Arrigo, K. R., van Dijken, G. L., and Bushinsky, S., 2008. Primary production in the Southern Ocean, 1997–2006. *J. Geophys. Res., Oceans*, 113, C08004.
- Bercovici, S. K., Huber, B. A., DeJong, H. B., Dunbar, R. B., and Hansell, D. A., 2017. Dissolved organic carbon in the Ross Sea: Deep enrichment and export. *Limnol. Oceanogr.*, 62, 2593–2603.
- Carlson, C. A., 2002. “Production and removal processes,” in *Biogeochemistry of Marine Dissolved Organic Matter*, eds D. A. Hansell and C. A. Carlson (New York: Academic), 91–151.
- Carlson, C. A., Hansell, D. A., Peltzer, E. T., and Smith, W. O. Jr., 2000. Stocks and dynamics of dissolved and particulate organic matter in the southern Ross Sea, Antarctica. *Deep-Sea Res. II*, 47, 3201–3225.
- Cochlan, W. P., and Bronk, D. A., 2001. Nitrogen uptake kinetics in the Ross Sea, Antarctica. *Deep-Sea Res. II*, 48, 4127–4153.
- Ducklow, H., Carlson, C., Church, M., Kirchman, D., Smith, D., and Steward, G., 2001. The seasonal development of the bacterioplankton bloom in the Ross Sea, Antarctica, 1994–1997. *Deep-Sea Res. II*, 48, 4199–4221.
- Hansell, D. A., and Carlson, C. A., 2001. Marine dissolved organic matter and the carbon cycle. *Oceanography*, 14, 41–49.
- Orsi, A. H., Smethie, W. M. Jr., and Bullister, J. L., 2002. On the total input of Antarctic Waters to the Deep Ocean: a preliminary estimate from chlorofluorocarbon measurements. *J. Geophys. Res.*, 12, 12.
- Smith, W. O. Jr., Ainley, D. G., Arrigo, K. R., and Dinniman, M. S., 2014. The oceanography and ecology of the Ross Sea. *Annual. Rev. Mar. Sci.*, 6, 469–487.

2.3. Particulate Organic Carbon and Photochemistry

Sun-Yong Ha and Jun-Oh Min

Korea Polar Research Institute, Incheon, Republic of Korea

E-mail: syha@kopri.re.kr; jomin@kopri.re.kr

2.3.1. Introduction

The Ross Sea is the Antarctic's productive region (Arrigo et al., 1998) and considered one of the most important ocean sinks of atmospheric CO₂ by biological uptake. Particularly, rates of annual primary production (PP) can be very high in Ross Sea Polynya, more than 150 g C m⁻² yr⁻¹ (Smith and Gorden, 1997; Arrigo et al., 2003). The magnitude of PP and phytoplankton physiology are likely to influence carbon export to deep water. Active (and fast) fluorometry is a non-destructive and rapid method, and it has been used to monitor variations in the photochemistry (Kolber and Falkowski, 1993; Falkowski and Kolber, 1995). Especially, variable fluorescence is the most sensitive signal recorded in the upper ocean that reflects phytoplankton photophysiology. The extent to which biological degradation of particulate organic matter (POM) also plays an important role in oceanic carbon cycling and the efficiency of the carbon export. Concerted measurements for PP have been made, during the last decade (Smith, 2022), but in situ field data are scarce recently. To improve our understanding of biological processes such as variations of PP and photochemical efficiency of PSII, we measured carbon uptake rates and the ratio of variable to maximal fluorescence (Fv/Fm) using ¹³C tracer technique and Miniaturized Fluorescence Induction and Relaxation (mini-FIRe) and Picosecond Lifetime Fluorometer (PicoLiF) System, respectively. Particulate organic matter is also investigated to better understand the role of the Ross Sea in the cycles of carbon.

2.3.2. Material and methods

2.3.2.1. Sample collection

Sampling for particulate organic carbon (POC), and primary productivity were carried out in

Ross Sea aboard R/V ARAON in February 2023. We selected 13 sampling stations (blue and red dots) and 6 ~ 12 depths, from surface to bottom depth (~ 3570 m) (Fig. 2.3.1). Water samples were collected using a Sea Bird sampler (24 Niskin bottles, 10 L each) attached to a conductivity–temperature–depth (CTD) rosette system.

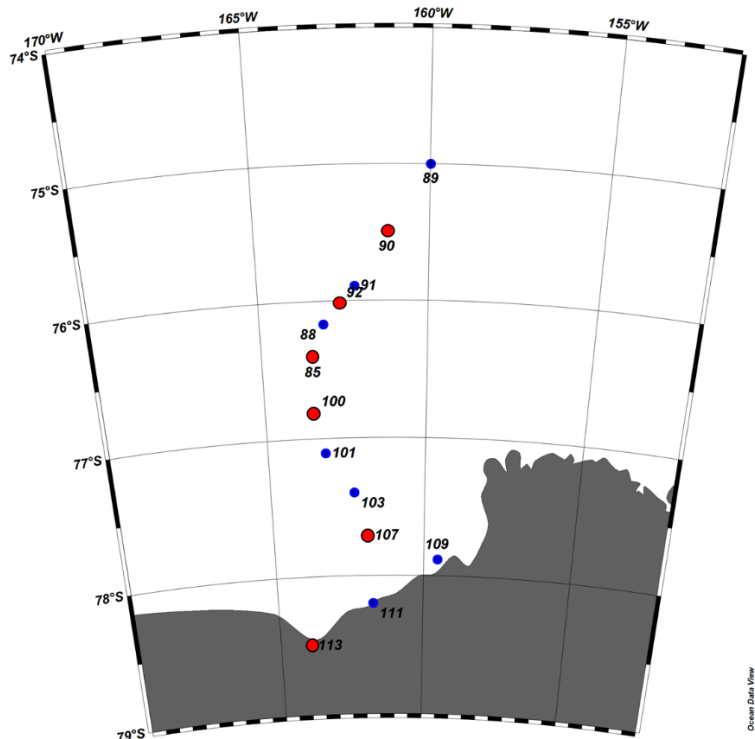


Figure 2.3.1. Sampling site at Little American Basin, Ross Sea.

2.3.2.2. Particulate organic carbon (POC) sampling

POC was measured by filtering 1L of seawater on pre-combusted (4 h, 450°C) 25mm GF/F glass fiber filters (Whatman, nominal pore size 0.7 µm). The filters were stored frozen (-80°C) until processed. Prior to analysis, the filters for POC will be dried and acidified to removed carbonates and then analyzed using elemental analyzer after this cruise.

2.3.2.3. Primary productivity of phytoplankton

To estimate carbon and nitrogen uptake of phytoplankton at different locations, productivity experiments were executed by incubating phytoplankton in the incubators on the

deck for 4-5 hours (Fig. 2.3.2) after stable isotope (^{13}C) as tracer were inoculated into each bottle. Total 6 productivity experiments (Fig. 2.3.1; red dots and Table 2.3.1) were completed during this cruise. At every CTD station, the productivity waters were collected by CTD rosette water samplers at 6 different light depths (100, 50, 30, 12, 5, and 1%). The samples were kept in an on-deck incubator equipped with surface seawater flowing facility to maintain the temperature. Immediately after the incubation period samples were filtered under low vacuum (<75 mm Hg or 0.1 MPa) to retain particulate materials on pre-combusted. on GF/F ($\phi = 25$ mm) filters for laboratory isotope analysis at University of Alaska Fairbanks after this cruise.

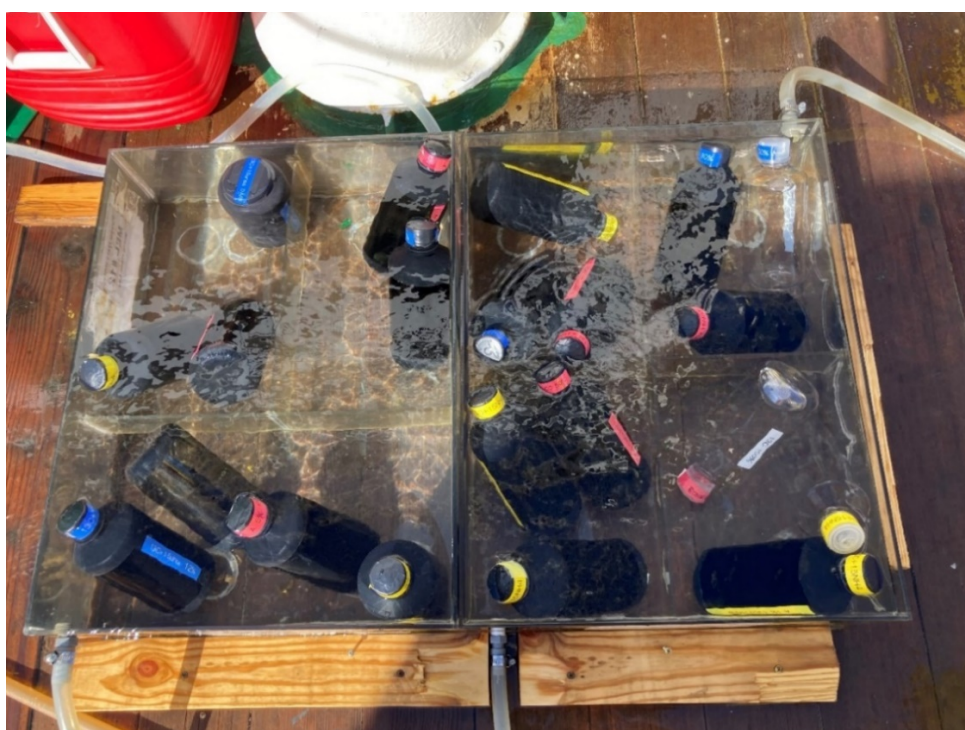


Figure 2.3.2. *In situ* incubation on deck for 4-5 hours.

2.3.2.4. Photochemistry

To investigate the impact of physico-chemical conditions on photosynthesis in the Little American Basin, we measured photosynthetic characteristics of phytoplankton at total 12 stations (Fig.1 and Table 1; red and blue dots except station 88) using mini-FIRe (Fig. 2.3.3). After collection of seawater from Niskin bottles at five to six depths in upper layer (0 – 100m) (Table 1), samples

were kept under in situ temperature in light bottles. These samples were measured after 30 minutes low light adaptation. Photosystem II (PSII) parameters such as the minimal fluorescence yield (F_0 ; when all reaction centers are open), the maximal fluorescence yield (F_m ; all reaction centers are closed), the quantum efficiency of PSII (F_v/F_m), the functional (or effective) absorption cross-section of PSII (σ_{PSII}) were measured as described in Kolber et al. (1998). Quantum efficiency of photochemistry in PSII (F_v/F_m) was calculated as a ratio of variable fluorescence ($F_v=F_m-F_0$) to the maximum one (F_m). The fluorescence measurements were corrected for the blank signal recorded from filtered seawater (by 0.2 μm syringe filter set) because of background fluorescence (Dissolved organic matter and dissolved degradation products in water). When the ship was moving (from New Zealand to Ross sea), underway pumped on the seawater near surface (ca. 7 m depth) and the fluorescence was measured continuously on real time.



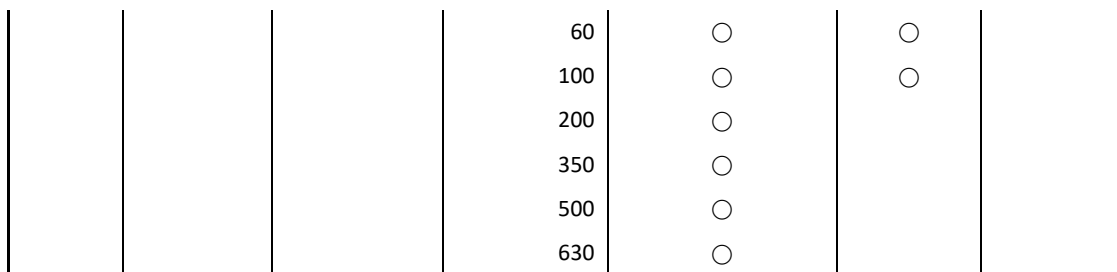
Figure 2.3.3. Miniaturized Fluorescence Induction and Relaxation (mini-FIRe) onboard Araon.

Table 2.3.1. Sampling information of POC, F_v/F_m , and primary production during ANA13B

			9			○	
			10		○		○
			13			○	
			15	○			○
			20		○		○
			45	○		○	
			70		○		
			100	○		○	
			200	○			
			300	○			
			500	○			
			700	○			
			1000	○			
			2000	○			
			3000	○			
			3328	○			
91	-75.89149	-162.1611	0	○		○	
			10			○	
			20			○	
			30	○		○	
			50	○		○	
			100	○		○	
			250	○			
			350	○			
			500	○			
			700	○			
			1000	○			
			2000	○			
			2822	○			
92	-76.01936	-162.5866	0	○		○	○
			6				○
			10			○	○
			18				○
			20	○		○	
			26				○
			35			○	
			40				○
			60	○		○	
			100	○		○	
			230	○			
			300	○			
			415	○			

			500	○		
			700	○		
			1000	○		
			1500	○		
			2240	○		
100	-76.80682	-163.464	0	○	○	○
			5			○
			8			○
			10		○	○
			14			○
			15	○		
			20		○	○
			30	○	○	○
			60	○	○	
			100	○	○	
			250	○		
			420	○		
			560	○		
101	-77.10515	-163.1742	0	○	○	
			10		○	
			20	○	○	
			40		○	
			50	○		
			60		○	
			100	○	○	
			200	○		
			350	○		
			500	○		
			600	○		
103	-77.39774	-162.289	0	○	○	
			10		○	
			20	○	○	
			40		○	
			60	○		
			70		○	
			100	○	○	
			200	○		
			350	○		
			500	○		
			632	○		
107	-77.71053	-161.8531	0	○	○	○
			5			○

			8			○
			10		○	○
			14			○
			20			○
			25	○	○	
			30			○
			50	○	○	
			100	○	○	
			170	○		
			275	○		
			500	○		
			665	○		
109	-77.88224	-159.5415	0	○	○	
			10		○	
			15	○	○	
			40	○	○	
			70	○	○	
			100		○	
			150	○		
			250	○		
			380	○		
			439	○		
111	-78.19982	-161.7228	0	○	○	
			10		○	
			20		○	
			30	○		
			40		○	
			60		○	
			65	○		
			100	○	○	
			200	○		
			300	○		
			450	○		
113	-78.49574	-163.9227	592	○		
			0	○	○	○
			5			○
			8			○
			10		○	
			14			○
			20	○	○	○
			30			○
			40	○		



References

- Arrigo, K. R., and van Dijken, G. L. (2003) Phytoplankton dynamics within 37 Antarctic coastal polynya systems. *Journal of Geophysical Research*, 108(C8), 3271, doi:10.1029/2002JC001739.
- Arrigo, K. R., Worthen, D. L., and Lizotte, S. M. P. (1998) Primary production in Southern Ocean waters. *Journal of Geophysical Research: Oceans*, 103, 15587–15600. <https://doi.org/10.1029/98JC00930>.
- Falkowski, P. G. and Z. Kolber (1995) "Variations in chlorophyll fluorescence yields in phytoplankton in the world oceans." *Aust. J. Plant Physiol.* 22(2): 341-355.
- Kolber, Z. and P. G. Falkowski (1993) "Use of active fluorescence to estimate phytoplankton photosynthesis in situ." *Limnol. Oceanogr.* 38(8): 1646-1665.
- Kolber, Z. S., O. Prasil, et al. (1998) "Measurements of variable chlorophyll fluorescence using fast repetition rate techniques: defining methodology and experimental protocols." *Biochimica et Biophysica Acta-Bioenergetics* 1367(1-3):88-106.
- Smith, W. O. Jr. (2022) Primary productivity measurements in the Ross Sea, Antarctica: a regional synthesis. *Earth System Science Data*, 14: 2737-2747.
- Smith, W. O. Jr. and Gordon, L. I. (1997) Hyperproductivity of the Ross Sea (Antarctica) polynya during austral spring. *Geophysical Research Letters*, 24: 233-236.

2.4. Trace Metal

Taejin Kim, Ijin Lim

Pukyong National University, Busan 48513, Korea

Email: tkim@pknu.ac.kr; ijinlim@pukyong.ac.kr

2.4.1. Introduction

Dissolved trace metals generally present in seawater at low concentrations ($10^{-12} - 10^{-9}$ mol/L). Trace metals, such as iron (Fe), copper (Cu), nickel (Ni), zinc (Zn), cobalt (Co), are well known essential micro-nutrients for many marine microorganisms (Anderson, 2020). However, detailed distributions of trace metals have not been investigated well in the Little American Basin, Ross Sea. Therefore, we will study the distributions of dissolved trace metals (Fe, Mn, Zn, Cu etc.) in the Little American Basin.

Moreover, chemical speciation of trace metals is also considered to be an important factor of the biological availability of these trace metals. For example, organic complexed Zn, which is bound with organic ligands, reduces the fraction of free metal ion (Zn^{2+}) to a level as $10^{-15}M$, which could limit the growth of some phytoplankton species (Sunda and Huntsman, 1992). On the other hand, dissolved Cu can be toxic to most microorganisms in the absence of Cu binding organic ligands. But in most ocean environments, Cu is not toxic to microorganisms because of Cu is bound with organic ligands (Sunda and Huntsman, 1998). For better understanding of biogeochemical cycles of trace elements in the ocean, it is the first step to clarify the speciation of these elements in seawater. However, little is known about the organic complexation of trace metals in open-ocean waters. In this study, therefore, we will investigate trace metal speciation in the Little American Basin using cathodic stripping voltammetry (CSV).

Rare earth elements (REEs), comprising 15 lanthanide elements (La to Lu), are an extremely coherent group in terms of their chemical behavior. Among the REEs, neodymium (Nd) isotopes have been used as a water mass tracer due to the shorter residence time of Nd (300–500 yr) (Amakawa et al., 2004), compared to the global ocean mixing time (1500 yr) (Broecker and Peng, 1982). In addition, the major source of REEs in ice-covered oceans is probably

particulate matter rafted by sea ice and glacial ice (Winter et al., 1997). However, REEs and Nd isotopes data in the Southern Ocean are scarce. Therefore, we will investigate distributions of dissolved REEs and the water mass structure and ocean circulations using Nd isotopic composition in the Ross Sea, the most important area for the formation of ocean bottom waters.

2.4.2. Material and methods

2.4.2.1. Sampling location

Trace metal samples were collected at 12 stations (Fig. 2.4.1) during ice breaker R/V Araon research cruise (ANA13B) from February 2 to 8, 2023. Detailed information of stations is described in Table 2.4.1.

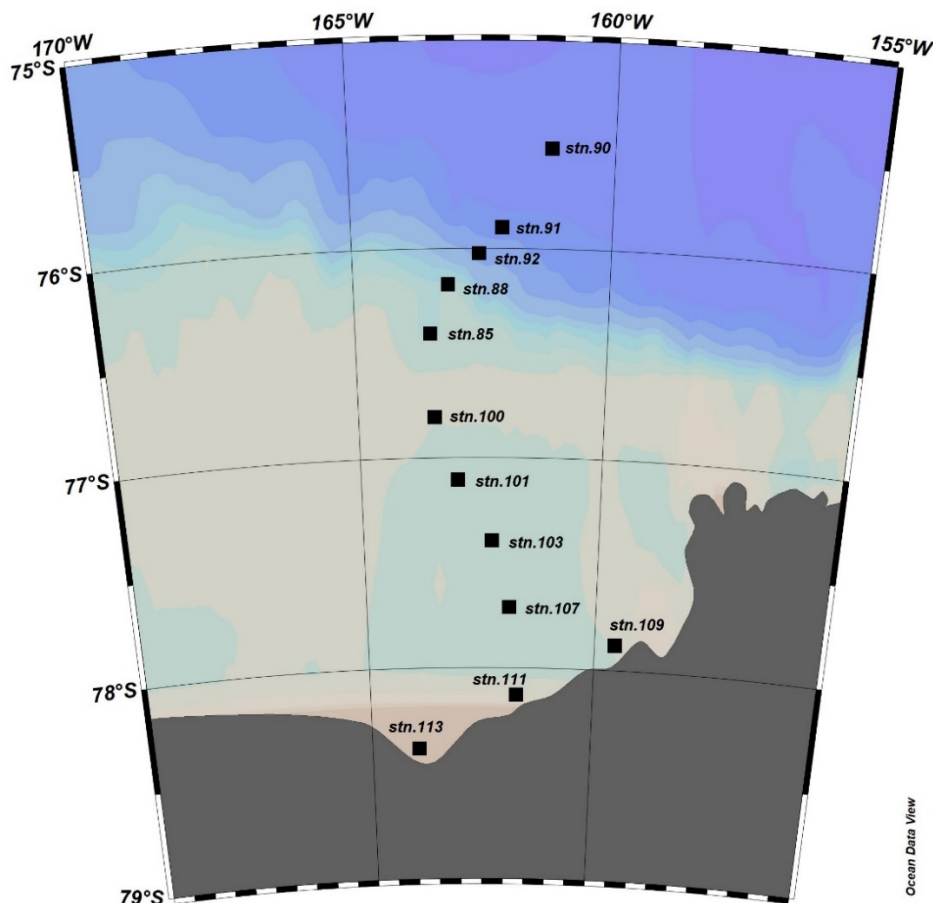


Figure 2.4.1. Map of sampling locations during ANA13B research cruise.

Table 2.4.1. Information of sampling locations and water samplings

Station	Latitude	Longitude	Date (UTC) (YYYY.MM.D D)	Arrival Time (UTC)	Bottom Depth (m)	Trace Metal	Speciatio n	Nd isotopes
85	76°24.6304'S	163°27.4880'W	2023.02.02	02:25	537	O	O	
88	76°10.0502'S	163°5.9232'W	2023.02.02	14:21	981	O	O	O
90	75°30.0010'S	161°12.7170'W	2023.02.03	13:18	3348	O	O	O
91	75°53.4895'S	162°9.6629'W	2023.02.03	22:55	2845	O	O	
92	76°01.1615'S	162°35.1930'W	2023.02.04	13:00	2256	O	O	O
100	76°48.4100'S	163°27.8337'W	2023.02.05	20:49	573	O		
101	77°6.3095'S	163°0.4502'W	2023.02.06	01:46	616	O	O	O
103	77°23.8651'S	162°17.3355'W	2023.02.06	09:30	645	O		
107	77°42.6337'S	161°51.1755'W	2023.02.07	09:16	678	O	O	
109	77°52.9335'S	159°32.4950'W	2023.02.07	06:41	459	O	O	
111	78°11.9905'S	161°43.3694'W	2023.02.07	13:12	603	O	O	O
113	78°29.7447'S	163°55.3636'W	2023.02.07	20:29	642	O	O	
						Total Samples	106	180
								32

2.4.2.2. Clean seawater sampling

The clean seawater sampling system for trace metal sample is consisted of a polyurethane coated Al frame holding acid-cleaned 12 L Teflon coated Niskin-X samplers (General Oceanics Inc., USA) mounted on a Carousel array with auto firing module (Sea Bird Electronics Inc., USA), which attached to an Ultra High Molecular Weight Polyethylene (UHMWPE) rope (Fig. 2.4.2). After seawater collection, sampling system was moved into the trace metal clean van. Samples for trace metal concentration analysis were obtained through an acid-cleaned 0.2 μm filter cartridge (Acropak, Pall, USA) connected to sampler directly with pressured air (Fig. 2.4.3). Filtered samples (125 mL LDPE bottle) were acidified to pH<1.8 by adding ultra-pure HCl (ODLAB, Korea) and stored. Samples for chemical speciation analysis were filtered in the same way with those of trace metal samples. Filtered samples (500 mL LDPE bottle) were then frozen at -18°C and stored until analysis. Samples for Nd isotopic composition analysis were collected in the same way with those of trace metal except for sampling volume (6 L in LDPE collapsible containers). Subsequently, 5 mg/L of Fe was added into each sample for iron coprecipitation. After 24 h equilibrium, ammonia solution (20–22%, OPTIMA, Fisher Chemical, USA) was added into each sample to increase the pH to 8.0. After 48 h, the supernatant was discarded. The collected iron hydroxide will be determined in the on-land laboratory.

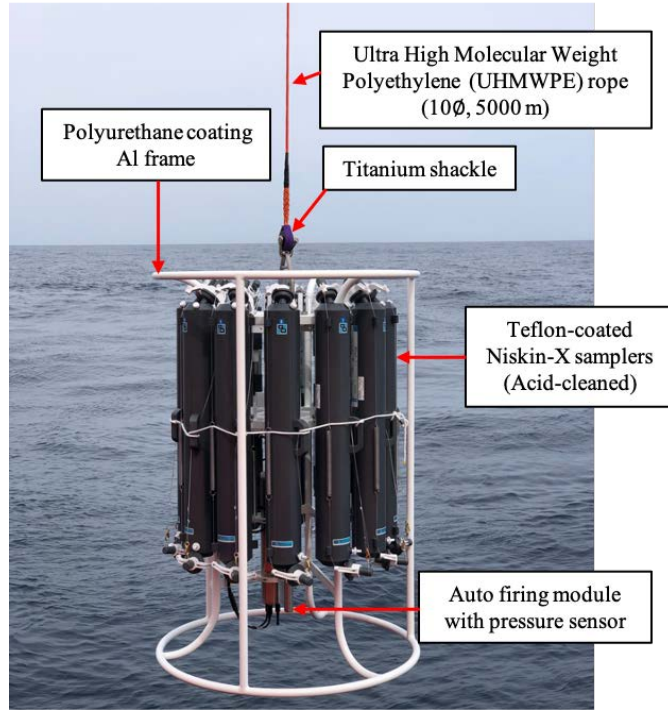


Figure 2.4.2. Clean seawater sampling system for trace metal samples.



Figure 2.4.3. Subsampling for clean seawater samples.

2.4.2.3. Analytical method

Concentrations of trace metals will be determined by an automated system (SC-DX seaFAST, ESI) with online pH buffering connected to a high-resolution inductively coupled plasma mass spectrometry (HR-ICP-MS) (Kim et al., 2020). Chemical speciation such as Cu or Fe will be determined by a titration method using cathodic stripping voltammetry (CSV) (Kim et al., 2015; Wong et al., 2018) in the on-land laboratory. Neodymium isotopic compositions will be determined using a multi-collector inductively coupled plasma mass spectrometer (MC-ICP-MS) (Amakawa et al., 2019).

References

- Amakawa, H., Yu, T. L., Tazoe, H., Obata, H., Gamo, T., Sano, Y., Shen, C-C., Suzuki, K. (2019). Neodymium concentration and isotopic composition distributions in the southwestern Indian Ocean and the Indian sector of the Southern Ocean. *Chemical Geology*, 511, 190-203. <https://doi.org/10.1016/j.chemgeo.2019.01.007>
- Amakawa, H., Alibo, D.S., Nozaki, Y., 2004. Nd abundance and isotopic composition distributions of surface seawaters of the Northwest Pacific Ocean and its adjacent seas. *Geochem. J.* 38, 493–504. <https://doi.org/10.2343/geochemj.38.493>.
- Anderson, R.F., 2020. GEOTRACES: Accelerating Research on the Marine Biogeochemical Cycles of Trace Elements and Their Isotopes. *Annual Review of Marine Science*, 12(1): 49 - 85. doi:10.1146/annurev-marine-010318-095123
- Broecker, W.S., Peng, T.-H., 1982. Tracers in the Sea. Eldigio Press, Palisades, New York (689 pp).
- Kim, T., Kim, H. and Kim, G., 2020. Tracing river water versus wastewater sources of trace elements using rare earth elements in the Nakdong River estuarine waters. *Marine Pollution Bulletin*, 160: 111589. doi:10.1016/j.marpolbul.2020.111589
- Kim, T., Obata, H., Kondo, Y., Ogawa, H. and Gamo, T., 2015. Distribution and speciation of dissolved zinc in the western North Pacific and its adjacent seas. *Marine Chemistry*, 173: 330 - 341. doi:10.1016/j.marchem.2014.10.016
- Sunda, W.G. and Huntsman, S.A., 1992. Feedback interactions between zinc and phytoplankton in seawater. *Limnology and oceanography*, 37(1): 25 - 40. doi:10.4319/lo.1992.37.1.0025
- Sunda, W.G. and Huntsman, S.A., 1998. Interactions among Cu²⁺, Zn²⁺, and Mn²⁺ in

controlling cellular Mn, Zn, and growth rate in the coastal alga Chlamydomonas. Limnology and oceanography, 43(6): 1055 – 1064

Winter, B.L., Johnson, C.M., Clark, D.L., 1997. Strontium, neodymium, and lead isotope variations of authigenic and silicate sediment components from the Late Cenozoic Arctic Ocean: implications for sediment provenance and the source of trace metals in seawater. Geochim. Cosmochim. Acta 61, 4181e4200.

Wong, K.H. et al., 2018. Organic complexation of copper in estuarine waters: An assessment of the multi-detection window approach. Marine Chemistry, 204: 144 - 151. doi:10.1016/j.marchem.2018.07.001

2.5. Deploying Biogeochemical Profiling Floats in the Southern Ocean and Ross Sea

Jennifer Magnusson

Monterey Bay Aquarium Research Institute; Moss Landing, CA

E-mail: jenn.magnusson@gmail.com

2.5.1. Introduction

The ***Southern Ocean Carbon and Climate Observations and Modeling (SOCCOM) Project*** aims to collect as much information as possible about the Southern Ocean and its connection to the climate. The goal of the SOCCOM float program is to produce a climate-quality data record for carbon cycling. Using 200 autonomous profiling floats, SOCCOM has been taking measurements on the Southern Ocean's oxygen, nitrate, and carbon content in order to investigate its role in the global carbon cycle. It's clear that the Southern Ocean absorbs enormous amounts of anthropogenic carbon dioxide, but as it continues to be flushed with carbon dioxide, the absorption power of the Southern Ocean will begin to wane, and Southern Ocean sponge may only be able to hold back the effects of climate change for so long.¹

SOCCOM uses biogeochemical data from the floats to design and support climate models, building high-resolution projections of the Southern Ocean. This open-source data can help support climate models throughout the world and hopefully lead to further innovations in climate research. SOCCOM float data will be made available in digital form in real time without restriction using a data policy similar to that of the Argo system. If there are adjustments to float raw data based on sensor calibrations during the deployment, then these adjusted data will also be available in near real time shortly after the float is deployed.

SOCCOM is supported by the National Science Foundation under NSF Award PLR-1425989 and OPP-1936222, with additional support from NOAA and NASA.

The ***Global Ocean Biogeochemistry (GO-BGC) Array*** is a project funded by the US National Science Foundation to build a global network of chemical and biological sensors that will monitor ocean health. Scientists at the Monterey Bay Aquarium Research Institute, the University of Washington, Scripps Institution of Oceanography, Woods Hole

Oceanographic Institution, and Princeton University will build and deploy 500 robotic ocean-monitoring floats around the globe as part of NSF's Mid-scale Research Infrastructure-2 program.

This network of floats will collect data on the chemistry and the biology of the ocean from the surface to a depth of 2,000 meters, augmenting the existing Argo array that monitors ocean temperature and salinity. Data streaming from the float array will be made freely available within a day of being collected via the Argo data system and will be used by researchers around the world. These data will allow scientists to pursue fundamental questions concerning ocean ecosystems, observe ocean health and productivity, and monitor the elemental cycles of carbon, oxygen, and nitrogen in the ocean through all seasons of the year. Such essential data are needed to improve computer models of ocean fisheries and climate, and to monitor and forecast the effects of ocean warming and ocean acidification on sea life.

In addition to NSF support, the US contribution to the Core-Argo array and the US Argo Data Center are supported by NOAA. These contributions provide a conduit for GO-BGC data into the Argo system. Development of the SIO BGC-SOLO II float for GO-BGC and the Argo community was supported by the US National Oceanographic Partnership Program and by NASA.

The GO-BGC Array is led by Director Ken Johnson and administered by the Monterey Bay Aquarium Research Institute, and is supported by NSF Award 1946578.

SOCCOM and GO-BGC are partnering with teachers and classrooms across the country and around the world to inspire and educate students about global ocean biogeochemistry and climate change through our "Adopt-A-Float" initiative. This program creates a powerful opportunity for students of all ages to engage directly with world-class scientists and learn about their research by naming and tracking BGC (biogeochemical) floats. There is no financial cost to adopting a float. Teachers, students and scientists have expressed strong support for the program, citing a unique opportunity to interact around a shared passion for not only better understanding the Southern Ocean's outsized role in our climate system but also improving climate models for the global ocean.

2.5.2. Material and methods

2.5.2.1. Float Deployment

Ten biogeochemical profiling floats were successfully deployed during the expedition. All ten floats were adopted and named by educators, classrooms, programs, and schools in the US and Canada, with ages ranging from grade 4 through grade 12.

Table 2.5.1. Float deployments during ANA13B

Float ID (UW)	Type	Sta #	Date (UTC)	Time (UTC)	Latitude	Longitude	Adopt-a-float name
1121	Navis	Argo1	12 JAN 2023	01:01	-50.0004	153.0837	Adventure
1119	Navis	ANA13B-01	13 JAN 2023	20:49	-58.3273	160.9760	Project Smiley
21951	Apex	Argo2	14 JAN 2023	04:04	-59.9998	160.9878	HK LEO
20109	Apex	Argo3	14 JAN 2023	12:30	-62.0004	160.9886	Angel Ice Cream Float
21302	Apex	Argo4	14 JAN 2023	21:05	-63.9985	160.9876	Davis Drive Davie Dolphin
21871	Apex	ANA13B-41	26 JAN 2023	00:15	-74.9012	175.4942	Sir Float a Lot
21838	Apex	ANA13B-50	27 JAN 2023	10:17	-74.9008	179.9953	My Buddy Eric
20572	Apex	ANA13B-61	29 JAN 2023	14:00	-76.0998	-175.0060	QE Explorer
21803	Apex	ANA13B-80	01 FEB 2023	07:34	-77.7999	-169.9967	Ariana Grande
21888	Apex	ANA13B-103	06 FEB 2023	12:37	-77.3982	-162.2963	TIMA Tide 2023



Figure 2.5.1. Shelf float 20572 (QE Explorer) is launched from the deck of the IBRV Araon.

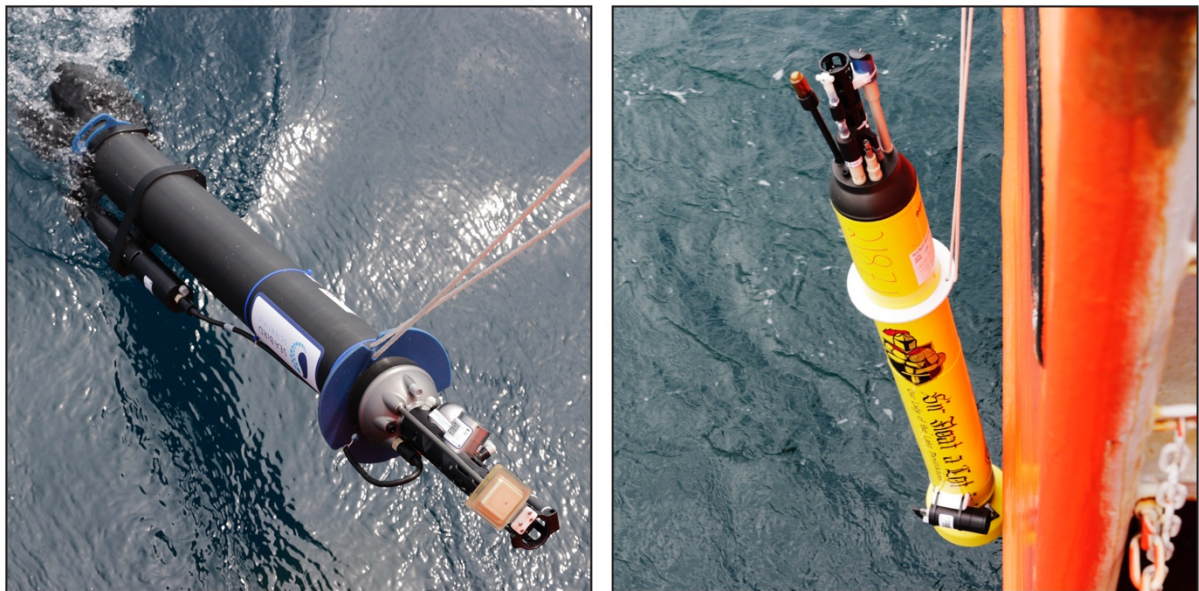


Figure 2.5.2. Deploying a Navis (L) and Apex (R) float.



Figure 2.5.3. Artwork on all ten adopted floats aboard the IBRV Araon.

2.5.2.2. HPLC Sampling

At six of the float deployment stations where CTD casts were also completed, water samples were collected to be processed for High Performance Liquid Chromatography (HPLC). Approximately two litres of seawater were collected from two depths at each station: the surface and the chlorophyll maximum (as determined by the CTD profile). An additional two litres were collected as a duplicate sample at one of the depths at each

station, alternating between surface and chlorophyll maximum between stations. Water samples were processed through vacuum filtration and then the filtered samples were frozen at -80°C. Upon disembarkation, the samples will be shipped in a dry shipper to Scripps Institute of Oceanography to be further processed and analyzed.

Table 2.5.2. Water samples processed for HPLC during ANA13B.

	sta & cast	niskin	trip depth	Bottle IDs	Type HPLC/POC	seq #	volume
float #	1119						
total water depth =	4290	ANA13B01-01	22	0	1,2	HPLC	1 2124
Lat N (dec degrees)	-58.3334	ANA13B01-01	22	0	3,4	HPLC	2 2121
Long E (dec degree)	160.9878	ANA13B01-01	16	75	5,6	HPLC	3 2139
GMT date (yyyymmdd)	20230113						
float #	21871						
total water depth =	292	ANA13B41-01	24	0	1,2	HPLC	1 2124
Lat N (dec degrees)	-74.9000	ANA13B41-01	20	35	3,4	HPLC	2 2121
Long E (dec degree)	175.4999	ANA13B41-01	20	35	5,6	HPLC	3 2139
GMT date (yyyymmdd)	20230125						
float #	21838						
total water depth =	418.5	ANA13B50-01	16	60	1,2	HPLC	1 2124
Lat N (dec degrees)	-74.9000	ANA13B50-01	22	0	3,4	HPLC	2 2121
Long E (dec degree)	179.9996	ANA13B50-01	22	0	5	HPLC	3 1068
GMT date (yyyymmdd)	20230127						
float #	20572						
total water depth =	547	ANA13B61-01	14	20	1,2	HPLC	1 2124
Lat N (dec degrees)	-76.1000	ANA13B61-01	14	20	3,4	HPLC	2 2121
Long E (dec degree)	174.9998	ANA13B61-01	24	0	5,6	HPLC	3 2139
GMT date (yyyymmdd)	20230129						
float #	21803						
total water depth =	542	ANA13B80-01	22	0	1,2	HPLC	1 2124
Lat N (dec degrees)	-77.8000	ANA13B80-01	22	0	3,4	HPLC	2 2121
Long E (dec degree)	-170.0000	ANA13B80-01	19	35	5,6	HPLC	3 2139
GMT date (yyyymmdd)	20230201						
float #	21888						
total water depth =	645	ANA13B103-01	21	20	1,2	HPLC	1 2124
Lat N (dec degrees)	-77.3978	ANA13B103-01	21	20	3,4	HPLC	2 2121
Long E (dec degree)	-162.2889	ANA13B103-01	24	0	5,6	HPLC	3 2139
GMT date (yyyymmdd)	20230206						

2.5.3. Preliminary results and discussion

Sensors on all floats are working properly and floats have successfully returned their first profiles. The five deep-water floats are central to maintaining circumpolar coverage for SOCCOM/GO-BGC. The first float deployed (#1121) returned some inconsistent data, so an updated pH calibration file was obtained from Seabird. The data has now been reprocessed and the pH is now consistent with nearby floats. The profile shown for #1121 in Figure 2.5.4 shows the first 2 profiles with the updated calibration.

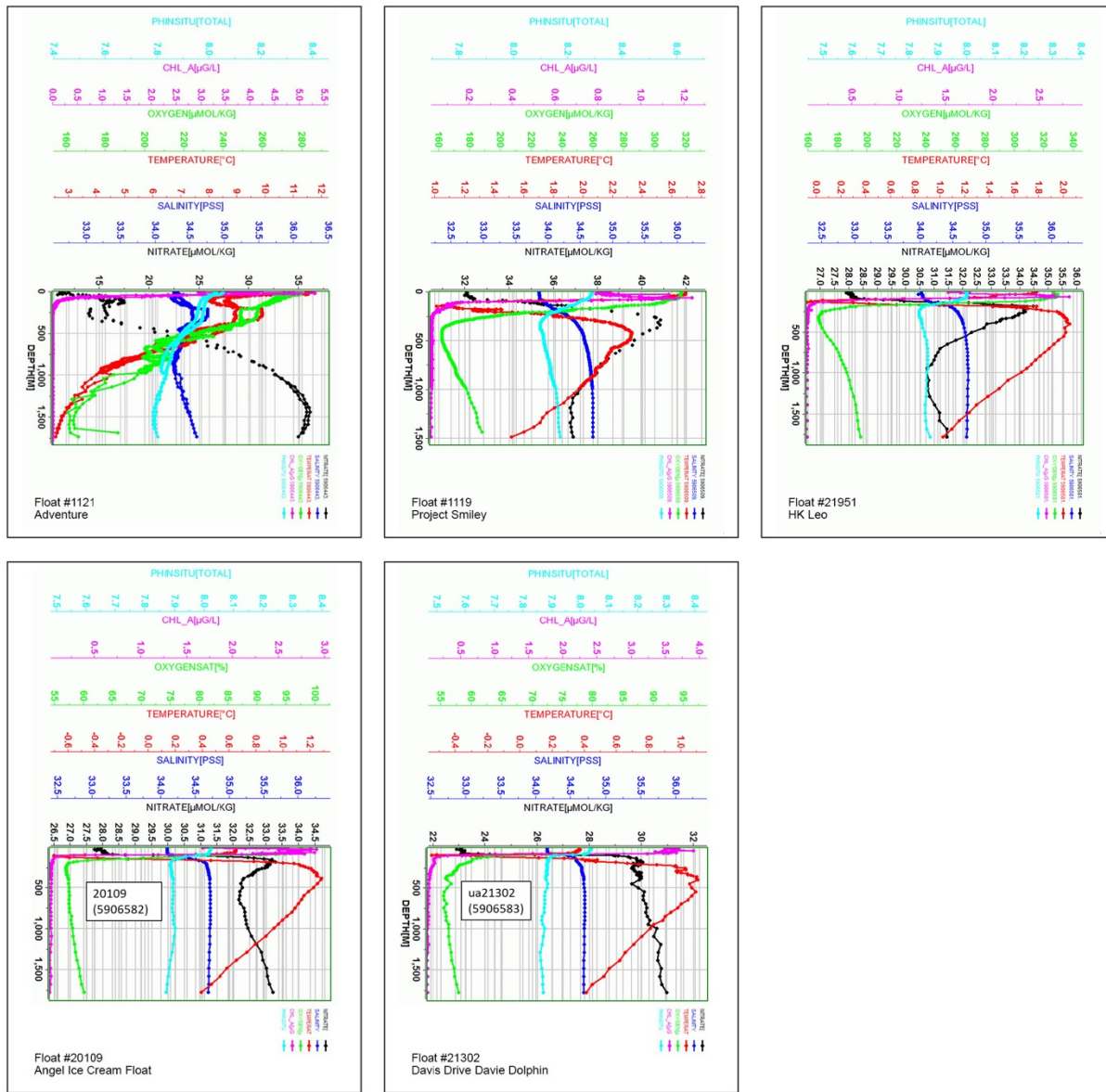


Figure 2.5.4. Profiles from the five floats deployed during transit in the Southern Ocean.

The five shelf floats, which are a special supplementary program within SOCCOM, are particularly exciting as they now include the southernmost floats in the program.

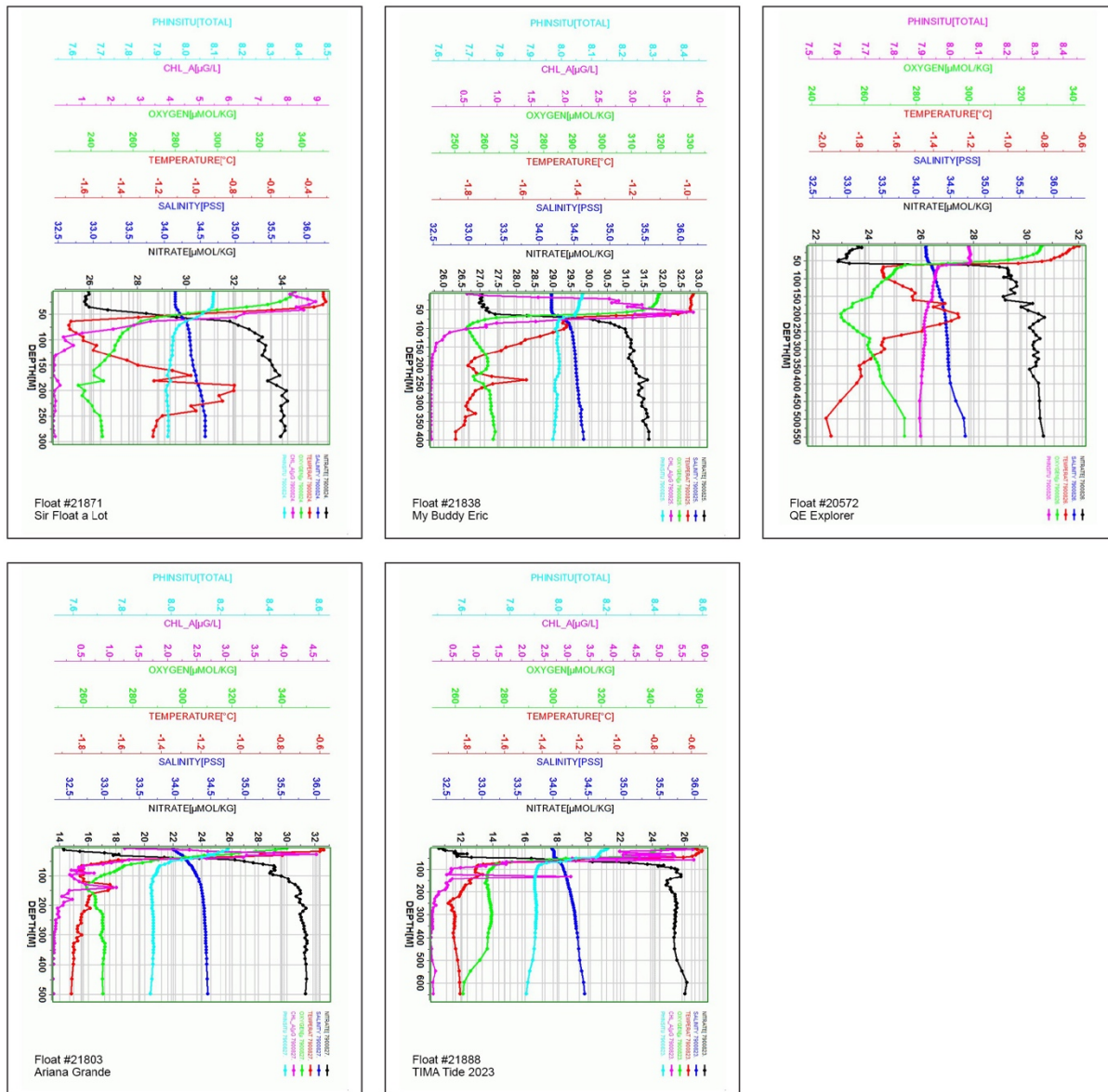


Figure 2.5.5. Profiles from the five shelf floats deployed in the Ross Sea.

All of the float data will be in the public domain through the Argo GDAC, although they might not appear there until after initial processing is completed and links are set up. All floats were funded by NSF through the separate programs SOCCOM and GO-BGC, so the internal processing and links appear in both projects at the following websites:

<http://soccom.princeton.edu/> Click on **Observations > Map Room** for interactive map

<https://www.go-bgc.org/> Click on **Map Room > Float Locations and Data** for interactive maps, listings, etc.

On both interactive maps, you can hover over the float dot and get a link to data sets.

Table listings for both SOCCOM and GO-BGC can be found in the GO-BGC webpage. The direct links to the tables are as follows:

Table 2.5.3. Floats available at http://go-bgc.ucsd.edu/GOBGC_float_performance.html

WMO	Serial Number	Float Name	Ship Station
5906581	21951	HK Leo	Argo2
5906582	20109	Angel Ice Cream Float	Argo3
5906583	21302	Davis Drive Davie Dolphin	Argo4

Table 2.5.4. Floats available at http://socomm.ucsd.edu/SOCCOM_float_performance.html

WMO	Serial Number	Float Name	Ship Station
5906443 (SBE Navis)	1121	Adventure	Argo1
5906509 (SBE Navis)	1119	Project Smiley	ANA13B01
7900824	21871	Sir Float a Lot	ANA13B41
7900825	21838	My Buddy Eric	ANA13B50
7900826	20572	QE Explorer	ANA13B61
7900827	21803	Ariana Grande	ANA13B80
7900823	21888	Tima Tide 2023	ANA13B103

References

- ¹ A. K. Morrison, T. L. Frölicher, J. L. Sarmiento. "Upwelling in the Southern Ocean" Physics Today. 68 (1), 27. 2015. For more information, contact socomm@climatecentral.org

Chapter 3. Biological Oceanography

3.1. Phytoplankton Ecology

Youngju Lee

Korea Polar Research Institute, Incheon, Republic of Korea

E-mail: yjlee@kopri.re.kr

3.1.1. Introduction

The Southern Ocean is a net sink for atmospheric CO₂ on annual timescales, accounting for 20% of global ocean (Takahashi et al., 2009) due to high primary productivity (Arrigo et al., 2008). Phytoplankton bloom appeared in austral summer in the coastal Polynya which is local areas of reduced ice cover that generally form due to offshore katabatic winds and seasonal ice melt (Tremblay and Smith, 2007). In the growing season, higher insolation and thinner sea ice allow sufficient irradiance to penetrate and drive photosynthesis in this continental shelf area. Seasonal variation of phytoplankton biomass and primary production in the Antarctic shelf waters plays an important role in the biogeochemical cycle in the Southern Ocean.

Several researches have been intensively studied the dynamics of phytoplankton in the Antarctic coastal waters and revealed that diatoms and prymnesiophyte *Phaeocystis antarctica* formed massive bloom in different season and area in the coastal waters (Arrigo et al., 1999). However, variations occur among years not only in the dominant rate of these two major groups, but also in the controlling mechanisms, and it is hard to predict their distribution (Smith Jr et al., 2006). Moreover, most studies were mainly concerned with regions in the western area of the Ross Sea, Weddell Sea, and eastern Antarctica (Arrigo et al., 1999; Lancelot et al., 1993; Wright et al., 2010).

Ross Sea Polynya (ASP) is the most productive area of the 37 identified coastal polynya systems in the Antarctic (Arrigo and van Dijken, 2003). However, phytoplankton community distribution has rarely been reported in the eastern area of the Ross Sea. Therefore, the distribution and response of whole phytoplankton groups in the Ross Sea including the Little American basin area need to be understood for prediction of phytoplankton response under

climate change.

3.1.2. Materials and methods

3.1.2.1. Field survey

Field survey was conducted onboard the Korean Research IBRV Araon in the Ross Sea during austral summer from January 14 ~ February 8, 2023 (Fig. 3.1.1). Water samples for chlorophyll *a* (Chl-a) concentration, picophytoplankton, and pigments were collected from 2~12 depths in the whole water column using a 10-L PVC Niskin water sampler attached to a CTD rosette system (Table 1).

3.1.2.2. Total and size-fractionated Chl-a concentration

Subsamples from the Niskin bottles were filtered through a cascade connection of 20- μm nylon mesh, Nuclepore filter (Whatman International) with pore size of 3 μm , and a Whatman GF/F filter to determine size-fractionated Chl-a (Sieburth 1978). Thus, micro-Chl-a (>20 μm), nano-Chl-a (3-20 μm), and pico-Chl-a (<3 μm) could be measured directly. Subsamples for total Chl-a were filtered onto 47 mm GF/F Whatman filters. Each filter was extracted in 90% acetone, and Chl-a concentrations were measured with a fluorometer (model Trilogy, Turner Designs, USA; method: Parsons et al., 1984).

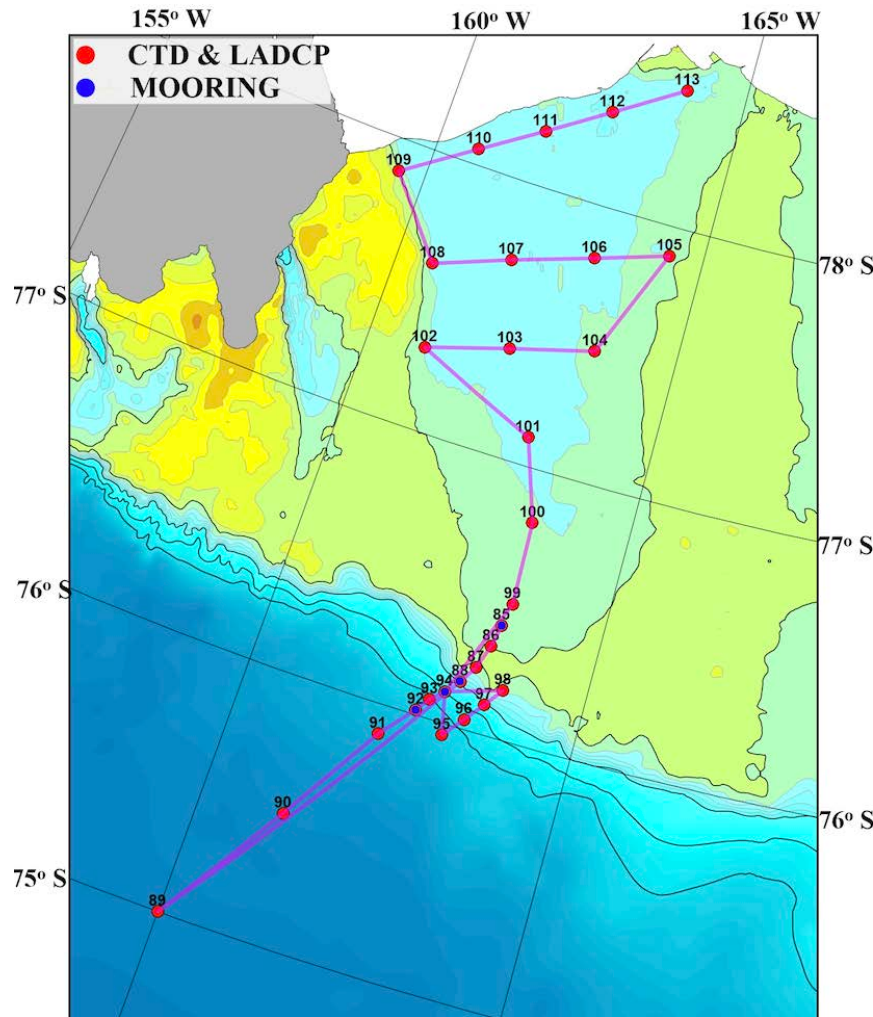


Figure 3.1.1. Sampling stations of phytoplankton community in the Little American Basin area of the Ross Sea during the 2023 cruise.

Table 3.1.1. Stations for phytoplankton biomass and community structure during the 2023 cruise

Station	Sampling time (Local, GMT+13)	Latitude	Longitude	Phytoplankton Net	Chl-a concentration	Size-fraction chl-a	Picophytoplankton abundance	Photosynthetic pigments
ANA13B001	2023.1.14 7:33	58° 20.0013' S	160° 59.2677' E	x	o	o	o	o
ANA13B002	2023.1.16 9:50	68° 10.7855' S	165° 40.0855' E	o	o	o	o	o
ANA13B085	2023.2.2 17:00	76° 24.6301' S	163° 27.4873' W	o	o	o	o	o
ANA13B087	2023.2.3 0:31	76° 14.0705' S	163° 15.9754' W	x	o	x	x	o
ANA13B088	2023.2.3 16:30	76° 10.0512' S	163° 5.9200' W	o	o	o	o	o
ANA13B089	2023.2.3 22:54	74° 59.9994' S	159° 59.9969' W	o	o	o	o	o
ANA13B090	2023.2.4 8:05	75° 30.0013' S	161° 12.7187' W	o	o	o	o	o
ANA13B091	2023.2.4 16:24	75° 53.4922' S	162° 9.6230' W	o	o	o	o	o
ANA13B092	2023.2.5 5:37	76° 1.1600' S	162° 35.2460' W	o	o	o	o	o
ANA13B094	2023.2.5 17:18	76° 6.9217' S	162° 55.2736' W	x	o	x	x	o
ANA13B099	2023.2.6 7:36	76° 29.8524' S	163° 31.5554' W	x	o	x	x	o
ANA13B100	2023.2.6 11:44	76° 48.4090' S	163° 27.8434' W	o	o	o	o	o
ANA13B101	2023.2.6 16:18	77° 6.3110' S	163° 0.4720' W	o	o	o	o	o
ANA13B102	2023.2.6 20:12	77° 18.2208' S	160° 56.8858' W	x	o	x	x	o
ANA13B103	2023.2.7 0:18	77° 23.8625' S	162° 17.3253' W	o	o	o	o	o
ANA13B104	2023.2.7 4:30	77° 28.7858' S	163° 38.7838' W	x	o	x	x	o
ANA13B105	2023.2.7 7:37	77° 53.5688' S	164° 24.7721' W	x	o	x	x	o
ANA13B106	2023.2.7 10:00	77° 48.4595' S	163° 11.3989' W	x	o	x	x	o
ANA13B107	2023.2.7 13:59	77° 42.6327' S	161° 51.1790' W	o	o	o	o	o
ANA13B108	2023.2.7 17:05	77° 36.2863' S	160° 36.9695' W	x	o	x	x	o
ANA13B109	2023.2.7 21:23	77° 52.9364' S	159° 32.5006' W	o	o	o	o	o
ANA13B110	2023.2.8 0:13	78° 3.4997' S	160° 42.9781' W	x	o	x	x	o
ANA13B111	2023.2.8 3:53	78° 11.9898' S	161° 43.3673' W	o	o	o	o	o
ANA13B112	2023.2.8 6:30	78° 20.4361' S	162° 44.9708' W	x	o	x	x	o
ANA13B113	2023.2.8 11:14	78° 29.7475' S	163° 55.3981' W	o	o	o	o	o

3.1.2.3. Phytoplankton community structure

To estimate the phytoplankton abundance, water samples from Niskin bottles were collected in 200-mL high density polyethylene bottles, preserved with glutaraldehyde (final concentration 1%), and stored at 4°C until analysis. Sample volumes of 50 - 150 mL were filtered through nucleopore filters (0.8 µm pore size, black, 25 mm diameter). During filtration, the samples were drawn down until 5 mL remained in the filtration tower. Concentrated DAPI (50 µg mL⁻¹ final concentration) was then added and allowed to sit briefly (5 seconds) before filtering the remaining sample until dry (Taylor et al., 2011). The total 100 slides were made for identifying species compositions of phytoplankton.

Phytoplankton was sampled with 20 µm mesh plankton net hauled vertically from 100 m to the surface. The samples were preserved with Lugol's solution (final concentration 1%) and

will be transported to the laboratory for further analysis.

3.1.2.4. Heterotrophic bacteria and picophytoplankton abundance

Water samples for flow cytometry analysis were fixed for 15 min with paraformaldehyde (final concentration: 1%) and stored at -80 °C. Since fixation with added chemical reagents may result in loss of cells, natural samples were also analyzed on a Accuri C6 flow cytometer (Becton Dickinson) equipped with an air-cooled argon laser (488 nm, 15 mW), placed on-board so that after sample collection the analyses could immediately be performed. Picophytoplankton groups were identified and their abundance enumerated using the characteristics of 90°-angle light scatter, orange fluorescence from phycoerythrin, and red fluorescence from chlorophyll (Marie et al., 1997). For the enumeration of heterotrophic bacteria, seawater samples were stained with SYBR green I (Molecular Probes), and incubated in the dark at room temperature for 15 min before analysis. Bacteria were identified for their side light scatter and green fluorescence signals. Raw data from the flow cytometer will be processed using the FlowJo program (Tree Star, www.flowjo.com).

3.1.2.5. Photosynthetic pigments

The CHEMTAX program based on photosynthetic pigments data has potential benefits for the estimation of phytoplankton composition, including small and fragile forms. For photosynthetic pigments analysis, 0.5~4 L subsamples from the Niskin bottles were filtered onto 47 mm GF/F Whatman filters, flash frozen in liquid nitrogen, and stored at -80 °C until analysis. The pigments will be analyzed with high performance liquid chromatography (HPLC) in the laboratory.

3.1.2.6. Automated continuous measurements

Continuous variables were measured while underway, using the seawater supply of the ship, at a nominal depth of 7 m along the cruise track (Fig. 3.1.2). Seawater temperature and salinity were measured using a thermosalinograph (SBE45). Chlorophyll fluorescence was measured

using a Algae Online Analyzer (Fig. 3.1.3 and 3.1.4). Surface photosynthetically active radiation (PAR) was determined using a quantum sensor (LI-1500, LI-COR Inc., USA) every 5 min during the cruise (Fig. 3.1.5).

Phytoplankton species abundance was acquired with the Imaging FlowCytobot (IFCB), which collects images of particles containing chlorophyll fluorescence (Fig. 3) (Olson and Sosik, 2007). The seawater continuously flowed into a sample reservoir (approximately 2 L), and the bottom water (typically 5 mL) of the reservoir was pumped into the sample syringe of the IFCB. A Nitex screen with a mesh size of 150 µm was placed over this sample intake to prevent larger particles from clogging the flow cell.

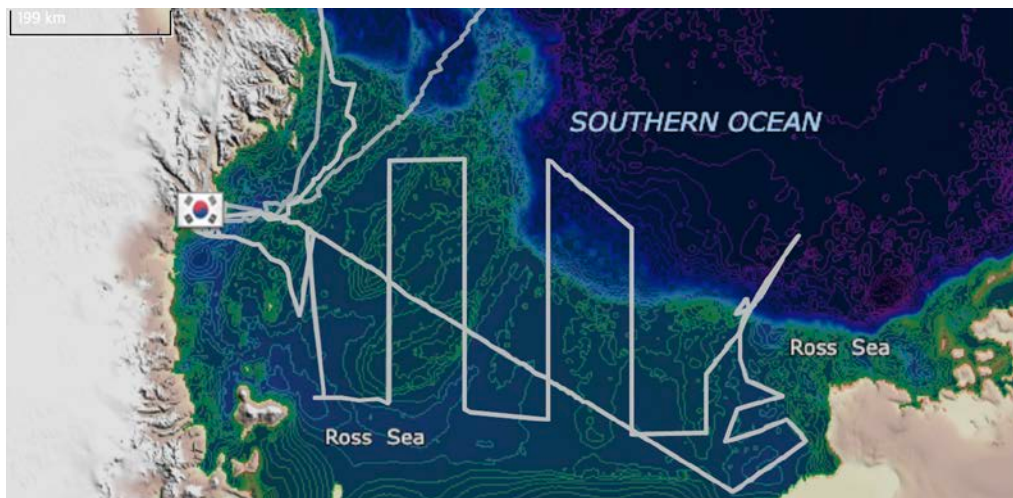
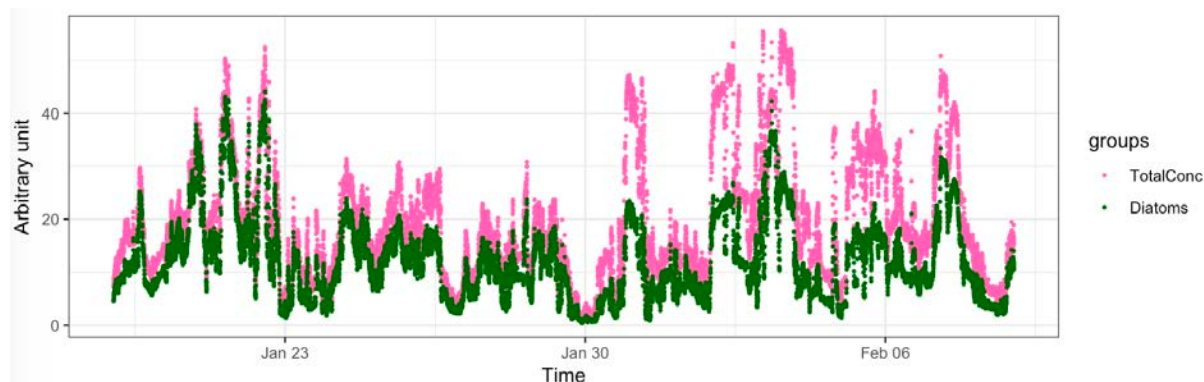


Figure 3.1.2. Cruise track of the IBRV in the Ross Sea coastal waters during the 2023 cruise.



Figure 3.1.3. Continuous measurements phytoplankton groups biomass and species abundance using the Algae Online Analyzer and the Imaging FlowCytobot, respectively in the Ross Sea coastal waters during the 2023 cruise.

(a)



(b)

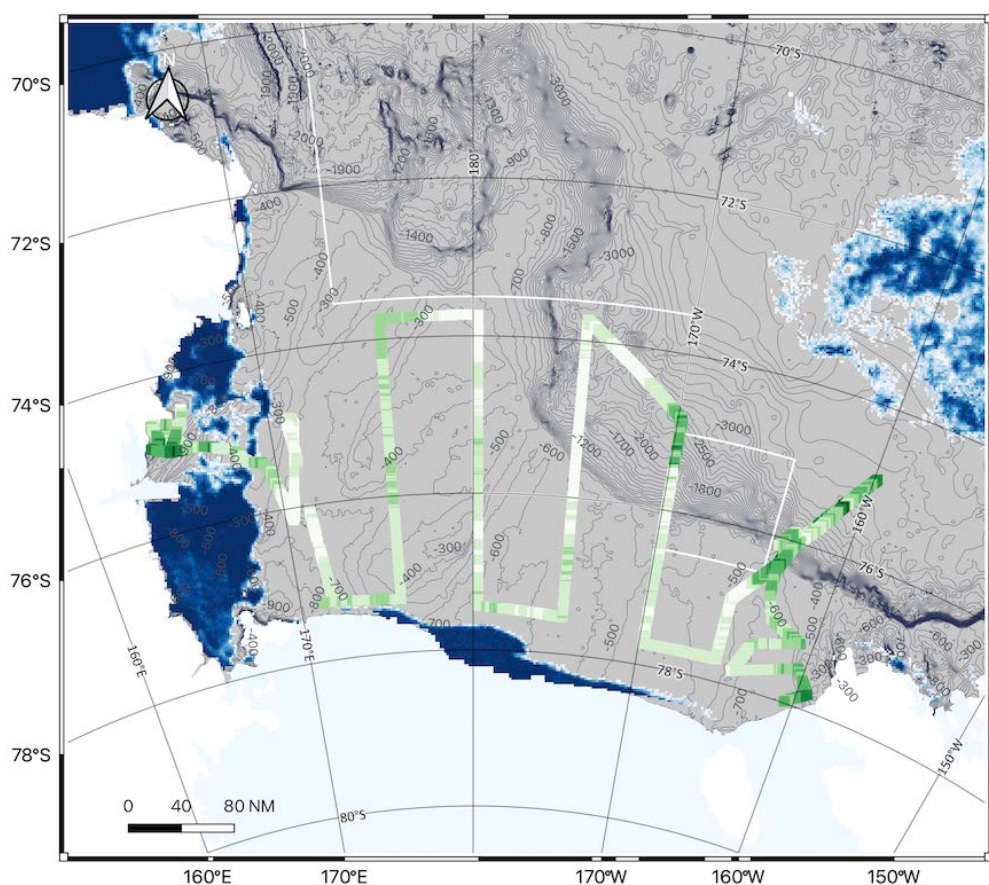


Figure 3.1.4. (a) Time series of the phytoplankton biomass (Chlorophyll fluorescence, arbitrary unit) and diatoms contribution and (b) spatial distribution of phytoplankton biomass (Chlorophyll fluorescence, arbitrary unit) using the Algae Online Analyzer along the 2023 cruise track in the Ross Sea, Antarctica (Preliminary results).

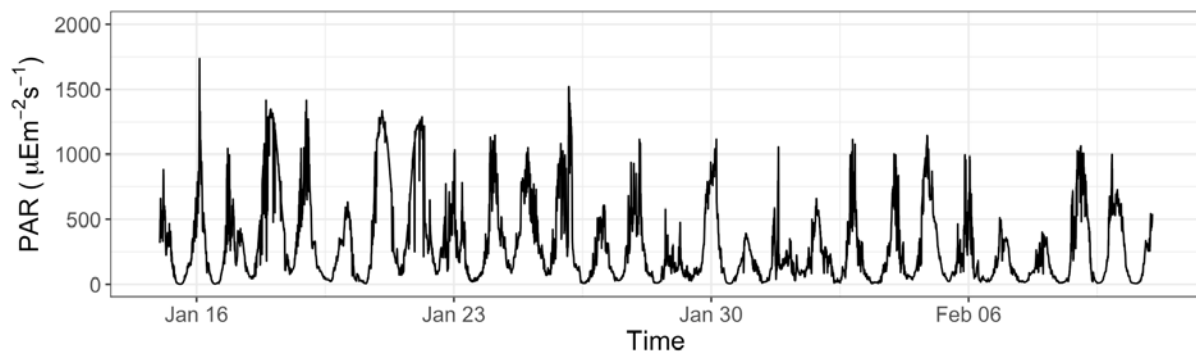


Figure 3.1.5. Photosynthetically active radiation, PAR ($\mu\text{Em}^{-2}\text{s}^{-1}$) throughout the field survey in the Ross Sea area.

3.1.2.7. Experimental design for iron and light limitation

Experiments were conducted during the Ross Sea cruise in January and February 2023, onboard the icebreaker Araon. For the experiments, 20 - 60 L water was collected from the mixed layer (10m depth) at four stations using the Niskin-X samplers in the clean container. Water collected into a 2-L or 4-L cubitainer. Half of the bottles were added iron (4 nM) at the beginning of the experiment. Bottles were incubated in two light controlled deck-board incubators. Two incubators were screened to 70% and 99% of incident light, respectively, using sunscreen filters and those were kept at sea surface temperature. Bottles were incubated for seven days, after which three different treatments were applied to triplicate bottles and subsampled at noon. Samples were taken at time zero, on day 3 and the final day for iron concentration, macro nutrients concentrations, phytoplankton species abundance. Samples for photosynthetic pigments were taken on the initial and final days of the experiments.

References

- Arrigo, K.R., Robinson, D.H., Worthen, D.L., Dunbar, R.B., DiTullio, G.R., VanWoert, M., Lizotte, M.P., 1999. Phytoplankton community structure and the drawdown of nutrients and CO₂ in the Southern Ocean. *Science* 283 (5400), 365-367.
- Arrigo, K.R., van Dijken, G., Long, M., 2008. Coastal Southern Ocean: A strong anthropogenic CO₂ sink. *Geophysical Research Letters* 35 (21).
- Arrigo, K.R., van Dijken, G.L., 2003. Phytoplankton dynamics within 37 Antarctic coastal

- polynya systems. *Journal of Geophysical Research: Oceans (1978–2012)* 108 (C8).
- Lancelot, C., Mathot, S., Veth, C., de Baar, H., 1993. Factors controlling phytoplankton ice-edge blooms in the marginal ice-zone of the northwestern Weddell Sea during sea ice retreat 1988: field observations and mathematical modelling. *Polar Biology* 13 (6), 377-387.
- Marie, D., Partensky, F., Jacquet, S., Vaultot, D., 1997. Enumeration and cell cycle analysis of natural populations of marine picoplankton by flow cytometry using the nucleic acid stain SYBR Green I. *Appl. Environ. Microbiol.* 63 (1), 186-193.
- Olson, R.J., Sosik H.M., 2007. A submersible imaging-in-flow instrument to analyze nano- and microplankton: Imaging FlowCytobot. *Limnol. Oceanogr. Methods* 5, 195-203.
- Parsons, T., Maita, Y., Lalli, C., 1984. Fluorometric determination of chlorophylls A manual of chemical and biological methods for seawater analysis. ed. T Parsons et al., Oxford: Pergamon, p. 173.
- Sieburth, J.McN., 1978. Pelagic ecosystem structure: Heterotrophic compartments of the plankton and their relationship to plankton size fractions. *Limnology and Oceanography*, 23: 1256-1263.
- Smith Jr, W.O., Shields, A.R., Peloquin, J.A., Catalano, G., Tozzi, S., Dinniman, M.S., Asper, V.A., 2006. Interannual variations in nutrients, net community production, and biogeochemical cycles in the Ross Sea. *Deep-Sea Research Part II: Topical Studies in Oceanography* 53 (8-10), 815-833.
- Takahashi, T., Sutherland, S.C., Wanninkhof, R., Sweeney, C., Feely, R.A., Chipman, D.W., Hales, B., Friederich, G., Chavez, F., Sabine, C., 2009. Climatological mean and decadal change in surface ocean pCO₂, and net sea-air CO₂ flux over the global oceans. *Deep Sea Research Part II: Topical Studies in Oceanography* 56 (8), 554-577.
- Taylor, A.G., Landry, M.R., Selph, K.E., Yang, E.J., 2011. Biomass, size structure and depth distributions of the microbial community in the eastern equatorial Pacific. *Deep Sea Research Part II: Topical Studies in Oceanography* 58 (3), 342-357.
- Tremblay, J.-É., Smith, W., 2007. Primary production and nutrient dynamics in polynyas. *Elsevier Oceanography Series* 74, 239-269.
- Wright, S.W., van den Enden, R.L., Pearce, I., Davidson, A.T., Scott, F.J., Westwood, K.J., 2010. Phytoplankton community structure and stocks in the Southern Ocean (30-80°E) determined by CHEMTAX analysis of HPLC pigment signatures. *Deep-Sea Research Part II: Topical Studies in Oceanography* 57 (9-10), 758-778.

3.2. Microzooplankton Community and Grazing

Hyeju Yoo, Jong Kuk Moon

Korea Polar Research Institute, Incheon, Republic of Korea

E-mail: hjyoo@kopri.re.kr; jkmoon@kopri.re.kr

3.2.1. Introduction

Heterotrophic protists ingest a broad size spectrum of prey, from bacteria to phytoplankton, and are themselves important prey items for mesozooplankton. Many researchers suggest that heterotrophic protists contribute to the trophic linkage between phytoplankton and mesozooplankton and are important in the pelagic food webs of many oceanic waters. Microzooplankton defined as taxa ranging in size 20-200 µm and usually are dominated by ciliate and dinoflagellate taxa. The importance of heterotrophic protists in pelagic ecosystems has become increasingly evident in the past two decades, and trophic interaction between heterotrophic protists and phytoplankton has been reported in various marine. However, there is no information on the relative importance of heterotrophic protists in the pelagic ecosystem of the Ross Sea. In the past, many heterotrophic protist studies in Antarctic water have focused on the waters of the Weddell Sea and Antarctic Peninsula. While the Ross Sea is today one of the best studied of the Antarctic Seas related to the dynamics of phytoplankton, the microzooplankton have been relatively neglected. In this study area, we investigated the meso-scale variations and structure of heterotrophic protist communities and grazing rates on phytoplankton in the various environmental conditions such as open ocean. During this cruise, we investigated protozoa abundance, biomass in total 13 stations. Experiment for grazing rates of heterotrophic protists was conducted in total 10 stations. (Table 3.2.1).

3.2.2. Materials and methods

3.2.2.1. Abundance and community structure of heterotrophic protists

To determine the abundance of heterotrophic protists, a CTD-Niskin rosette sampler was used to take water samples from the following 3 or 4 depths. For ciliates and sarcodina, 500

ml water from the vertical profiles was preserved with 1% acid Lugol's iodine solution these samples were then stored in darkness. For heterotrophic nanoflagellates and heterotrophic dinoflagellates smaller than 20 µm, 500 ml of water was preserved with glutaraldehyde (0.5% final concentration) and stored at 4° C.

3.2.2.2. Grazing experiments

Grazing rates of heterotrophic protists were determined by the dilution method (Landry and Hassett 1982). Water for grazing experiments was collected from 2 depth (surface, SCM) of each station, and gently filtered through a 200 µm mesh. Due to using 200 µm pre-screened sea water, the water in incubation for microzooplankton grazing on phytoplankton included all of <200µm grazers (e.g. small heterotrophic and mixotrophic flagellates, the larger ciliates and heterotrophic and mixotrophic dinoflagellates). At each station, 20L seawater were collected in a Niskin bottle and transferred to a polycarbonate carboy. Part of this water was filtered through the 0.22-µm filtration system. Dilution series were set up in ten 1.3-l PC bottles. Ten bottles were used to establish a nutrient-enriched dilution series consisting of replicate bottles with 20% and 100% natural seawater. The bottles were incubated on deck for 24 – 48 h at ambient sea surface temperatures and screened to the ambient light level with neutral density screening (Figure 3.2.1). Subsamples were collected from replicate bottles at 0 and 24-48h to determine chlorophyll-a concentrations.

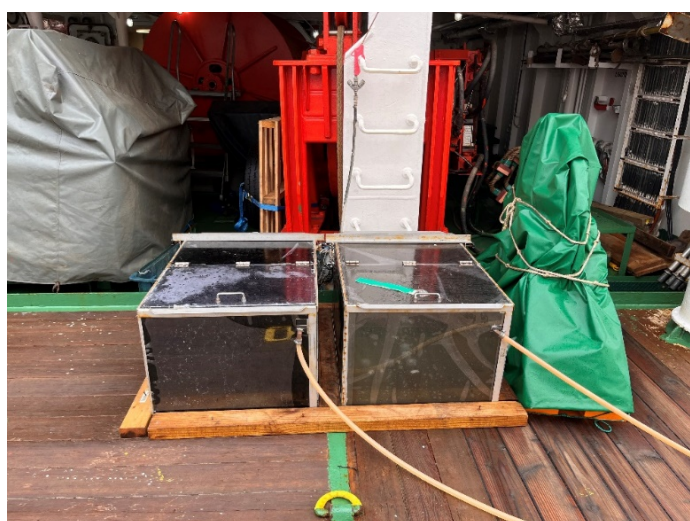


Figure 3.2.1. Incubation for grazing experiments.

Table 3.2.1. Sampling locations of heterotrophic protists community structure and grazing rates during the ANA13B 2023 SOLOMON cruise

Cruise	St.	Lat_Deg10	Lon_Deg10	Depth (m)	Net (Depth)	Net (Volume)	Heterotrophic protists community	Grazing Exp. (Depth)
ANA13B(SOLOMON)	85	-76.4104667	-163.4581	537	-	-	o	0m, 22m
ANA13B(SOLOMON)	88	-76.1674833	-163.0986	970	100m	190ml	o	0m, 30m-
ANA13B(SOLOMON)	89	-75.0000000	-160.0000	3797	100m	150ml	o	0m, 22m
ANA13B(SOLOMON)	90	-75.5000000	-161.2121	3616	100m	190ml	o	-
ANA13B(SOLOMON)	91	-75.8915333	-162.1612	2746	100m	210ml	o	0m, 30m-
ANA13B(SOLOMON)	92	-76.0193667	-162.5866	2247	100m	300ml	o	-
ANA13B(SOLOMON)	100	-76.8069667	-163.4635	577	100m	350ml	o	0, 20m-
ANA13B(SOLOMON)	101	-77.1051333	-163.0070	649	100m	250ml	o	-
ANA13B(SOLOMON)	103	-77.3977667	-162.2888	711	100m	360ml	o	0m, 22m
ANA13B(SOLOMON)	107	-77.7105333	-161.8530	681	100m	330ml	o	0m, 25m-
ANA13B(SOLOMON)	109	-77.8823333	-159.5418	498	100m	390ml	o	0m, 15m
ANA13B(SOLOMON)	111	-78.1997500	-161.7233	675	100m	290ml	o	0m, 10m-
ANA13B(SOLOMON)	113	-78.4957000	-163.9230	630	100m	230ml	o	0m, 38m

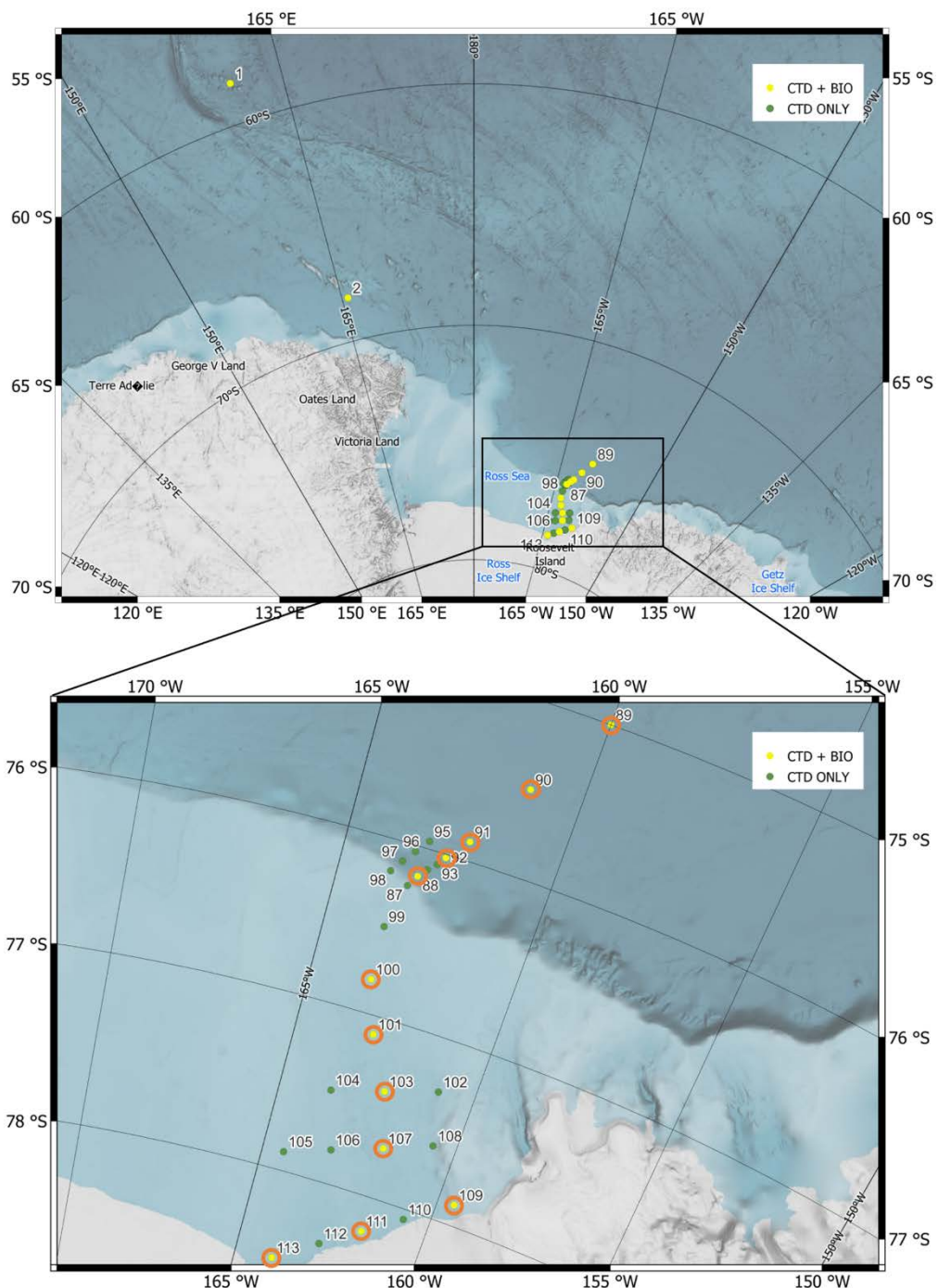


Figure 3.2.2. A map shows study area(Little America Basin, Ross Sea) and sampling stations during the 2023 Antarctic cruise. Small orange circles represent the station conducting experiment for grazing rates of heterotrophic protists.

3.3. Mesozooplankton Ecology

Jee-Hoon Kim

Korea Polar Research Institute, Incheon, Republic of Korea

E-mail: jeehoonkim@kopri.re.kr

3.3.1. Introduction

Across the whole oceans, mesozooplankton are easily affected by the physical fluctuations of the oceans that accompany climate change (due to their short lifespan, small body size, and weak swimming capability), they have been used as ecological indicators for global climate change in the ocean. Mesozooplankton play a crucial role in the trophic web by transferring materials and energy from lower to higher trophic levels in the ocean, as well as in the biological carbon pump by exporting carbon vertically from the surface to the deep ocean and seabed in the ocean. In particular, several macrozooplankton taxa, including *Euphausia superba*, *Metridia* spp., *Clione* spp., *Limacina helicina*, and Chaetognaths are known to account for almost 90% of the total abundance of zooplankton in the Southern Ocean. For these reasons, many large-scale meso- and macrozooplankton surveys have been conducted to estimate the impact of climate change on the marine ecosystem in the Southern Ocean.

For instance, Long-term programs such as the Southern Ocean CPR survey have provided information on the patterns of abundance and distribution of zooplankton for much of East Antarctica; however, they do not cover the Little American Basin (LAB), the focus of the current study. The LAB is an area of significant ecological value, with high krill biomass, and seabirds, seals and whales, using the plateau for migration and feeding. Finally, to evaluate the effects of environmental factors on zooplankton distribution, and to determine whether distinct communities were associated with large-scale oceanographic features we applied multivariate statistics. This approach has the potential to provide powerful insights into the influence of environmental factors on zooplankton distributions in the Southern Ocean, particularly environmentally variable regions such as the LAB.

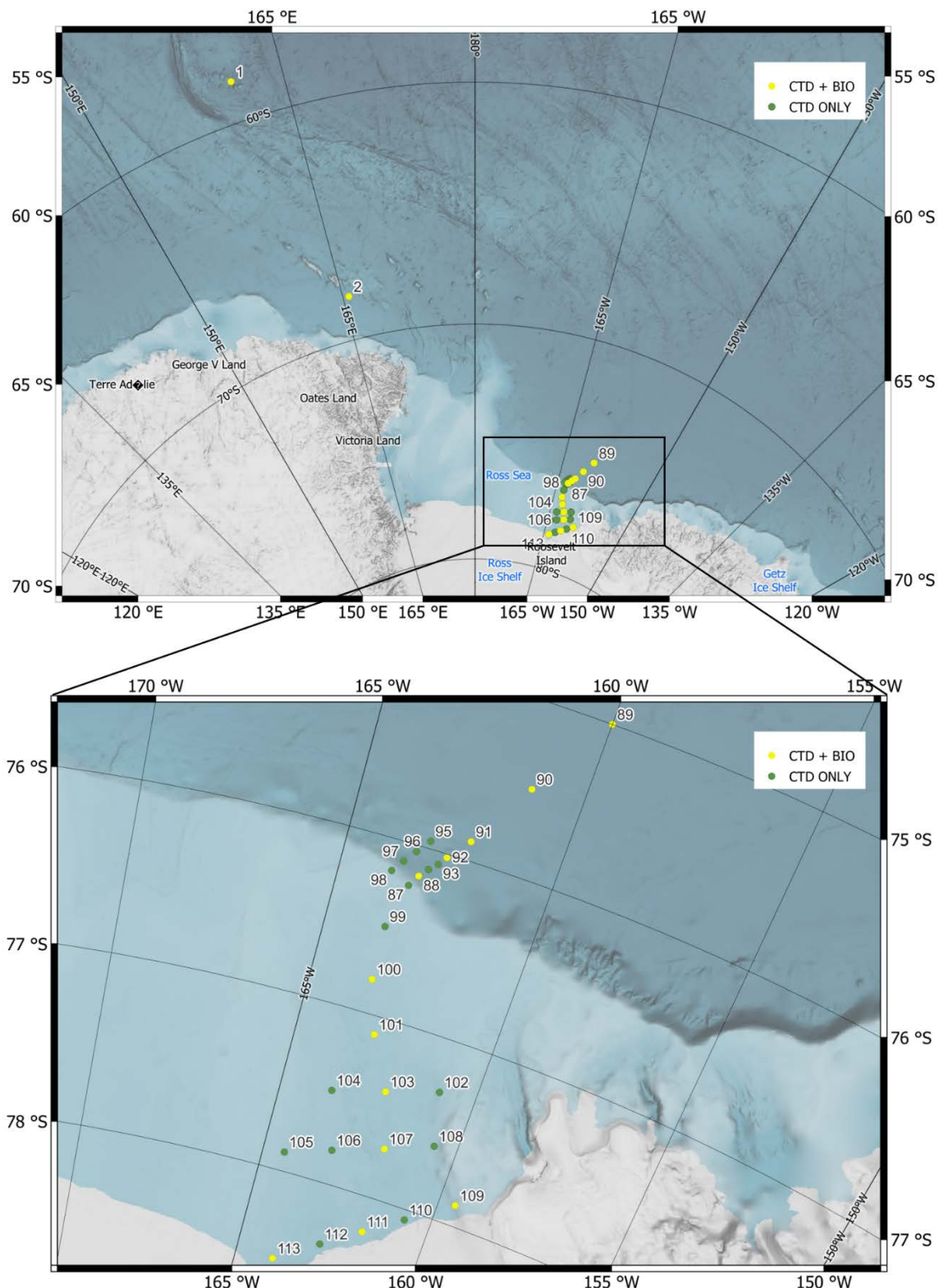


Figure 3.3.1. Study area with sampling sites during the 2023 Antarctic cruise (Yellow dots: Bio stations, Green dots: CTD only).

3.3.2. Material and method

Sample collection and Processing

Zooplankton net hauls were carried out in the LAB in 14 JAN 2023 to 08 FEB 2023 (Figure 3.3.1; Table 3.3.1). In all cases a bongo net was used, hauled vertically between 200 m and the surface. The bongo net and 150 net had 330 & 500 µm mesh and 150 µm mesh, respectively (a mouth diameter of 60 cm). There were 30 net hauls at 15 stations (Table 3.3.1), and the volume of seawater filtered was estimated from flow meter measurements. Samples were immediately fixed and preserved with 5% neutralized formaldehyde for quantitative analyses and were identified to the lowest taxonomic level using a microscope. Sub-samples from 500 µm net were transferred into 2 ml vial and 250 ml bottle with 99% ethanol, which were frozen at –20 °C for the post analysis.



Figure 3.3.2. Zooplankton Sampling with Bongo (330 and 500 µm mesh)

Table 3.3.1. Sampling locations of zooplankton composition during ANA12B

항차	St.	Date (Local)	Bongo (150X2)				Bongo (330, 500)			
			Time Start	Time End	Flow	Depth (m)	Time Start	Time End	Flow	Depth (m)
ANA13B	1	2023.01.14	9:30	9:42	1297	200	9:10	9:23	1093	200
ANA13B	2	2023.01.16	12:57	13:08	614	200	13:14	13:25	923	200
ANA13B	83	2023.02.02	17:43	17:56	423	200	18:07	18:21	675	200
ANA13B	88	2023.02.03	6:23	6:36	545	200	6:50	7:04	1181	200
ANA13B	89	2023.02.03	22:05	22:19	572	200	22:26	22:38	695	200
ANA13B	90	2023.02.04	8:49	9:03	635	200	9:10	9:24	982	200
ANA13B	91	2023.02.04	17:04	17:18	590	200	17:27	17:40	1051	200
ANA13B	92	2023.02.05	6:22	6:35	805	200	6:44	6:57	1183	200
ANA13B	100	2023.02.06	12:26	12:39	577	200	12:46	12:59	1086	200
ANA13B	101	2023.02.06	16:58	17:12	438	200	17:19	17:23	652	200
ANA13B	103	2023.02.07	0:56	1:11	483	200	1:16	1:28	883	200
ANA13B	107	2023.02.07	14:41	14:54	496	200	15:16	15:28	897	200
ANA13B	109	2023.02.07	22:02	22:14	505	200	22:23	22:35	1086	200
ANA13B	111	2023.02.08	4:29	4:43	306	200	4:49	5:03	1046	200
ANA13B	113	2023.02.08	11:55	12:09	354	200	12:14	12:27	636	200

3.3.3. Preliminary results and discussion

A total 13 taxonomic communities of zooplankton, Copepoda (Over 15 Species), Cnidaria, Chaetognatha, Pteropoda, Polychaeta (larvae), Cirriped (larvae), Euphausiacea, Amphipoda, Isopoda, Ostracoda, Tunicata, Fish larvae, Gastropoda (larvae), were identified at 15 stations. Copepods were dominant species with more than 60% of total meso-zooplankton communities at all stations. Copepod and Euphausiacea (Krill) are the most important biomass species and the prime omnivores in the Southern Ocean. The greatest diversity of Antarctic holo-zooplankton occurs within the copepods, which dominate the mesozooplankton community in both abundance and biomass (Kosobokova and Hopcraft, 2010). Copepods constitute over 80% of the total mesozooplankton community in Southern Ocean, which they play a major role in energy flow and biogeochemical cycles. Some of the ingested organic carbon of zooplankton is used for metabolic activities, so quantifying this carbon is of prime importance to better understand energy transfer and elemental cycling via zooplankton in Southern Ocean ecosystems.

3.4. Krill Acoustics

Wuju Son, Hyoung Sul La

Korea Polar Research Institute, Incheon, Republic of Korea

E-mail: swj5753@kopri.re.kr; hsla@kopri.re.kr

3.4.1. Introduction

The Ross Sea is noted for sustaining enhanced levels of biological production and biogeochemical activity during spring and summer (Arrigo, 2003). This place is considered significant regions from low- to high-trophic levels showing one of the most productive areas in the Southern Ocean. In addition, in recent, the Ross Sea was selected Marine Protect Area (MAP), which is the largest MPA of Southern Ocean. Thus, sustainable long-term observation would be necessary to monitor the marine ecosystems in the Ross Sea. The EK80 was run throughout ANA13B to collect information on the horizontal and vertical distribution of zooplankton and krill to derive estimates of zooplankton density around Cape Hallett. The overall purposes of acoustic observation are:

- To collect acoustic data to accompany all stations, transects, and net tows around Little America Basin during the Ross Sea survey.
- To determine the temporal and spatial distribution of relative abundance of krill around Little America Basin
- To estimate the krill density around Little America Basin

3.4.2. Materials and methods

3.4.2.1. Acoustic data

Multidisciplinary oceanographic survey was conducted from 2 to 8 February, 2023 during the Korean research ice breaker ARAON expedition. Acoustic data were collected using a multi-frequency echo sounder (EK80, Simrad) configured with down-looking 38, 120, and 200 kHz split-beam transducers mounted in the hull of the IBRV Araon (Figure 3.4.1). Because of instability of sync unit, there were continuous interference noise from EM122 during the entire running time. Simrad EK80 v.1.12.4 was used for EK80.raw data files, which were logged to extra hard drive using a USB cable. All raw data were collected

to 1000 m and Echolog was run on the EK80 workstation. All raw data were saved in a general folder ANA13B/raw, all echolog data were saved in the folder ANA13B/data/EK60. All files were prefixed with ana13b. The echosounder was calibrated near the sea of Jangbogo research station. The calibration was followed the standard procedures (Foote et al., 1987). The EK60 was run initially using calibrated settings (Table 3.4.1).

Post processing will be followed to remove the non-biological signals (surface bubbles, ice fragments, false bottom echoes, frequency interference from other acoustic instruments) and background noise using virtual echogram (Myriax, Echoview software) (Figure 3.4.2). The raw acoustic data will convert to raw volume backscattering strengths (S_v) binned into mean S_v cells with an interval of 1 nautical mile (nmi) horizontal distance. The background noise will be removed with a proper threshold at each frequency.

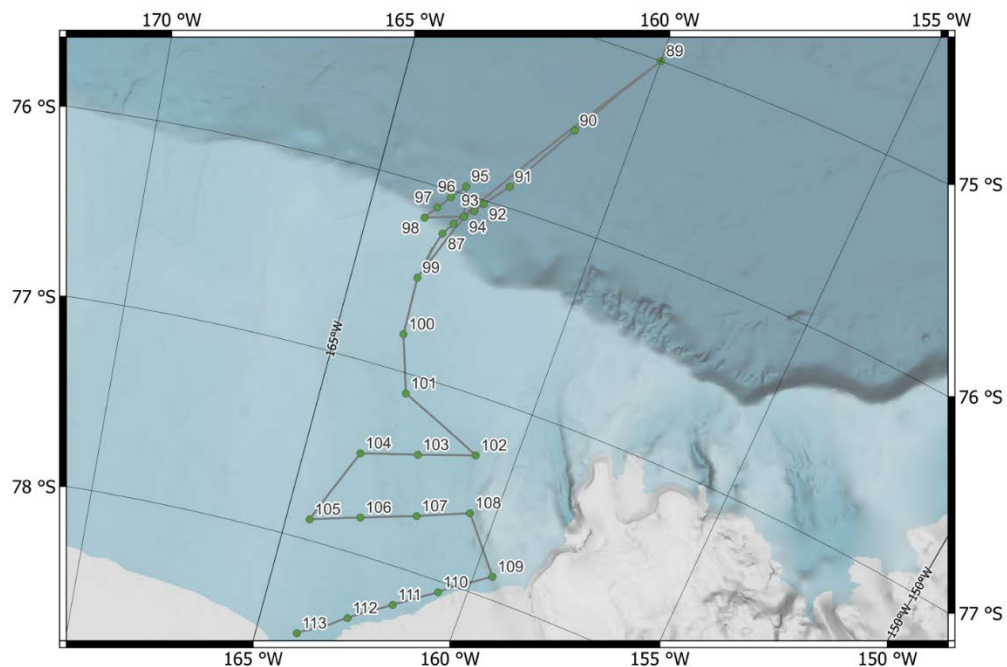


Figure 3.4.1. Bathymetry in the Little America Basin.

Table 3.4.1. System parameters of scientific echosounder

Frequency(kHz)	38	120	200
Beam type	Wide	Narrow	Narrow
Transmitted power (W)	500	250	150
Pulse duration (ms)	1.024	1.024	1.024
Transducer gain (dB)	–	25.15	25.60
Beam width (along/athwart) (°)	–	6.23 / 6.36	6.07 / 6.01
Absorption coefficient (dB km ⁻¹)	–	38.7	38.9
Sa correction (dB)	–	0.0018	-0.04
Sound Velocity (m s ⁻¹)	1450.5	1450.5	1450.5
RMS Error (dB)	–	0.21	0.35

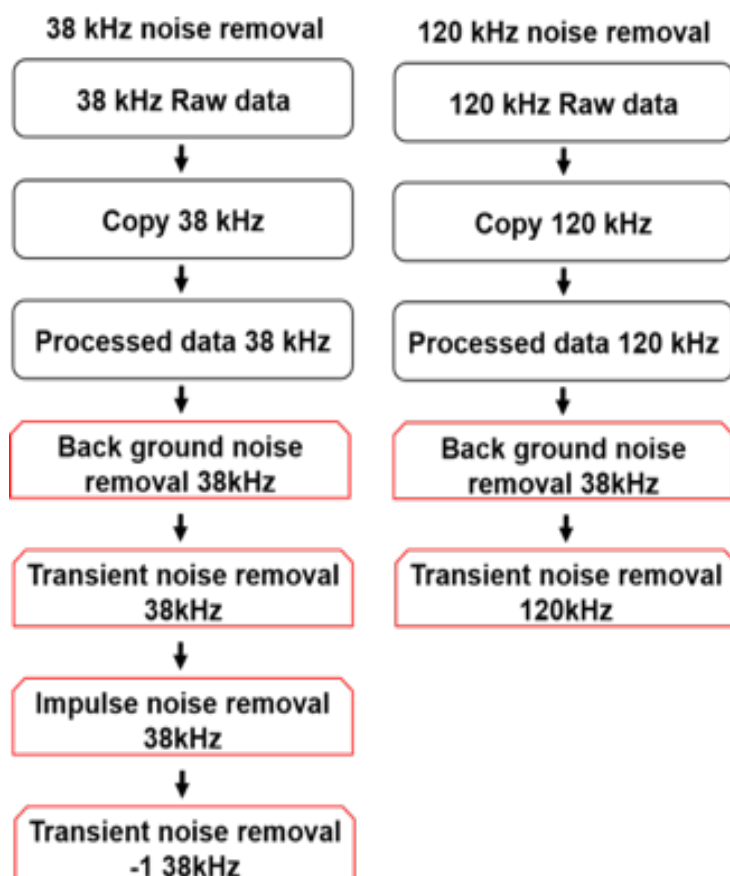


Figure 3.4.2. Flow diagram for noise removal using acoustic analyze software algorithms.

3.4.2.2. Krill sampling

To estimate length distribution of krill, krill samples were collected in the Little America Basin with a small frame net. The mouth opening of small frame net was 4 m² and the mesh size was 4 mm. Each net was equipped with a mechanical flowmeter (HYDRO-BIOS, Germany) attached to the net mouth to determine the water volume filtered in each haul. The small frame net was targeted to collect krill and micronekton upper 200 m of the water column at two stations (Table 2). The average towing speed during each haul was 3 knots for about 0.8 hours and wire-up speed was 1 m/s. At each station, 100 individual krill were subsampled and measured their body length (Figure 3.4.3). Just after length measurement finished, subsamples were immediately frozen in -80 °C for further analysis such as estimation of weight-length relationship and identification of the krill. If the total number of individuals caught was lower than 100, the whole net-sample was frozen in -80 °C.

Table 3.4.2. Sampling station details including start date and time, station location, sampling depth

Station	Latitude (°)	Longitude (°)	Date (YYYY-MM-DD)	Time (UTC)	Net type	Flow meter	Sampling Depth(m)
103	77° S 26.289'	162° W 55.664'	2023-2-6	13:34-14:04	FTN	21898 - 29428	95
112	78° S 25.426'	163° W 19.469'	2023-2-7	19:03-19:21	FTN	29428 - 30761	30



Figure 3.4.3. Krill length measurement during ANA13B SOLOMON cruise.

3.4.3. Preliminary results

At each station, 100 individual krill were subsampled and krill body lengths were measured from the anterior edge of the eye to the tip of the telson. All lengths were measured to the nearest 0.1 millimeter (mm) using a vernier caliper. Ice krill was predominant and Figure 3.4.4 shows the length distribution of ice krill during ANA13B cruises. The mean length of ice krill was 30.9 mm (SD=3.3, N = 200) and varied from 20.2 to 38.4 mm during the cruise.

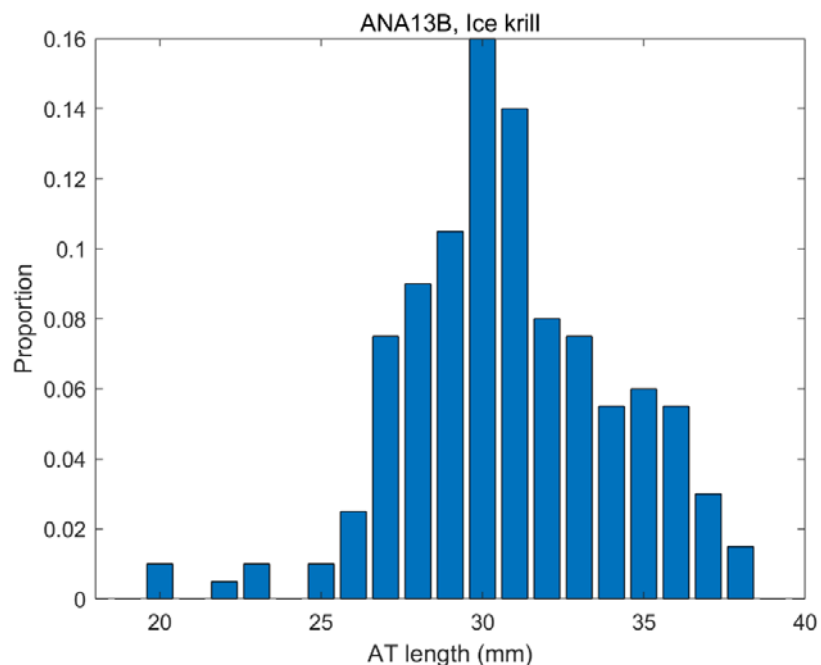


Figure 3.4.4. Ice krill length-frequency distribution during ANA13B SOLOMON cruise.

References

- Arrigo K. R., van Dijken G. L. (2003) Phytoplankton dynamics within 37 Antarctic coastal polynyas. *J Geophys Res* 108: doi:10.1029/2002JC001739.
- Foote, K.G., Knudsen, H.P., Vestnes, G., MacLennan, D.N., Simmonds, E.J. (1987) Calibration of acoustic instruments for fish density estimation: a practical guide. *ICES Coop. Res. Rep* 144, 69.

3.5. Biochemical Composition of POM

Sanghoon Park

Department of Oceanography, Pusan National University, Korea

E-mail: mossinp@pusan.ac.kr

3.5.1. Introduction

The Ross Sea has been recognized as an important reservoir of anthropogenic carbon dioxide (Arrigo et al., 2008). The export of carbon from the atmosphere to the bottom of the Ross Sea is mostly driven by the biological pump, which is the sequestration of organic carbon mainly attributed to phytoplankton into the deep sea (Smith et al., 2013). Particulate organic carbon (POC) is generally known as the important components of the biological pump in this region (Fabiano et al., 1997; Bercovici et al., 2017).

Another component that is known to play a pivotal role in the carbon cycle is transparent exopolymer particle (TEP). TEP is carbon-rich sticky organic particle, mostly formed by dissolved acidic polysaccharides (Alldrege et al., 1993). TEP mainly originates from dissolved precursors, mostly dissolved polysaccharides released by phytoplankton (Passow, 2000). These precursors contribute to the DOM pool in the water column. Therefore, the formation of TEP is important as a major pathway in which the DOM is switched into the particulate organic matter (Passow, 2000). Because of their high stickiness, TEP enhances the formation of large aggregate, increasing the vertical transport of POC to the deep ocean (Passow et al. 2001). However, despite the important of TEP in the carbon cycle, little information on the stocks and contributions of TEP to the organic carbon pool in the Ross Sea is currently available (Hong et al., 1997; Park et al., 2021).

Furthermore, few studies have been conducted on the different particulate organic carbon compositions depending on each dominant algal group in the Ross Sea. Therefore, in this study, we aimed to identify the spatial variations in particulate organic carbon composition including biopolymeric particulate carbons (BPC) and TEP in the Little American Basin in the Ross Sea, Antarctica.

3.5.2. Material and methods

3.5.2.1. TEP Sampling

Seawater samples were obtained at 11 stations over the Ross Sea (Figure 3.5.1, Table 3.5.1) using CTD/rosette sampler equipped with 24-10L Niskin bottles. Water samples for TEP (0.1-0.3L) collected from different 10 depths were filtered through 0.4 µm pore sized polycarbonate membrane filters (ADVANTEC; 25mm, Toyo Roshi Kaisha, Tokyo, Japan) under low vacuum (<150 mm Hg) (Figure 3.5.2). The filters were stained with 500 µL of Alcian Blue solution (8GX, Sigma), rinsed with distilled water, and immediately kept at -20 °C until further analyses. At the home laboratory, the stained TEP on the filters will be soaked in 6 mL of 80 % sulfuric acid for 3 hours. According to the spectrophotometric method of Passow and Allredge (1995) with consideration of the updated method described in Bittar et al (2018), the absorbance for TEP concentration will be measured at 787nm with a spectrophotometer (Hitachi-UH 5300, Hitachi, Tokyo, Japan).

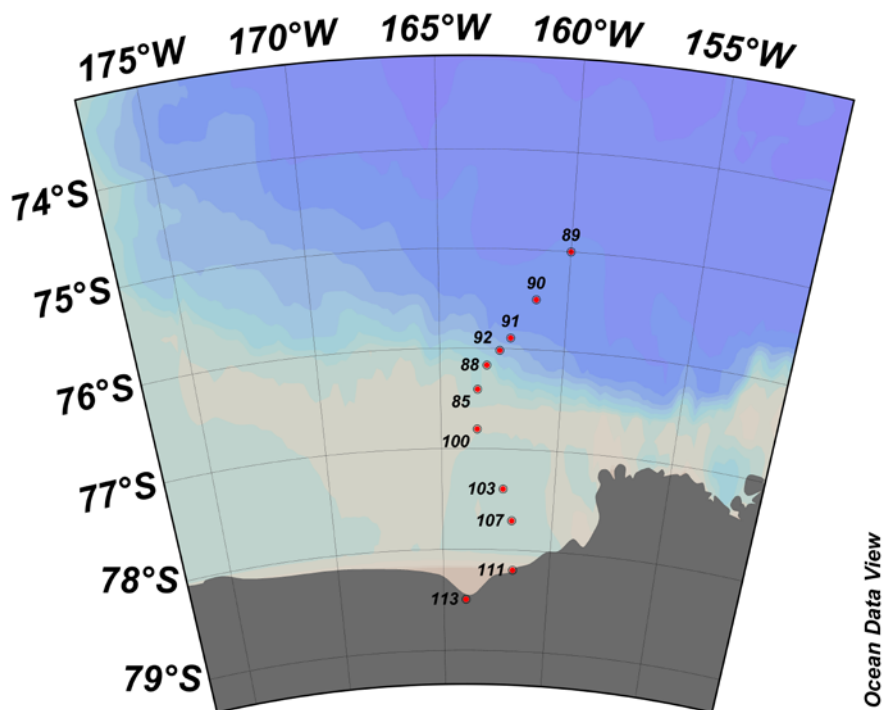


Figure 3.5.1. Sampling stations for transparent exopolymer particle and biopolymeric particulate carbons during the ANA13B SOLOMON Cruise.

3.5.2.2. BPC Sampling

Water samples for macromolecular composition of phytoplankton obtained from different 10 depths at selected 11 stations in the Ross Sea. All sample waters for macromolecular composition of phytoplankton were filtered on GF/F ($\phi = 47$ mm) filters and was then immediately stored at -20°C until analysis (Figure 3.5.2). The content of total carbohydrates will be determined by the phenol–sulfuric acid method from with a glucose standard (1 mg mL⁻¹, 108 Sigma, St. Louis, MO, USA), and the protein concentration of POM will be analyzed with a protein standard solution (2 mg mL⁻¹, Sigma). For lipid extraction and assay, the methods will be used with the chloroform–methanol mixture (1:2 v/v). Tripalmitin solution will be used as a standard for the lipid concentration. The sum of carbon equivalents of total carbohydrates, proteins, and lipids is indicated as the total biopolymeric particulate carbons (BPC) (Danovaro et al., 2000).



Figure 3.5.2. Sampling for transparent exopolymer particle and biopolymeric particulate carbon.

Table 3.5.1. Sampling information during the ANA13B SOLOMON Cruise

Station	Lat	Long	Secchi Depth (m)	Bottom Depth (m)	TEP	BPC	POC
85	76°24.628	163°27.488	6	537	o	o	o
88	76°10.049	163°05.916	7	965	o	o	o
89	75°00.000	160°00.000	5	3797	o	o	o
90	75°30.000	161°12.724	5	3348	o	o	o
91	75°53.492	162°09.671	6	2840	o	o	o
92	76°01.162	163°35.193	11	2247	o	o	o
100	76°48.418	163°27.812	6	576	o	o	o
103	77°23.866	162°17.326	6	645	o	o	o
107	77°42.632	161°51.180	8	681	o	o	o
111	78°11.985	161°43.396	5	603	o	o	o
113	78°29.742	163°55.379	7	640	o	o	o

References

- Allredge, A. L., Passow, U., & Logan, B. E. (1993) The abundance and significance of a class of large, transparent organic particles in the ocean. Deep-Sea Research Part I, 40(6), 1131– 1140.
- Arrigo, K. R., van Dijken, G., & Long, M. (2008) Coastal Southern Ocean: A strong anthropogenic CO₂ sink. Geophysical Research Letters, 35(21).
- Bercovici, S. K., Huber, B. A., DeJong, H. B., Dunbar, R. B., & Hansell, D. A. (2017) Dissolved organic carbon in the Ross Sea: Deep enrichment and export. Limnology and Oceanography, 62(6), 2593–2603.
- Bittalr, T.B., Passow, U., Hamaraty Li., Bidle, K. D., Harvey, E.L. (2018) An updated method for the calibration of transparent exopolymer particle measurements. Limnology and oceanography: Method.
- Danovaro, R., Dell'Anno, A., Pusceddu, A., Marrale, D., Della Croce, N., Fabiano, M., & Tselepidis., A. (2000) Biochemical composition of pico-, nano- and micro-particulate organic matter and bacterioplankton biomass in the oligotrophic Cretan Sea (NE Mediterranean). Progress in Oceanography.
- Fabiano, M., Chiantore, M., Povero, P., Cattaneo-Vietti, R., Pusceddu, A., Misic, C., & Albertelli, G. (1997) Short-term variations in particulate matter flux in Terra Nova Bay, Ross Sea. Antarctic Science, 9(2), 143-149.
- Hong, Y., Smith, W. O., & White, A. M. (1997) Studies on transparent exopolymer particles (TEP) produced in the ross sea (Antarctica) and by Phaeocystis antarctica (Prymnesiophyceae). Journal of Phycology, 33(3), 368–376.

- Park, S., Park, J., Yoo, K. C., Yoo, J., Kim, K., Jo, N., Jang, H. K., Kim, J., Kim, J., Kim, J., & Lee, S. H. (2021) Seasonal variations in the biochemical compositions of phytoplankton and transparent exopolymer particles (Teps) at Jang Bogo station (terra nova bay, ross sea), 2017–2018. *Water* (Switzerland), 13(16) 2173.
- Passow, U., & Alldredge, A. L. (1995) A dye-binding assay for the spectrophotometric measurement of transparent exopolymer particles (TEP). In *Limnology and Oceanography*, 40(7), 1326–1335.
- Passow, U., Shipe, R. F., Murray, A., Pak, D. K., Brzezinski, M. A., & Alldredge, A. L. (2001) The origin of transparent exopolymer particles (TEP) and their role in the sedimentation of particulate matter. *Continental Shelf Research*, 21(4), 327–346.
- Passow, Uta. (2000) Formation of transparent exopolymer particles, TEP, from dissolved precursor material. *Marine Ecology Progress Series*, 192, 1–11.
- Smith, W. O., Tozzi, S., Long, M. C., Sedwick, P. N., Peloquin, J. A., Dunbar, R. B., Hutchins, D. A., Kolber, Z., & DiTullio, G. R. (2013) Spatial and temporal variations in variable fluorescence in the Ross Sea (Antarctica): Oceanographic correlates and bloom dynamics. *Deep-Sea Research Part I: Oceanographic Research Papers*, 79, 141–155.